KTH Industrial Engineering
and Management

Desalination Using Membrane Distillation

Experimental and Numerical Study

Alaa Kullab

Doctoral Thesis 2011
Division of Heat and Power Technology
Department of Energy Technology
Royal Institute of Technology
SE-100 44 STOCKHOLM

Trita KRV-11-7
ISSN 1100-7990
ISRN KTH-KRV-11-07-SE
ISBN 978-91-7501-133-2

ABSTRACT

.
Desalination has been increasingly adopted over the last decades as an option, and sometimes as a necessity to overcome water shortages in many areas around the world. Today, several thermal and physical separation technologies are well established in large scale production for domestic and industrial purposes. Membrane distillation is a novel thermally-driven process that can be adapted effectively for water desalination or water treatment in industrial applications, due to its potential lower energy consumption and simplicity.

The general objective of this thesis is to contribute to the technical understanding of membrane distillation as a new technology in water treatment for both industrial and drinking water purposes, as a starting point for further improvement. The thesis includes experimental and numerical investigations that highlight some aspects of the technology application and fundamental aspects.

In the field of industrial application, an experimental and numerical assessment has been carried out on an Air Gap Membrane Distillation (AGMD) prototype to assess the utilization of the technology in thermal cogeneration plants; in particular, demineralization of water boiler feed water and treating flue gas condensate. The main assessment parameters were water quality and energy consumption. The results from full-scale simulations of a system of 10 m^3/hr production capacity, connected to the district heating network were as follows: 5 to 12 kWh/m^3 specific thermal energy consumption, and 0,6 to 1,5 kWh/m^3 specific electricity consumption, depending upon the heat source (district heat supply line or low-grade steam).

For desalination applications, experimental and simulation work was conducted on an AGMD semi-commercial system as part of the EU MEDESOL project. The aim was to evaluate AGMD performance with saline water of 35 g/l NaCl in order to establish an operation data base for simulation of a three-stage AGMD desalination system. Specific thermal energy consumption was calculated as 950 kWh_t/m^3 for a layout without heat recovery, and 850 kWh_t/m^3 for a layout with one stage heat recovery. The lack of internal heat recovery in the current MD module means that most of the heat supplied to MD system was not utilized efficiently, so the thermal energy consumption is high. This would mean that a large solar field is needed.

In order to analyze the flow conditions in feed flow and cooling channels, CFD was used as tool to analyze a spacer-obstructed flow channel for different types of spacer geometrical characteristics: flow of attack angle, spacer to channel thickness ratio, and void ratio. Velocity profiles, shear stress, and pressure drop were the main assessment criteria. Results show the flow of attack angle has a very minimum effect on the performance of spacers. The effect of spacer to channel thickness ratio was significant in all assessment parameters. Higher void ratios were found advantageous in promoting flow mixing, but resulted in lower sheer stress and hence reduced heat transfer.

Physical modifications were implemented on a semi-commercial AGMD prototype to assess experimentally any improvement in its performance. These modifications were mainly focused on reducing the conductive heat transfer losses by modifying the physical support in the air gap that separates the membrane from the condensation surface. In addition, several feed channel spacers were tested and assessed based on their effect in increasing the mass

transfer while maintaining or reducing pressure drop. The modifications yielded a two-fold augmentation: slight increase in the distillate mass flow rate (9-11%), and increased thermal efficiency (6%). The pressure drop in the module was reduced by 50% through selecting the appropriate spacer that would achieve the above mass flow rate increase.

Keywords: Air gap membrane distillation, applications, experimental and simulation, CFD, physical modification, performance improvement.

SAMMANFATTNING

Avsaltning har blivit alltmer aktuellt under de senaste decennierna som ett alternativ, och ibland som en nödvändighet för att hantera vattenbristen i många områden runt om i världen. Idag finns flera termiska och fysikaliska separationstekniker för storskalig produktion både för hushålls och industriella ändamål. Membrandestillation är en ny process som kan anpassas effektivt för avsaltning eller vattenrening i industriella applikationer på grund av potentialen för lägre energiförbrukning och ökad enkelhet.

Målet med denna avhandling är att bidra till den tekniska förståelsen av membrandestillation som en ny teknik i vattenrening för både industri- och dricksvatten, som utgångspunkt för ytterligare förbättringar. Avhandlingen innehåller experimentella och numeriska undersökningar som belyser vissa aspekter av teknikens tillämpningsområden samt grundläggande aspekter.

För industritillämpningar har experimentell och numerisk analyser gjorts för en luftspalt membrandestillation (AGMD) prototyp för att bedöma utnyttjandet av processen i termiska kraftvärmeverk, i synnerhet demineralisering av matarvatten och rening av rökgaskondensat. De huvudsakliga parametrarna är vattenkvalitet och energiförbrukning. Resultaten från en fullskalig simulering av ett system med 10 m^3/tim produktionskapacitet, ansluten till fjärrvärmenätet: 5 till 12 kWh/m^3 specifik termisk energi, och 0,6 till 1,5 kWh/m^3 specifik elförbrukning beroende på värmekällan (fjärrvärmeledning eller låg temperatur ånga).

För avsaltning har experimentella och numeriska analyser genomförts på en AGMD enhet inom ramen för EU MEDESOl-projektet. Syftet var att utvärdera MD:s prestanda med saltvatten (35 g/l NaCl) för att upprätta en databas om en trestegs MD-system. Specifik värmeförbrukningen beräknades till 950 kWh_t/m^3 för systemet utan värmeåtervinning och 850 kWh_t/m^3 för systemet med ett-stegs värmeåtervinning. Bristen på intern värmeåtervinning i den aktuella MD-modul leder till en hög termisk energiförbrukningen, som i sin tur leder till stora solfångarytor.

För att analysera flödesförhållanden i inloppskanalen och i kylkanalerna har numeriska beräkningsverktyg (CFD) använts. Olika typer av nät har studerats med följade parametrar i fokus: infallsvinkel, avstånd mellan nätet och kanalytor, och nätöppning. Hastighetsprofiler, skjuvspänning och tryckfall var de primära bedömningskriterier som används för utvärderingen. Resultaten visar att infallsvinkeln har en mycket minimal verkan på prestandan. Avståndet mellan nätet och kanalytorna visade stor påverkan. Högre nätöppningar var fördelaktigt för att de bedrog till bättre blandning, men resulterade i lägre skjuvspänningar och därmed minskade värmeöverföring.

Fysiska modifieringar har genomförts på en semi-kommersiell AGMD prototyp för att utvärdera experimentellt dess förbättring i prestanda. Modifieringarna var fokuserade på att minska förluster i värmeledningen genom att minska stödet i luftspalten som skiljer membranet från kondensytan. Flera typer av nät som stöd testades utifrån förmågan att öka masstransport med bibehållen eller minskad tryckfall. Resultaten visar att modifieringarna

ökade något destillatets massflödet (9-11%) samt termiska verkningsgrad (6%). Tryckfallet minskade med 50% med denna konfiguration.

Nyckelord: membrandestillering, tillämpningar, numeriska beräkningar, modifiering, prestandaförbättring.

PREFACE

1. List of publications included in the thesis (Appended)

Alaa Kullab, Andrew Martin; 2011 "Membrane distillation and applications for water purification in thermal cogeneration plants" Separation and Purification Technology, Volume 76, 2011, pp 231-237

Alaa Kullab, Andrew Martin, Elena Guillén-Burrieza; 2011 "Experimental and Simulation of an Air Gap Membrane Distillation System", *Manuscript submitted to Journal of Desalination*

Alaa Kullab, Reza Fakhrai, Andrew Martin; 2011 "CFD Analysis for Spacer-Obstructed Channel in Membrane Distillation", *Manuscript to be submitted to Journal of Membrane Science*

Alaa Kullab, Andrew Martin; 2011 "Experimental Evaluation of a Modified Air-Gap Membrane Distillation Semi-Commercial Prototype", *Manuscript submitted to Journal of Desalination*

2. List of publications not included in this thesis

Reviewed conference/research papers

Kullab, A.; Liu, C.; Martin, A; 2005 "Solar Desalination Using Membrane Distillation – Technical Evaluation Case Study" *International Solar Energy Society Conference, Orlando, FL, August 2005.*

Alaa Kullab and Andrew Martin, 2006 "Treatment and Reuse of Flue Gas Condensate by Membrane Distillation," *The International Conference on Renewable Energies and Water Technologies (CIERTA) October 2006*

Technical reports

Alaa Kullab and Andrew Martin; 2007 "Membrane Distillation and Applications for Water Purification in Thermal Cogeneration – Pilot Plant Trials," *VÄRMEFORSK Service AB, (2007) Stockholm.(reviewed report; published December 2007)*

Alaa Kullab and Andrew Martin; 2007 "Review of the Membrane Distillation Technology" *Internal report included in Deliverable 1; part of official EU MEDESOL project reports submitted to EC in March 2007.*

Alaa Kullab and Andrew Martin; 2007 "Prototype design of 3-stage membrane distillation unit" *Deliverable 3; part of official EU MEDESOL project reports submitted to EC in November 2007.*

ACKNOWLEDGEMENTS

It has been a long journey of work and thought, but mostly wondering. During the past few years, I enjoyed the guidance, help, support and the company of many people to whom I am grateful. First, I would like to express my sincere appreciation to my supervisor Associate Professor Andrew Martin. Your guidance, support and the method of constructive encouragement and trust will be the manners I wish to follow.

At the Energy Department, I am grateful to Reza Fakhrai for his great help and valuable discussions in numerical simulations. Special thanks to Seksan Udomsri, my office mate for his support in work and personal level.

I would like to thank Anders Wik for his help and fruitful discussions during Värmeforsk project. I wish to thank my colleagues in Spain during the work on MEDESOL project; special thanks to Elena Guillen and Wolfgang Gernjak.

Many thanks to Aapo Sääsk from SCARAB AB for his support, enthusiasm and willingness to explore any new idea. My appreciation to Henrik Dolfe, Miriam Aslin and Louise Andersson for continues and valuable help for many years.

I wish to thank my collogues in the Energy Department for the time and experience. My friends who are still in the department and the ones who already left; I am grateful for the pleasure of your friendship.

Special thanks to Jan-Erik Gustafsson, Lennart Johansson and Nabil Kassim for their support in professional and personal levels.

My great appreciation to my friends in Sweden: Samer, Lina, Nasrin, Mohammad, Khamis, Baha, Sara, Jaime, Sikander, Rabie, Houssien, Helen and Feras.

I will be always grateful and indebted to my family for their unconditional love and support; without you I wouldn’t have come all that way.

For my father Ibrahim who left this world three years ago; for my mother Nazira, who fills this world; no words, will ever be sufficient.

Alaa Kullab

October, 2011

CONTENTS

LIST OF FIGURES

LIST OF TABLES

NOMENCLATURE

Abbreviations	Description	Units
F	Mass flux	kg/m^2-s
r	Average pore size	µm
ε	membrane porosity	%
τ	membrane tortuosity	
d	thickness	m
B	geometric factor determined by pore structure	
γ_L	liquid surface tension	
θ	liquid-solid contact angle/ flow of attack angle	
T	temperature	ºC
Q	Heat flux	kJ/ m^2-s
h	Heat transfer coefficient	W/ m^2-s
C	Specific heat capacity	kJ/kg-K
k	Thermal conductivity	W/m-K
λ	Latent heat of evaporation	kJ/kg
K	mass transfer coefficient/permeability	s^{-1}
P	Partial pressure	Pa
R	ideal gas constant	J/mol/K
M	molecular mass	kg/mol
f	Molar flux	mol/s
l	litre	l
h	hour	h
S	siemens	
α	Angle between filaments	
ℓ	Length of the flow channel	m
b	Air gap width	m
e	Thickness of condensation plate	m
η	Thermal efficiency	
g	gram	
Subscript		
m	membrane	
a	air	
e	evaporation	
c	cooling	
h	hot	
f	film	
w	water	
l	liquid	
p	plate	
s	Solid/sensible	
g	gas	
b	bulk	
r	ridge	

Acronyms

PR	Performance ratio
MD	membrane distillation
RO	reverse osmosis
AGMD	air gap membrane distillation
DCMD	Direct contact membrane distillation
SGMD	sweep gas membrane distillation
VMD	vacuum membrane distillation
PTFE	polytetrafluoroethylene
PVDF	polyvinylidenedifluoride
PP	polypropylene
MF	microfiltration
LEP	liquid entry pressure
TPC	temperature polarization coefficient
CPC	concentration polarization coefficient
SEK	Swedish Kronor
CHP	combined heat and power
PSA	Plataforma Solar de Almería
MSF	Multi-stage Flush
MED	Multi-effect Distillation
MVC	Mechanical vapor compression
ED	Electrodialysis
IDA	International Desalination Association
CFD	Computational fluid dynamics
UF	ultrafiltration

1 INTRODUCTION

1.1 Background and motivation

Water supply and management plays a major role in societies' development and wellbeing of their citizens. The need for water covers not only the water needed for human consumption, but also, and most of the time, mainly the consumption in agriculture and industry. While the amount of available fresh water in the natural occurrence is constant, the population growth and the consumption level are constantly increasing. According to the Worldwatch Institute, more than two-thirds of the world's population may experience water shortages by 2025 [Karagiannis and Soldatos, 2008]. The challenge becomes even more critical when it comes to distribution and local conditions which expected to be more hardship for countries already suffering from critical water shortages, especially in the Middle East and sub-Saharan countries.

Industry accounts for about a quarter of all water consumption worldwide. In industrialized countries significant quantities of water are needed for various industrial processes, greatly exceeding the quantities of water used for all other purposes [Judd and Jefferson, 2003]. While overcoming the shortage problem would need efficient water governance programmes and tools; still, in many areas around the world, desalination option is bound to play a more increasing role in the future of water management schemes.

According to the International Desalination Association (IDA), the overall worldwide installation of desalination plants, distributed over almost 120 countries (with production capacity of nearly 26 million m^3/d and number of plants, actually operating or ready for production), amounts to more than 12,500 installations [Sharma et al, 2003]. Even for countries of abundant water resources, like Sweden, desalination or water demineralization as usually referred to, is a common practice in industrial process up-stream and more increasingly, in the processes' downstream for economical and environmental reasons. For instance, thermal cogeneration plants require purified or treated water for a number of processes, i.e. boiler/district heat make-up water systems and flue gas condensate treatment. The selection of the exact water treatment process is of course dependent upon the final water quality along with the volume of water to be treated [Kullab and Martin, 2007].

The technologies used on the industrial scale are generally classified into the following categories:

Thermal processes

1. Multi-stage flash (MSF): The by far most commonly used process for the desalination of seawater is the Multi Stage Flash (MSF) distillation. It is a process that involves evaporation and condensation of water, where pressurized feed water is heated in the brine heater before entering a chamber under partial vacuum. The latent heat of evaporation is recovered for reuse by preheating the incoming water. To maximize water recovery, each stage of an MSF unit operates at a successively lower pressure [Ettouney et al, 1999; Darwish and Al Najem, 2000].

2. Multiple effect distillation (MED): Multiple Effect Distillation (MED) utilizes the principle of distillation that it involves boiling of the feed water. Therefore, this method encounters problems with scaling and has in general a more complex installation and control as compared to MSF. MED also uses different pressure vessels or effects, and the feed water is evaporated in the first vessel at its boiling point [El Dessouky et al, 2000; Al-Shammiri and Safar, 1999].
3. Mechanical vapor compression (MVC): The MVC process is characterized by being driven solely by electric current, which is used to drive the mechanical vapor compressor. Start-up of the MVC process requires use of an external heating steam. Vapor compression (VC) is similar to the MED principle. Feed water entering the effect is evaporated and the produced vapor leaves by passing a moisture separator. Instead of condensing in the next subsequent effect as the case MED, the feed water is compressed and hence its condensing temperature is elevated [Mandany et al, 2000; Ettouney, 2004].

Membrane technologies

1. Reverse osmosis (RO): Desalination plants based on reverse osmosis are one of the most popular types installed nowadays, although their overall capacity is comparatively small [Ribeiro, 1996]. Reverse osmosis is a membrane process; the salt is separated from the water by means of a selective membrane. Theoretically, the only energy requirement is to pump the feed water at a pressure above the osmotic pressure. However, higher pressures must be used, typically 50-80 bar, in order to have a sufficient amount of water pass through a unit area of membrane [Van der Bruggen, 2003].
2. Electrodialysis (ED): As implied by its name, this technology utilizes an electrochemical separation process in which charged membranes are applied to separate ionic species from a mixed aqueous solution of varied components imposed by an electrical potential difference. In the ED process, multi-forces such as potential and concentration differences lead to the transport of solute and water through ion exchange membranes, which cause the concentration variations of solute in dilute and concentrated compartments [Wang et al, 2004].

While these technologies are well established, they are energy intensive and are ultimately linked to fossil-based or non-renewable energy sources, in addition their complexity and different related operational problems. Other technologies like Membrane Distillation (MD) have been investigated due to its potential advantages regarding energy consumption, simplicity and its ability to be coupled with solar energy [Al-Obaidani et al, 2008], combined heat and power production, or polygeneration.

Membrane Distillation is a novel process that can be adapted effectively for water desalination or water treatment in industrial applications. A difference in partial pressure serves as the driving force, and the presence of a hydrophobic membrane ensures high water quality regardless of feedstock parameters. Hot-side temperatures under 90 °C are suitable; hence this process is ideal for exploiting waste heat or solar thermal resources. However a number of issues remain before this technology is fully deployed commercially.

In general MD has a several advantages and disadvantages including [Lawson and Lloyd, 1997; Liu and Martin, 2005]:

Advantages of MD:

- 100% (theoretical) rejection of ions, macromolecules, colloids, cells, and other non-volatiles
- Lower operating temperatures than conventional distillation
- Lower operating pressures than conventional pressure-driven membrane separation processes
- Low sensitivity to variations in process variables (e.g. pH and salts)
- Good to excellent mechanical properties and chemical resistance
- Reduced vapor spaces compared to conventional distillation processes

Disadvantages of MD:

- High energy intensity (although energy, i.e. heat, is usually low grade)
- Low yield in non-batch mode; high recirculation rates in batch mode
- Sensitive to surfactants
- Undesirable volatiles such as ammonia or carbonates must be treated separately (degassing, pH control, or other methods required)

The potential for employing MD is not yet utilized in practice. Such potential of membrane distillation in energy consumption, water quality and simplicity has driven many researchers to carry on several theoretical and lab scale researches in order to employ it as a commercial technology.

1.2 Research background and objectives

Membrane Distillation research was initiated at KTH in 2002 in conjunction with Scarab Development AB and its subsidiaries, in order to find viable applications for MD technology in the field of desalinization and water treatment. Within the scope of this study started in March 2006, the application of the technology in two main fields, desalination for industrial purposes and desalination for drinking purpose are main focus. A semi-commercial MD unit owned by Swedish company (SCARAB AB) was utilized in this study. Despite the theoretical and lab scale studies, very few semi-commercial size membrane distillation technology prototypes have been tested and evaluated in the world. Moreover, there are no viable technical and commercial data available about these technologies and their performance. On the other hand, most of the lab scale tests gave a large variance in performance ranging from very promising ones to almost non-interesting ones.

The general objective of this study is to contribute to the technical understanding of membrane distillation as a new technology in water treatment for both industrial and drinking water purposes, as a starting point for further improvement. Specific objectives (which are also outlining the work stages) of the current study are the following:

- Literature review of membrane distillation technology and its theoretical aspects *(Chapetr 2).*
- Performance evaluation of MD technology in industrial applications: focuses mainly on pilot plant trials at Idbäcken Cogeneration Plant in Nyköping in order to evaluate the on-site performance of five MD modules for the purpose of studying the viability of MD for water demineralization used in boiler feed and make-up water *(Chapter 3).*
- Performance evaluation of MD technology in drinking water applications: this part of the research was conducted within an EU project, MEDESOL, with the purpose to design, construct and test multi-stage MD desalination pilot plants driven by solar energy. System simulation tools (Aspen Utilities package) will be employed in order to analyze the multi-stage MD plant. Experimental work was used to evaluate the performance of the MD plant under the real life conditions in water demineralization using sea water as a feed stock *(Chapter 3).*
- Computational fluid dynamics analysis (CFD) in order to point out areas for potential improvements; this works covers the following areas *(Chapter 4)*:
  - Flow in spacer obstructed flow channel.
  - Flow conditions in the actual MD prototype cooling channel.
- Experimental tests and evaluation for a partially modified MD unit *(Chapter 5).*

2 LITERATURE SURVEY OF MEMBRANE DISTILLATION

2.1 Introduction

Membrane distillation (MD) is a thermally driven process that utilizes a hydrophobic micro-porous membrane to support a vapor-liquid interface. If a temperature difference is maintained across the membrane, a vapor pressure difference occurs. As a result, volatiles (water in this case) evaporates at the hot interface, crosses the membrane in the vapor phase and condenses at the cold side, giving rise to a net trans-membrane water flux. Membrane distillation (MD) is a relatively new process and was introduced in the late 1960s [Lawson and Lloyd; 1997, Alklaibi and Lior, 2004]. At that time, MD did not receive significant interest due to several reasons, e.g. the observed lower MD production compared to the reverse osmosis technique and unavailability of suitable membranes for the process [Lawson and Lloyd; 1997; El-Bourawi, et al; 2006. The MD process received renewed interest within the academic communities in the early of 1980s when novel membranes and modules with better characteristics became available [El-Bourawi, et al; 2006]. Moreover, the ability of MD to utilize low grade heat in a form of waste heat/renewable energy source had boosted the interest and research in order to find suitable application areas as well as improving the merits of the technology. Nonetheless, MD is not implemented yet in industry for water purification or desalination. A thorough historical perspective of MD development can be found in the review articles by Lawson and Lloyd [1997], Alkaibi and Lior [2004], and El-Bourawi et al. [2006].

Within the field of MD a variety of terms are used to identify the process: membrane distillation, capillary distillation, trans-membrane distillation, osmotic distillation, pervaporation, etc [Lawson and Lloyd, 1997]. The term membrane distillation arises from the similarity of the process to conventional distillation, where both MD and conventional distillation rely on vapor-liquid equilibrium as a basis for separation, and both processes require that the latent heat of vaporization be supplied to achieve the phase change [Lawson and Lloyd, 1997]. A few of the early patents appear in review articles like Lawson and Lloyd [1997].

2.2 MD Configurations and Application Areas

A variety of methods may be employed to impose this vapor pressure difference, and in general there are four kinds of MD system configurations (Figure 2-1): (a) Direct contact membrane distillation (DCMD), (b) air gap membrane distillation (AGMD), (c) sweep gas membrane distillation (SGMD) and (d) vacuum membrane distillation (VMD).

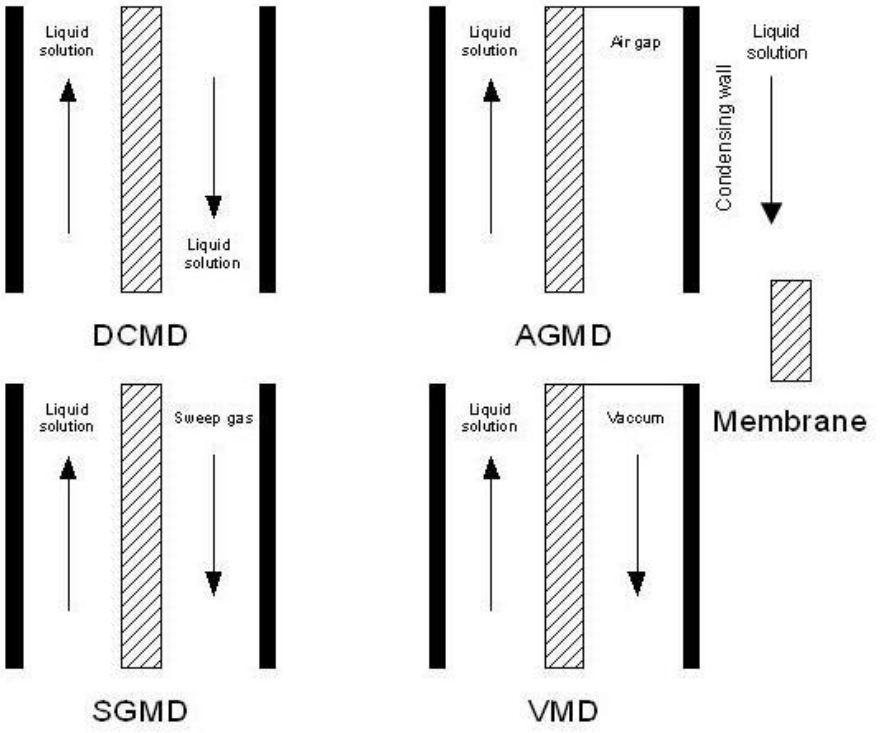

a) DCMD: The permeate side of the membrane may consist of a condensing fluid in direct contact with the membrane
b) AGMD: A condensing surface separated from the membrane by an air gap (AGMD)
c) SGMD: A condensing surface separated from the membrane by a sweeping gas
d) VMD: A condensing surface separated from the membrane by a vacuum gap.

Figure 2-1: Common configurations of membrane distillation [Lawson and Lloyd; 1997]

AGMD and DCMD are best suited for applications where water is the permeating flux. SGMD and VMD are typically used to remove volatile organic or dissolved gas from an aqueous solution [Alklaibi and Lior, 2004].

Table 2-2 shows some of the main advantages and disadvantages of each configuration; in addition to each one's application area [Lawson and Lloyd, 1997; Alklaibi and Lior, 2004; El-Bourawi et al, 2006].

Table 2-1: Main advantages, disadvantages and application area for MD configurations

MD configuration	Advantages	Disadvantages	Application area
DCMD	▪ High permeate flux ▪ Possible internal heat recovery	▪ High conductive heat losses ▪ High temperature polarization effect ▪ Risk of mass contamination of the permeate	▪ Desalination and water treatment ▪ Nuclear industry ▪ Food industry ▪ Textile industry ▪ Chemical and pharmaceutical industries
AGMD	▪ Low conductive heat losses ▪ Low temperature polarization effect ▪ Possible internal heat recovery	▪ Low permeate flux due to resistance to mass transfer	▪ Desalination and water treatment ▪ Food industry ▪ Chemical industry
SGMD	▪ Low conductive heat losses ▪ High permeate flux	▪ Complicated to handle the sweeping gas ▪ Difficult heat recovery	▪ Desalination and water treatment ▪ Chemical industry
VMD	▪ low conductive heat loses ▪ high permeate flux	▪ higher risk of pore wetting ▪ Difficult heat recovery	▪ Desalination and water treatment ▪ Food industry ▪ Textile industry ▪ Chemical industry

2.3 Membrane Materials and Characteristics

2.3.1 Membrane Material

MD is limited to the use of hydrophobic membranes. A wide variety of membranes matching such qualifications are commercially available in flat sheet or capillary form, and they are typically fabricated from polytetrafluoroethylene (PTFE), polypropylene (PP), and polyvinylidenedifluoride (PVDF) [Lawson and Lloyd, 1997]. Most of the membranes used are made originally for microfiltration (MF), and only few researchers considered designing or modifying these membranes [El-Bourawi et al., 2006; Khayet et al, 2005; Wu et al, 1992; Peng et al., 2005]. Modified membranes that consist of a hydrophobic layer and a hydrophilic layer or a hydrophobic layer sandwiched between two hydrophilic layers, have been also used [Lawson and Lloyd, 1997].

In general, the hydrophobic nature of the membrane prevents solution from penetrating into the pores, thus creating a vapour–liquid interface at each pore entrance. The microfiltration membranes manufactured from hydrophobic polymers such as polypropylene (PP), polytetrafluoroethylene (PTFE) and polyvinylidene fluoride (PVDF) are used in the MD process. The surface energies of PTFE and PVDF are 9,1 and 30,3 kN/m, respectively. They also have thermal conductivities as low as 0,22– 0,45 W/m-K and good chemical stability at the operating temperature of membrane distillation. Their pore sizes are in general in the range of 0,2–1,0 μm and thicknesses are in the range of 0,06–0,25 mm [Gray et al., 2010].

The relation between trans-membrane flux and membrane characteristics are given by the following relation [Lawson and Lloyd; 1997]:

$$N \propto \frac{r^{\alpha}\varepsilon}{\tau\delta_m}$$

where r^{α} is the average pore size for Knudsen diffusion (α = 1) or the average squared pore size for viscous flux (α = 2), ε is the membrane porosity, τ is the membrane tortuosity, and δ_m is the membrane thickness. The effect of these parameters on the flux will be described in later sections.

2.3.2 Membrane pore size

It is observed that greater distillate volumes are obtained for the membrane with a larger pore size [Izquierdo-Gil et al., 1999]. However, the larger the pore size, the lower is the liquid entry pressure (*LEP*). If the feed pressure is higher than the liquid entry pressure then the liquid penetrates through the pores and the hydrophobicity is lost [Chernyshov et al, 2003], according to the following relation:

$$LEP = \frac{-2B\gamma_L \cos\theta}{r_{\max}}$$

where γ_L is the liquid surface tension, θ is the liquid-solid contact angle, r_{max} is the largest pore radius, and B is a geometric factor determined by pore structure.

The effect of pore size becomes clear when a solution of low surface tension is processed [Kimura et al., 1987]. In order to avoid wetting of membrane pores, the pore size must be as small as possible, which contradicts the requirement of higher MD permeability. An optimum value is needed to be determined for each MD application depending on the type of the feed solution to be treated [El-Bourawi, et al; 2006].

2.3.3 Membrane porosity

Membranes with high porosity have higher fluxes regardless of which MD configuration used [El-Bourawi, et al., 2006; Schneider et al., 1988], since a larger percentage of area is available for evaporation. In terms of energy efficiency, since the heat transfer coefficient of the air/gas is smaller than that of the polymer, higher porosities decrease the conductive heat transfer through the membrane solid material. Typical membrane porosity ranges between 60-85% have been used in MD configurations [Alklaibi and Lior, 2004].

2.3.4 Membrane tortuosity

Membrane tortuosity is the average length of the pores channels relative to the membrane thickness. The higher tortuosity, the lower flux produced. In MD studies, a value of 2 is frequently assumed for tortuosity [El-Bourawi, et al; 2006].

2.3.5 Membrane thickness

Membrane thickness has an important role in the efficiency of heat and mass transfer in MD. The lower membrane thickness, the higher fluxes obtained [Schneider et al; 1988]. To obtain a high MD permeability, the membrane should be as thin as possible. On the other hand, to achieve better heat efficiency the membrane should be as thick as possible. In AGMD, the influence of membrane thickness is less influential relative to the air gap [Lawson and Lloyd; 1997, El-Bourawi, et al; 2006, Khayet et al; 2005, Schofield et al; 1987].

The kind of used polymers strongly affects the membrane properties and its processing procedure. Gryta and Barancewicz [2010] studied five different types of membranes, mainly, the influences of membrane morphology and hydrophobicity of membrane materials (water contact angle) on the membrane wettability. The PTFE membranes show the highest hydrophobic proprieties and are known as an excellent membrane material for MD. A disadvantage of PTFE is that the material is difficult to process and the PTFE membranes are usually produced through complicated extrusion, rolling and stretching procedures while PVDF membranes are relatively easy to produce and possess appropriate hydrophobic proprieties [Gryta and Barancewicz 2010].

The performances of various membranes were assessed by Gray et al [2010] in DCMD under different feed velocities and inlet temperatures. The membranes studied included a PVDF microfiltration membrane with a non-woven support layer, PTFE microfiltration membrane with a non-woven support layer, and three new MD membranes made from PTFE with a structured scrim support layer. The researchers concluded that new PTFE MD membranes in DCMD showed greater potential for use in desalination processes than the traditional microfiltration membranes due to higher flux, improved energy efficiency and doubled LEP [Gray et al, 2010].

2.4 Effect of Operating Parameters

2.4.1 Feed temperature

The effect of the feed temperature on permeate flux has been widely investigated in the different cited MD configurations. The feed temperature typically ranges between 60 °C and 90°C [Lawson and Lloyd; 1997] though lower temperatures have been used [Alklaibi and Lior; 2004]. Generally, there is exponential increase in flux with feed temperature in all MD configurations [El-Bourawi, et al; 2006]. As the driving force for membrane distillation is the difference in vapor pressure across the membrane, the increase in feed temperature increases the vapor pressure in the feed solution channel, which increases the trans-membrane vapor pressure.

According to several researchers, it is better to work under high feed temperature as the evaporation efficiency and the total heat from the feed to the permeate/cooling side is high although the temperature polarization effect increases with the feed temperature [Alklaibi and Lior; 2004, El-Bourawi, et al; 2006, Liu and Martin; 2005, Izquierdo-Gil et al; 1999, Walton et al; 2004]. However, it must be mentioned that operation on very high temperatures i.e. 90 °C may cause reduction of membrane selectivity [El-Bourawi, et al; 2006, Gryta and Karakulski; 1999] and severe scaling problems.

2.4.2 Coolant temperature

The general effect of increasing the permeate/cooling temperature is less influential than feed temperature, due to the exponential increase of the vapor pressure with feed temperature [Alklaibi and Lior; 2004, El-Bourawi, et al; 2006]. In AGMD, there is normally a minimal effect of coolant temperature on the permeate flux since the heat transfer coefficient in the air gap is much smaller than the hot and the cold side heat transfer coefficients [Banat and Simandl; 1994, Alklaibi and Lior; 2006].

2.4.3 Feed concentration

Feed concentration cause trans-membrane flux to decrease in all MD configurations [El-Bourawi, et al; 2006]. This is due to several causes; vapor pressure reduction due to the salt concentration, concentration boundary at the membrane surface and increased temperature polarization [Banat and Simandl; 1994]. However, the effect of increased feed concentration from different experimental studies could be classified as slight to modest [Khayet et al; 2005, Banat and Simandl; 1994; Criscuoli and Drioli, 1999; El-Bourawi, et al; 2006].

2.4.4 Feed flow rate

In most of the studies, the effect of the feed flow rate is to increase the permeate flux [Alklaibi and Lior; 2004, El-Bourawi, et al; 2006, Walton et al; 2004]. This is due to reeducation in temperature and concentration polarization effects by the mixing effect resulted from higher turbulence inside the feed channel. Such turbulence brings the temperature at the membrane surface closer to the bulk feed temperature. The effect of flow rate on yield is less than half of the influence of feed temperature [Alklaibi and Lior; 2004]; and its significance is obvious at higher temperatures especially associated with higher trans-membrane temperature drop [Walton et al; 2004]. In general, the relationship between the trans-membrane flux and feed flow rate is linear to a certain limit, after which has no effect where it then has no effect [Alklaibi and Lior; 2004; Sudoh et al, 1997].

2.4.5 Coolant flow rate

In the case of DCMD and SGMD configurations, an increase of the permeate flow velocity increases the heat transfer in the permeate side of the membrane module by reducing the temperature and concentration polarization effect. This will tend to increase the permeate flux as the temperature difference increases [El-Bourawi, et al; 2006]. In the case of AGMD, the effect is almost negligible relative to dominant effect of the air gap [Banat and Simandl; 1994, Alklaibi and Lior; 2006].

2.4.6 Trans-membrane temperature difference

The driving force in MD is the trans-membrane vapor pressure, as a result of temperature difference between the feed and permeate/cooling side of the membrane module [El-Bourawi, et al; 2006]. Flux increases linearly with hot to cold side temperature difference and increases slightly when coupled with a rise in feed concentration, as the boundary layer increases and contribute to the temperature polarization effect [Walton et al; 2004]. Moreover, the slope at which flux increases with temperature drop tends to decrease at higher values [Jönsson et al, 1985]. It should be noted that such tendencies are related to temperature and concentration polarization effects which are affected by feed flow rates.

2.4.7 Effect of non-condensable gases

Non-condensable gases evolve with the vapor, including dissolved. These gases are trapped in the membrane pores and tend to cause flux decline by imposing additional mass transfer resistance [Alklaibi and Lior; 2004]. When feed and permeate are degassed, the partial pressure of air within the pores becomes lower, hence, the molecular diffusion resistance decreases [Martínez and Florido-Díaz, 2001]. A study made by Schofield et al [1987] suggested two methods to de-aerate/degase the feed, either by de-aerating the feed/permeate prior to entering the module, which will increase the pressure difference across the membrane and may cause pore wetting, or by lowering the pressure of the feed/permeate. De-aeration could significantly increase the permeate flux when large pore size membrane is used [Alklaibi and Lior, 2006].

2.5 Modeling of Membrane Distillation

Water and volatiles evaporate from the liquid-vapor interface on the feed side, diffuse across the membrane, and condensed or removed from the membrane module as vapor on the permeate side [Lawson and Lloyd; 1997]. The main purpose of MD process modeling is to estimate the permeate flux depending on the membrane characteristics, module design and operation conditions [El-Bourawi, et al; 2006].

2.5.1 Heat and Mass Transfer

2.5.1.1 Heat Transfer

Heat transfer in all MD configurations is very important and assumed as the rate controlling mechanism [El-Bourawi et al; 2006]. To analyze the heat transfer mechanism, a cross section of AGMD cassette (Figure 2-2) is considered. Heat transfer is carried out in four steps: (1) heat flux from the feed solution to the liquid-vapor interface across the thermally boundary layer in the feed channel (2) heat flux by conduction and latent heat of vaporization across the membrane; (3) heat transfer from the permeate side of the membrane to the condensation layer/film on condensation plate; (4) heat transfer from the condensation film to the cooling liquid across the condensation plate and thermal boundary layer of the cooling liquid.

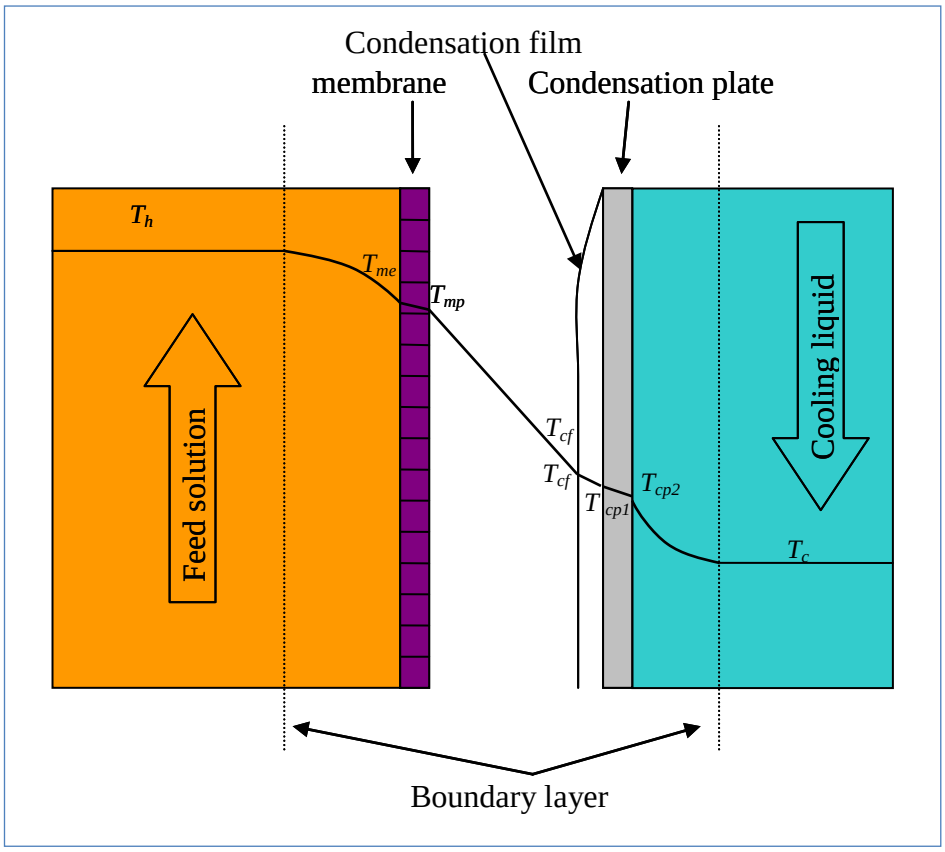

Figure 2-2: Cross section AGMD

2.5.1.1.1 Heat flux from the feed solution to the evaporation surface

The thermal boundary layer at feed side of the membrane imposes a resistance to heat transfer and creates a temperature difference between the membrane surface and the bulk liquid which creates heat transfer. The influence of this thermal layer in the feed channel (and cooling channel) is referred to as temperature polarization effect. Temperature polarization coefficient (*TPC*) is used to quantify this phenomena as following:

$$TPC = \frac{T_{me} - T_{cf}}{T_h - T_c}$$

where T_{me} is temperature at the membrane, T_{cf} is temperature at condensation film, T_h is temperature at hot/feed bulk solution and T_c is the temperature at the cooling bulk liquid. The lower *TPC* value, the higher temperature polarization effect, and vice versa. The temperature polarization effect increases with increase in feed temperature [Chernyshov et al, 2003]. The thermal boundary layers depend on fluid properties, operation condition and hydrodynamic conditions [El-Bourawi, et al; 2006].

The heat flux *Q* from the feed bulk to the interface at the membrane side can be described by [Dhahbi et al, 2002; Kubota et al, 1988]:

$$Q = (h_m + n_w C_l)(T_h - T_{me})$$

where h_m is the film heat transfer coefficient, n_w is the mass flux, C_l is liquid specific heat capacity.

2.5.1.1.2 Heat flux by conduction and latent heat of vaporization across the membrane

The total heat transfer across the membrane is the sum of the conductive heat transfer of the membrane material and membrane pores filled with air/gas which acts as a stagnant film; and the latent heat associated with evaporation. This heat flux is described by:

$$Q = \frac{k_m}{d}(T_{me} - T_{mp}) + n_w \lambda ;$$

$$k_m = \varepsilon k_g + (1-\varepsilon) k_s$$

where k_m is effective thermal conductivity of the membrane (solid material and air in the pores), d is the membrane thickness, T_{mp} is temperature at the permeate/air gap side of the membrane, λ is the latent heat of evaporation, ε is the membrane porosity, k_s is thermal conductivity of the solid material and k_a is the thermal conductivity of the air.

2.5.1.1.3 Heat transfer from the permeate side of the membrane to the condensation layer/film on condensation plate

The total heat transfer can be described by:

$$Q_T = (\frac{k_g}{b} + n_w C_g)(T_{mp} - T_{cf}) + n_w \lambda$$

where C_g is the specific heat at constant pressure in the gas phase of the water, n_w is the mass flux, λ is the latent heat of evaporation, k_g is the gas phase thermal conductivity and b is the air-gap width.

2.5.1.1.4 Heat transfer from the condensation film to the cooling liquid across the condensation plate and thermal boundary layer of the cooling liquid

From the condensation layer interface to the cold bulk liquid, the heat transfer rate can be described by:

$$Q = h_f (T_{cf} - T_{cp1}) - n_w C_l (T_{me} - T_{cf}) = \frac{k_p}{e}(T_{cp1} - T_{cp2}) = h_m (T_{cp2} - T_c)$$

where h_f is the heat transfer coefficient of condensation film, T_{cp1} and T_{cp2} are the temperatures of inner and outer side of the cooling plate respectively; k_p and e are the thermal conductivity and thickness of condensation plate respectively.

2.5.1.2 Mass Transfer

Mass transport of a volatile species occurs in two steps [El-Bourawi, et al; 2006], (1) mass transport from the bulk feed solution to the seed membrane surface, (2) mass transport through the membrane pores and (3) mass transport from the membrane surface to permeate bulk liquid. In the case of AGMD configuration, the mass transported through the membrane is affected by diffusion through the pores and free convection in the air gap [Dhahbi, 2002].

2.5.1.2.1 Mass transport from the bulk feed solution to the seed membrane surface

Considering only water; contain dissolved solids, the concentration of the solute at the membrane surface becomes higher than the one in the feed bulk due to mass transfer across the membrane. When the concentration of the solute increases; a concentration layer is formed on membrane surface reducing the flux as it constitutes a resistance to mass transfer. Concentration polarization coefficient (*CPC*) is used to quantify this resistance within the concentration layer [El-Bourawi, et al; 2006]. It is defined as:

$$CPC = \frac{C_m}{C_b}$$

where C_m is the concentration at the membrane side of the feed and C_b is the concentration at feed bulk. The molar flux N_w of the water through the concentration layer is defined by [El-Bourawi, et al; 2006]:

$$N_w = CK_{wf} \ln\left(\frac{C_b}{C_m}\right)$$

where C is the bulk total molar concentration, K_{wf} is the mass transfer coefficient of the volatile through the concentration layer.

2.5.1.2.2 Mass transport through the membrane

The mass transfer mechanism is governed by three mechanisms: Knudsen diffusion, Poiseuille flow, and molecular diffusion or combination between them, and the dusty-gas module is used as a general model describing the mass transport through the membrane generally [El-Bourawi, et al; 2006]. In general, the mass flux is described by the following relation:

$$n_w = K\Delta P$$

where K is membrane permeability and ΔP is the vapor pressure difference across the membrane. In the case of AGMD, the vapor flux is controlled by diffusion through membrane

pores and natural convection through the air gap and can be expressed by the following relation [Dhahbi et al, 2002]:

$$n_w = M_w\left[\frac{K_{total}}{R}\left(P_{me} - P_{cf}\right)\right];$$

$$K_{total} = \frac{1}{\frac{1}{K_D} + \frac{1}{K_a}}$$

where M_w is molecular weight of the water, P_{me} and P_{cf} are the partial pressure at T_{me} and T_{cf} respectively, R is the ideal gas constant, K_{total} is the total mass transfer coefficient, K_D is the diffusive mass transfer coefficient through the membrane and K_a is the convective mass transfer coefficient through the air gap.

2.6 Fouling and Scaling

Fouling and scaling are two important mechanisms that affect stability of the MD process and lead to reduce the overall efficiency. Despite the notation made in the review Lawson and Lloyd [1997] that membrane fouling problem is less in MD than in other membrane separations due the relatively large pores, the phenomena is less studied experimentally and analytically [El-Bourawi, et al; 2006]. Fouling and scaling can cause pore clogging in MD membranes which lead to reduce the membrane area available for water vaporization and hence reduce the flux. In addition, such build-up of fouling and scaling surfaces reduce the flow channel area which causes a pressure drop and lower flow rates. Such reduction will increase the temperature polarization effect and consequentially, reduces the flux [Gryta, 2005; Hsu et al, 2002; Gryta, 2002; Srisurichan et al, 2006]. Moreover, fouling and scaling may cause membrane partial wetting or severe membrane damage. There are several types of fouling and scaling.

Biological fouling is caused by microorganisms' growth on the membrane surface forming a biofilm [Gryta, 2002]. The hydrodynamic conditions and the chemical composition of feed liquid and operation conditions have significant effects on membrane fouling [Khayet and Mengual, 2004]. As MD typical temperature operational conditions, high salt concentration, and low pH due to acids (for scaling control) lead a low biofouling potential. However it is well known that bacteria are able to grow under extreme conditions such as high temperatures as 110 °C and pH values as low as 0,5 [Gryta, 2002; Gryta et al, 2006].

Particulate fouling is caused by the deposition of solid particles on the membrane. The rate and type of deposition is dependent on the size of these suspended solids [El-Bourawi, et al; 2006]. Mechanical pretreatment with on-line coagulation, sand filtration and/or rapid sand filtration and cartridge filtration are well practiced method to reduce particular fouling agents.

Scale formation results from formation of crystals on membrane surfaces [El-Bourawi, et al; 2006]. Scale formation also causes clogging of membrane pores and reduces its surface area, contributing to temperature polarization. Experimental results from direct application of tap water as a feed for the DCMD process resulted in a rapid decline of the permeate flux. Heating of the feed in the MD process caused decomposition of HCO^- ions present in the feed

water and precipitation of $CaCO_3$ on the membrane surface [Gryta and Karakulski, 2005]. Cleaning the membrane with HCl resulted in the dissolution of the deposit on the membrane surface, and the initial membrane permeability was restored. Acidification of the feed water to pH=4 was found to be efficient in controlling scaling formation caused by precipitation of $CaCO_3$. A rapid crystallization of salt on the membrane surface was observed during the concentration of saturated solutions experiment by Gryta et al [2006]. Crystal formations on membrane surface have been detected in other DCMD configuration, during crystallization of aqueous salt solutions of sodium sulfate and sodium chloride separately [Tun et al, 2005]; and sodium chloride and sugar solutions [Drioli and Wu, 1985]. On AGMD module Banat and Simandl [1994], claimed that no scaling or fouling was observed during a two-month operation with synthetic seawater feed.

Ding et al, [2010] had investigated the fouling resistance in concentrating traditional Chinese medicine (TCM) extract by direct contact membrane distillation. The concentrating experiments were conducted in batch mode, and each experiment lasted 200 to 400 min. The membrane fouling in this study was mainly caused by the deposition of suspended solid particles in TCM extract in a porous fouling layer covers the membrane surface. The study concluded that the growth of fouling layer can be effectively limited by increasing the feed temperature and feed flow velocity [Ding et al, 2010].

Treatment of wastewater from a petrochemical industry has been investigated using a novel submerged membrane distillation bioreactor (MDBR) in a bench scale system [Li et al, 2010]. During the first forty days of operation, the conductivity of the MDBR product was 33,7-82,1 µS/cm while the conductivity in the feed liquor was in a range of 20-30 mS/cm. The initial permeate flux of a new membrane was 8,6 L/m^2-h but a rapid decrease was reported in few hours, followed by a gradual permeate flux decreased up to the day 32. The researchers were able to restore permeate flux after conducting a chemical cleaning, using different strategies including distilled water, sodium hypochlorite, citric acid and HCl [Li et al, 2010].

2.7 Operation, Maintenance and Cost estimate

The commercial technology of MD is in an early stage, and a reasonable first step is to produce working, reliable membrane modules [El-Bourawi, et al; 2006]. Capital costs and operation cost are hard to estimate due to lack of experience and uncertainty. Walton et al. claimed that when fully developed, MD should be significantly lower in capital and operational expenses in comparison with RO [Walton et al; 2004]. Assuming the capital cost of AGMD facility is 0,375 $\$/m^3$, the total cost was made as a function of thermal energy cost; and found that MD is only competitive relative to reverse osmosis when low cost heat energy is available and/or when the water chemistry of the source water is too difficult for treatment with reverse osmosis [Walton et al; 2004].

Liu and Martin [2005] investigated a small-scale commercial AGMD demineralization plant for water production in thermal cogeneration plants. Data obtained from relevant experimental trials was scaled up to illustrate the performance of a 10 m^3/h unit supplied with heat either from the district heat supply line or low-grade steam. Heat and mass balance calculations show that the specific thermal and electricity demands lie around 4,0-5,0 kWh/m^3 and 1,5-4,0 kWh/m^3, respectively. (Thermal energy consumption was very low due to the fact that the district heating return line was used as the coolant; hence this heat was recovered by

the cogeneration facility.) Economic estimates place the cost of de-mineralized water production in the range of 10-14 SEK/m^3 (1,43-2,00 \$/m^3) excluding pretreatment [Liu and Martin; 2005].

A new AGMD technology, Memstill®, has been reported [Meindersma et al, 2006]. The projected cost for a seawater desalination capacity of 105,000 m^3/day was compared with RO. The authors estimated the total water costs with the Memstill® process as low as \$0,26/m^3.

In another study with a DCMD plant; assumption made on production rate of 4000 m^3/day and recovery rate of 30%. The capital and operation cost were assumed the same for a similar capacity RO desalination plant. The total production cost of water by DCMD process was estimated to be around 0,74 \$/m^3 [Sirkar and Li, 2004].

Al-Obaidani et al [2008] carried analysis on four different DCMD configuration adopting PP membranes. Feed solutions for the tests were aqueous NaCl solutions at concentration of 35 g/l. Exergy analysis, sensitivity study and economical evaluation were carried out to assess the feasibility of DCMD process. The researchers estimated the water cost for DCMD with heat recovery, to be \$1,17 per m^3, which is comparable to \$1,00 per m^3 water produced by multiple effect distillation (MED) and \$1,40 per m^3 for multi-stage flash (MSF). According to their conclusion, significant savings can be expected when using a low-grade thermal energy source, approaching the water cost for Reverse Osmosis [Al-Obaidani et al, 2008].

2.8 Comparative Analysis

In practical applications of the membrane distillation processes the most important and crucial issue is heat efficiency, which determines unit design and, eventually, the operating parameters. The process design should be optimized, taking into account various system schemes and costs factors [Kubota et al, 1988]. Choosing the optimum MD system is a process that starts with defining the application (the aqueous solution that is needed to be treated), the suitable MD configuration (i.e. DCMD, AGMD, VMD or SGMD), membrane material and its characteristics, and finally the operational conditions. In parallel, the pretreatment and/or fouling/scaling measures must be chosen carefully with regard to the composition of the feed water, membrane material and operation condition.

Choosing the suitable MD configuration depends on the type of aqueous solution to be treated and also, on the application in term of heat efficiency and heat recovery. It is known that the AGMD is more thermally efficient since the air gap reduces the conductive heat loses through the membrane solid matrix. The penalty of the air gap comes from the fact that it imposes additional resistance to mass transfer resulting of lower fluxes compared with other configurations.

Optimizing the operation conditions depends mainly on the source of energy utilized and the potential of maximizing the heat recovery. Other factors like fouling and scaling are important as well in determining the operation conditions, as they are partially dependent on the operating temperature and flow rate. It must be noted that optimizing the operation conditions for all-ready manufactured MD unit depends on the thermo-physical aspects and hydrodynamic conditions; and can be done iterative process.

With focus on the operational conditions, initially it seems favorable to operate with high feed temperature since the flux increases exponentially with temperature. However, it should be noted that the temperature polarization effect becomes more significant at higher temperature, though the overall heat consumption in terms of energy per unit distilled is higher. Another advantage comes from the fact that high feed temperature reduces the potential for biological fouling. On the other hand, scaling becomes more crucial at higher temperature especially with salts having inverse solubility. Decreasing the temperature polarization effect can be achieved by operating at turbulent flow regime either by increasing the flow rate and/or including turbulent promoters.

Choosing the low feed and cooling flow rates is favorable in systems where the heat recovery is crucial (e.g. solar powered MD). Moreover, lower flow rates reduce the electrical power consumption and enhance the overall energy efficiency. On the other hand, lower flow rates have negative effect of increasing the temperature polarization effect which tends to reduce the permeate flux. Lower flow rates has a disadvantage of increasing the potential for particulate fouling, though the resulting temperature polarization effect may help in reducing the scale formation due to the lower temperature at the membrane surface in comparison with the feed flow channel.

When operating with both high temperatures and low flow rate, the built up temperature polarization effect becomes more significant, and hence more attention is needed to optimize the those parameters taking not only the boundary layer formation, but also their effect on fouling and scaling. In such case, it is crucial to maintain a sufficient actual trans-membrane temperature difference to the drive the separation process in the first place and to minimize the expected penalty of resulting increased membrane area. Turbulence or mixing promoter is highly preferred to minimize the boundary layer effect and reduce the potential for particular fouling. Taking in account the high potential for scaling, a good pre-treatment system and scaling control measure is mandatory. Moreover, deaeration is quite significant in such case to reduce the mass transfer resistance. Though such effect could be small in small size membrane pores, it is still considerably significant in relative terms; and may be simply applied by lowering the feed pressure.

2.9 Background of semi-commercial air gap membrane distillation used in the study

The Air Gap Membrane Distillation (AGMD) module (Figure 2-3) consists of 10 cassettes with a total membrane area of 2,8 m^2. The size of module is 63 cm wide and 73 cm high with a stack thickness of 17,5 cm. The cassettes are designed so that they can be stacked together to form modules of varying size. The module is a property of SCARAB Development AB.

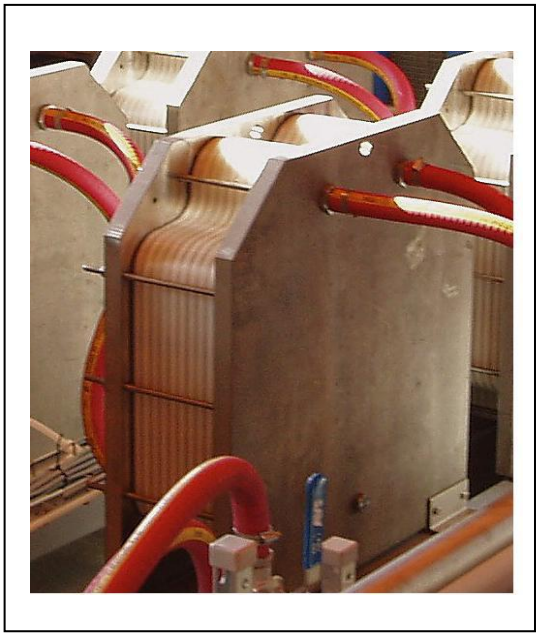

Figure 2-3: Picture of AGMD module

Each cassette consists of injection molded plastic frames containing two parallel membranes, feed and exit channels for the warm water, and two condensing walls. By interconnecting the cassettes, channels for the cooling water are formed between the condensing walls of adjacent cassettes. The membrane material is Polytetrafluoroethylene (PTFE) with a porosity of 80% and thickness of 0,2 mm. The width of the air gap is 1 mm.

The module has different operating parameters and restrictions that need to be accounted for during operation and in the design of production system. The main operating data are summarized in the following table:

Table 2-2 : Operational data.

Operation parameter	Specification	Remarks
Warm water flow, one module, nominal	Range (5-20 l/min)	Recommended 15-20 l/min
Cold water flow, one module, nominal	Range (5-20 l/min)	
Product water flow, one module, nominal	20- 50 l/h (temp dependent)	
Warm water operation temperature	40 – 95 ºC	Recommended >60 ºC & <90 ºC
Cold water operation temperature	20 – 40 ºC	
Temperature drop per pass	3,5-10 ºC	
Recommended Temperature difference	20 ºC	Temperature difference between feed and cooling inlets
Pressure drop per module per pass	0,02-0,1 (bar)	Tested value 0,02-0,04 (bar)
- Max operating pressure in system	300 kPa	
- Design pressure	600 kPa	

3 MEMBRANE DISTILLATION APPLICATIONS IN THERMAL COGENERATION AND SOLAR DRIVEN DESALINATION

This chapter includes the results of employing membrane distillation in thermal cogeneration (Värmeforsk research M06-611) and solar driven desalination (EU MEDESOL research project 036986).

3.1 Membrane Distillation and Applications for Water Purification in Thermal Cogeneration Plants (Appended Paper I)

This research is a continuation of a previously conducted theoretical study where the performance of MD-based water treatment was explored via laboratory testing, system simulations of thermodynamic performance, and economic evaluations.

3.1.1 Background

Thermal cogeneration plants require purified or treated water for a number of processes, i.e. boiler/district heat make-up water systems and flue gas condensate treatment. The selection of the exact water treatment process is of course dependent upon the final water quality along with the volume of water to be treated. Membrane-based technologies are an important component in such systems as they have been developed to meet the needs of the power generation industry. While such methods are well established and generally effective, there is still room for improvement regarding economy and enhanced water purity. In this context membrane distillation is a unit operation that deserves more attention as a promising alternative or complementary technology for water treatment in cogeneration facilities.

The need to purified water in thermal cogeneration plants can be addressed in a number of processes. **Make-up water and steam cycle water** require high quality water. A number of processes can be used depending on the particular requirements; softened water is used for hot water boiler while desalinated water (including softening, carbon adsorption, ultra filtration, reverse osmosis, and ion exchange) is used for both hot and steam boilers [Axby; 1998, 2004]. **Feed water/make-up water treatment in district heating networks:** here water quality should be relatively high in order to avoid corrosion in piping and heat exchangers, though the quality demand is slightly lower than for steam cycle water. Ammonia removal is an important factor as it causes corrosive damage to the copper and brass, which are common materials for valves in district heating networks [Axby; 1998]. **Flue gas condensate:** in this case treatment is more complicated and is highly dependent upon the fuel characteristics. There is significant interest to clean up effluents from flue gas condenser plant for the following reasons [Goldschmidt; 2009]:

- Better NOx capture
- Fuels containing heavy metals can be burned without emission levels being exceeded
- Recycling of treated condensate

In 2004 Värmeforsk (Thermal Engineering Research Institute) commissioned a pre-study in order to examine the potential of MD water purification for cogeneration applications [Liu and Martin; 2005]. Specific elements of this work included a literature survey, theoretical considerations of heat and mass transfer, and scale-up of experimental results for a case study involving a 10 m^3/h water treatment system. Results showed that MD is a promising alternative to membrane based treatment systems in existing or new treatment facilities. The most favorable results were obtained for alternatives where either the district heat supply line or low-grade steam is available. Specific energy consumption ranges were reported as follows: 4-5 kWh/m^3 thermal; and 1,5-4,0 kWh/m^3 electrical.

The purpose of the research highlighted in this section is to compliment the theoretical work performed in the previous Värmeforsk study with pilot-plant trials at Idbäcken Combined Heat and Power (CHP) Facility. Specific goals include the following: obtain long-term experimental performance data for product water quality for both municipal water and flue gas condensate feedstocks; and to observe any possible tendencies for performance deterioration (like leakage or fouling) under realistic operating conditions.

3.1.2 Experimental work

3.1.2.1 Test facility and plan

The test facility (Figure 3-1) comprises five AGMD modules connected in three parallel cascades. Each cascade (except the third) consists of two modules connected in series. Each module consists of 10 cassettes and the total membrane area for one module is 2,8 m^2. Details of the AGMD module is described in section 2.9.

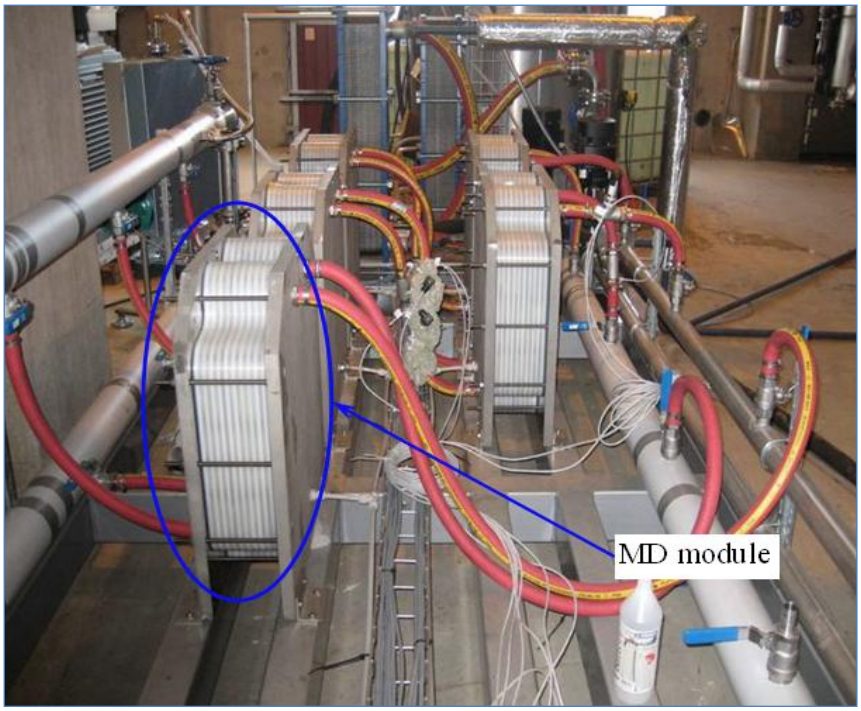

Figure 3-1: Test facility at Idbäcken Cogeneration Facility (Nyköping).

System control and primary data acquisition were handled via PLC connections to Citect Runtime software installed on a standard PC. A separate data logger recorded interstage inlet/outlet temperatures and inlet/outlet pressures. Flow rates were measured by visual flow meters (accuracy ± 5%), temperatures were measured by Pt 100s (accuracy 0,2%) and pressure with pressure transmitters (accuracy 0,25 %). On site conductivity measurements were also introduced to check the instant bulk quality of the product water. Product water yield was determined manually. A de-gassing unit is connected to the facility but failed to function properly during the test period. Operational temperatures were kept at 70° C for hot (feed) side and 15° C for cold (cooling) side. Flow rates were identical for both sides and ranged from 300 liters/hour to 1050 liters/hours.

Testing was divided into three phases: (1) parametric study of yield with municipal water as feedstock to validate previously tested performance of MD module; (2) long term operation with municipal water as feedstock; and (3) evaluation of flue gas condensate treatment as feedstock. The second phase aimed at testing the facility for long term performance (continuous operation) for around one month. During the first ten days of operation, the MD facility was operated continuously without a major disturbance noticed. However, by the 13th day a 20% reduction in permeate flow rate was observed (described in section 5.1.2.1) coupled with an increase of pressure at the feed inlet along with a lower flow rate. By the end of the test period, the permeate flow rate reduction reached a level of 32%. During this phase, a sample of the product water was taken and analyzed.

The third phase was conducted by testing one of the modules with flue gas condensate as a feed stock. This phase was done on two separate days. Samples of the product water and the raw flue gas condensate were taken and analyzed. The total accumulated run time for facility was around 500 h covering the three phases.

3.1.2.2 Test results and discussion

3.1.2.2.1 Production Flow rate and Quality: Municipal Water Feedstock

The parametric study included mainly running tests with variable feed flow rates ranging from 300 to 1050 l/h for one cascade (i.e. two modules connected in series). Figure 3-2 shows the relation between the feed flowrate and permeate flow rate. Different points must be stated here. First, the curve is drawn for two units connected together in which the feed outlet for the first is used as a feed in the second. At high flow rates (1050 l/h) the second stage produces about 35% of the total product output, while at low flow rates this stage is virtually non-functioning. It is well known that low flow rates results in larger thermal boundary layer, i.e. larger temperature polarization effect [El- Bourawi et al; 2006]. Such effects result in a lower membrane surface temperature compared to the bulk temperature in the flow channels within the module, and hence lower trans-membrane temperature difference and lower permeate flow rate. Moreover, the large temperature drop exhibited at low flow rates causes the permeate flow rate in subsequent stages to drop significantly. Previous findings available in the literature reported a linear increase in permeate flow rate enhancement with higher feed flow rate [Alklaibi and Lior; 2004, El- Bourawi et al; 2006], and the present results largely follow this trend.

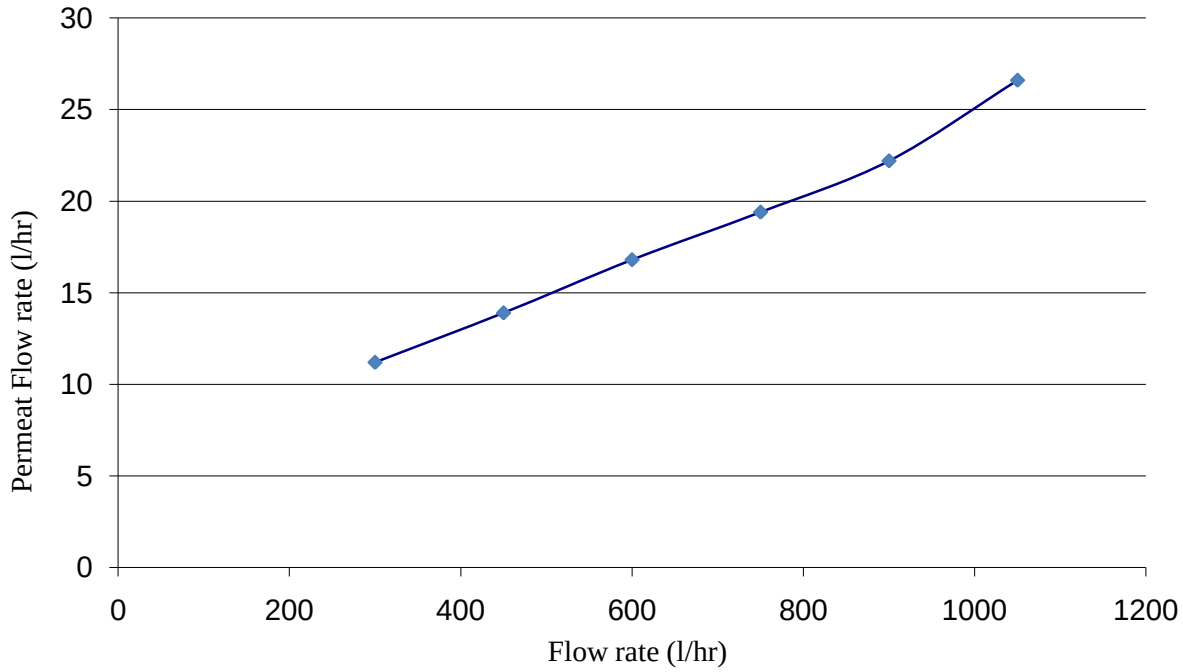

Figure 3-2: Water production for one cascade at various flow rates (70 ºC feed temperature and 15 ºC cold water supply temperature; cold water flow rate approximately the same as the feed flow rate).

A noticeable decay in permeate flow rate was noted during the second phase of testing, around the 13th consecutive day of operation (corresponding to around 370 cumulative hours of operation including the initial start up test). Approximately 20% reduction in product water flow rate was recorded, coupled with an increase of pressure at the feed head along with a lower flow rate. Thereafter the test could not be run on a 24-hour mode and was thus replaced by daily operation (8 hours continuous under supervision). At this point inlet pressure levels on the hot feed side began to rise, triggering membrane overpressure alarms that had to be handled manually). By the end of the test period, the permeate flow rate reduction reached a high level, over 30% and the first stage (modules 1, 3 and 5) had a very low product water flow rate, roughly half that measured in the beginning of the test. Figure 3-3 shows the decay of permeate flow rate by time. The data were not recorded daily, since the first speculation was that problem caused by the clogging of the micro flow channels with accumulated solid particles, and the main efforts was on trying to flush the system with deionized water to clean these micro channels with no success.

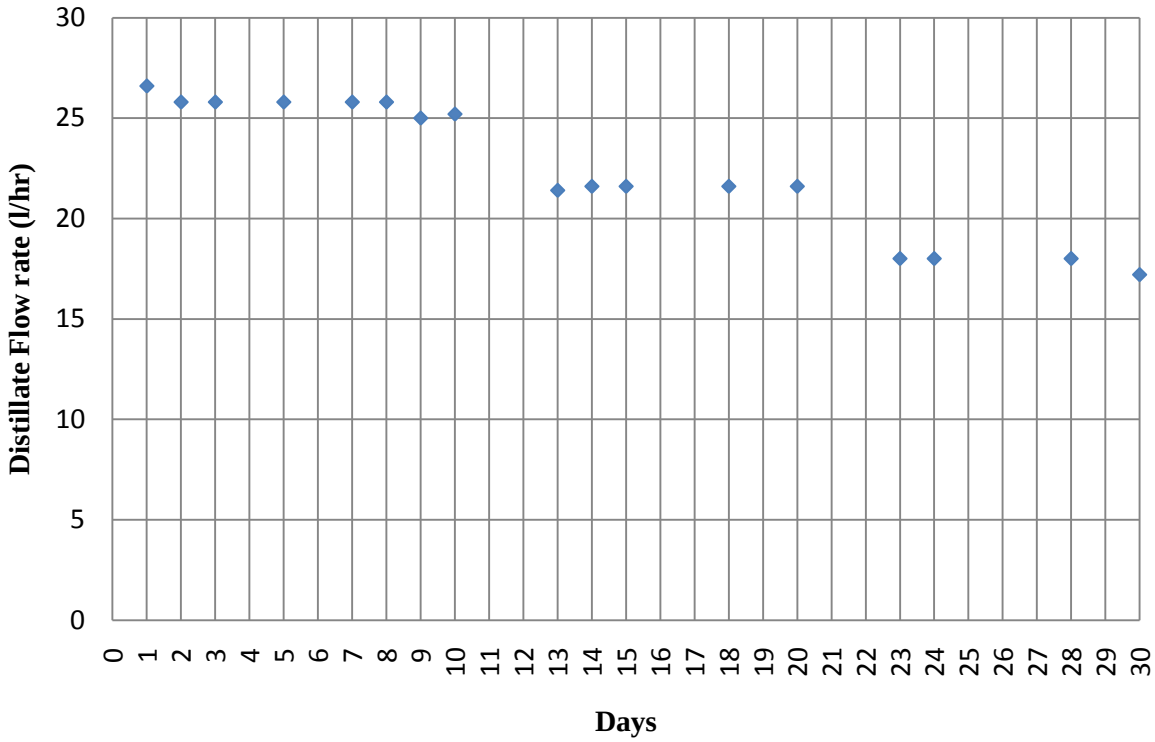

Figure 3-3: Permeate flow rate decay Vs time (two modules).

Shortly before the end of experiments (day 24), a light brownish color of the feed water in the tank was observed and it was attributed to contamination by dust and dirt from the open environment (the site where the facility was installed contained many airborne contaminants). However, a further investigation supported the assumption that the modules were subjected to scaling which caused a reduction in the flow passages and/or reduction on the membrane area available for evaporation.

The pressure drop measurement was important to consider in the study, since electrical energy consumption is directly linked to this. The measured values over one module ranged from 0,02 to 0,04 bar, corresponding to a flow rate range of 300 to 1200 l/h. Table 3-1 contains water analysis results obtained in the early phase of testing. Here SiO_2, Na and conductivity were selected as quality indicators, which is typically the design basis for a water treatment plant in cogeneration facilities. Comparisons are also made with the feed water as a base line. The bulk quality indication, represented by conductivity, shows high separation efficiency. Product water conductivities were around 1,5 µS/cm for most of the samples. Most of SiO_2 and Na levels were below the detection limit in the product water obtained from module 1, where a slightly higher level is presented. However, on-line conductivity checks did not reveal a different behavior for this module compared to the others, and the possible explanation for this irregularity is probably due to contamination during sampling. These results are favorable in respect towards meeting water quality guidelines for some process in cogeneration facilities. For instance the following limits have been recommended for boiler and steam in steam turbine cycles [Hellman; 2006]: SiO_2 < 5 µg/kg (≈ 5 µg/l); Na < 3-5 µg/kg (≈ 3-5 µg/l); and conductivity < 3-6 µS/cm (ammonia dosing for pH control).

Table 3-1: Water analysis for each module's product water

	SiO_2(µg/l)	Na (µg/l)	Conductivity (µS/cm)
Feed Water	5000-10000	17500	467
Product water			
Module 1	6	14	1.6
Module 2	≤ 5	≤10	1.5
Module 3	≤ 5	≤10	1.6
Module 4	≤ 5	≤10	1.4

Table 3-2 represents a more comprehensive analysis for the cations and anions in the MD product water sample collected. Analysis methods are detailed in the appendix. As stated previously, permeate flow rate decay was observed during this phase. The results shown below are for one sample collected after the permeate flow rate deterioration (day 23). Most of the elements are below the detection levels and others are slightly above, and comparable to results in Table 3-1. Sodium (Na) is considerably high compared with the cut-off represented in the previous analysis. There is no clear explanation that can be given in this case, although an error in chemical analysis could have occurred.

Table 3-2: MD product water analysis, municipal feedwater

Parameter	MD Product	Unit
Ca	0.297	mg/l
Fe	<0.004	mg/l
K	<0.5	mg/l
Mg	<0.09	mg/l
Na	0.175	mg/l
S	0.337	mg/l
Al	4.67	µg/l
As	<1	µg/l
Ba	<0.2	µg/l
Cd	<0.05	µg/l
Co	0.105	µg/l
Cr	<0.5	µg/l
Cu	<1	µg/l
Hg	<0.02	µg/l
Mn	<0.2	µg/l
Ni	2.55	µg/l
Pb	<0.2	µg/l
Zn	<2	µg/l
Chloride	<0.60	mg/l
Sulfate	<0.50	mg/l
Ammonia	<0.025	mg/l
Alkalinity	1.4	mg HCO_3/l
pH	5.9	
Conductivity	<1.0	mS/m

3.1.2.2.2 Production Test With Flue Gas Condensate as Feed stock

Flue gas condensate tests were conducted on two separate days mainly to confirm the results (day 28 and 30). The bulk quality of the product was checked via the on-site conductivity meter. The raw flue gas condensate was filtered with a 5-micron filter to remove larger particles. Product water flow rates recorded in this phase was similar to the one recorded at the end of phase two, when fouling effects were noted. Since the modules were affected by the scale, it was not possible to obtain more detailed measurements for long period of time. However, the main aim was to evaluate the separation efficacy and product water quality.

Water analysis of the raw and treated flue gas condensate is presented in Table 3-3. It can be seen that Na level is considerably high in the raw flue gas condensate, along with heavy metals (mainly Pb and Zn), high presence of chlorides, sulfate, ammonia and alkalinity. It must be noted that the flue gas condensate used in the test was simply filtered; typical pretreatment steps for flue gas condensate treatment plants would include sand filtration, volatile stripping, and pH adjustment [Axby; 2004].

Table 3-3: Analysis of raw and treated flue gas condensate

Parameter	Raw condensate	MD Product	Reduction (%)	Unit
Ca	35.0	<0.2	>99%	mg/l
Fe	0.0268	<0.004	>85%	mg/l
K	3.59	<0.5	>86%	mg/l
Mg	4.28	<0.09	>98%	mg/l
Na	902	1.27	99,90%	mg/l
S	60.6	0.274	99,50%	mg/l
Al	89.4	5.98	93,30%	µg/l
As	25.7	<1	>96%	µg/l
Ba	55.3	<0.2	>99,6%	µg/l
Cd	0.910	<0.05	>94,5%	µg/l
Co	0.422	0.105	75,10%	µg/l
Cr	3.21	<0.5	>84%	µg/l
Cu	32.7	<1	>96,9%	µg/l
Hg	5.64	<0.02	>99,6%	µg/l
Mn	28.6	<0.2	>99,9%	µg/l
Ni	7.20	1.62	77,50%	µg/l
Pb	46.0	<0.2	>99,6%	µg/l
Zn	387	<2	>99,5%	µg/l
Chloride	1490	1.5	99,90%	mg/l
Sulfate	168	<0.50	>99,7%	mg/l
Ammonia	115	49	57,40%	mg/l
Alkalinity	225	180	20%	mg HCO3/l
pH	8.4	8.7		
Conductivity	525	23.3	95,60%	mS/m

After treating the flue gas condensate in the MD facility, a quick check with the on-line conductivity meter showed high readings, up to 28 mS/m (280 µS/cm). The analysis of the product water indicates that such high conductivity was a result of volatile ammonia passing through the membrane and presence of alkalinity (HCO_3). However most problematic metals were successfully removed and their concentrations were below the detection limits. Sodium and chloride ions were quite high and exceeded the recommended values for boiler feed water

In future applications, membrane contactors or CO_2 stripper can be used for pretreatment to remove CO_2 which forms alkalinity. Ammonia stabilization by pH reduction (below 6) could be used in pretreatment as well, and then retained in the reject solution at the MD stage.

5.1.2.1 Scaling observed

As mentioned previously, scaling was encountered during the test period. The effect of scaling on the permeate flow rate was noticed clearly after 400 h of operation and had led to significant decay. However, one can say that scale was building up during the whole process. Factors like several shut downs and interruptions would be assumed to boost the process. No pretreatment or scale control measures were taken during the test period. Moreover, no rinsing (with acids) was conducted after the first test break.

First stage modules were more adversely affected by scaling as compared to second stage modules owing to higher operational temperatures. The second stage modules were subjected to feed flow with temperature ranging from 60 to 55 °C. In order to understand the mechanism of scaling in this particular module type, Module 1 was disassembled and inspected. Figure 3-4 and Figure 3-5 show the scale formation at the feed inlets of each cassette of the module and at the distribution channels inside one of the cassettes, respectively. The scale formation at the feed inlets was building up as finger-like crystals on the inlet openings causing a partial or total clogging. Inside the cassettes, the scale formed as loose flakes which accumulated and clogged the distribution channels. On the membrane surface, the scale layer was gradually decreasing with the length of the membrane flow direction (corresponding to change in tangential temperature decrease). On average, the scale layer covered one third of the membrane surface, while the rest of the membrane was free from significant deposits. The scaling pattern on the membranes gives an assumption of how the mass transfer takes place. Since the scale is dominant on the upper part where the highest temperature is expected, it is most probably in this region major part of the mass transfer of vapor takes place. The high presence of scale flakes in the flow distribution micro channels, and the fact that no permeate flow rate or quality decay was observed before the high pressure was recorded, suggest that scale was built up first in these micro channels. The resulting clogging of the flow micro channels reduced significantly the feed flow rate and hence, increased the rate of scale building on the membrane surface subjected to the higher temperatures around 70 °C (the upper one third). These findings highlight the importance of flow channel detailed design in industrial scale membrane distillation in relation to scale formation control.

Figure 3-4: Scale formation at the cassette entrances

Figure 3-5: Scale formation blocking the cassette flow channels

.

The content of the scale flakes was analyzed by the energy dispersion spectrometry (EDS) (Figure 3-6). The major ion found was Ca indicating the $CaCO_3$ scale, which is the most experienced one in running with tap water. Other elements such as Fe, Mg and S were also presented with a very low level though it is suggested that the light brown color of scale was due to Mg and Fe_2O_3. In practical operation, a softener could be sufficient to control such scale.

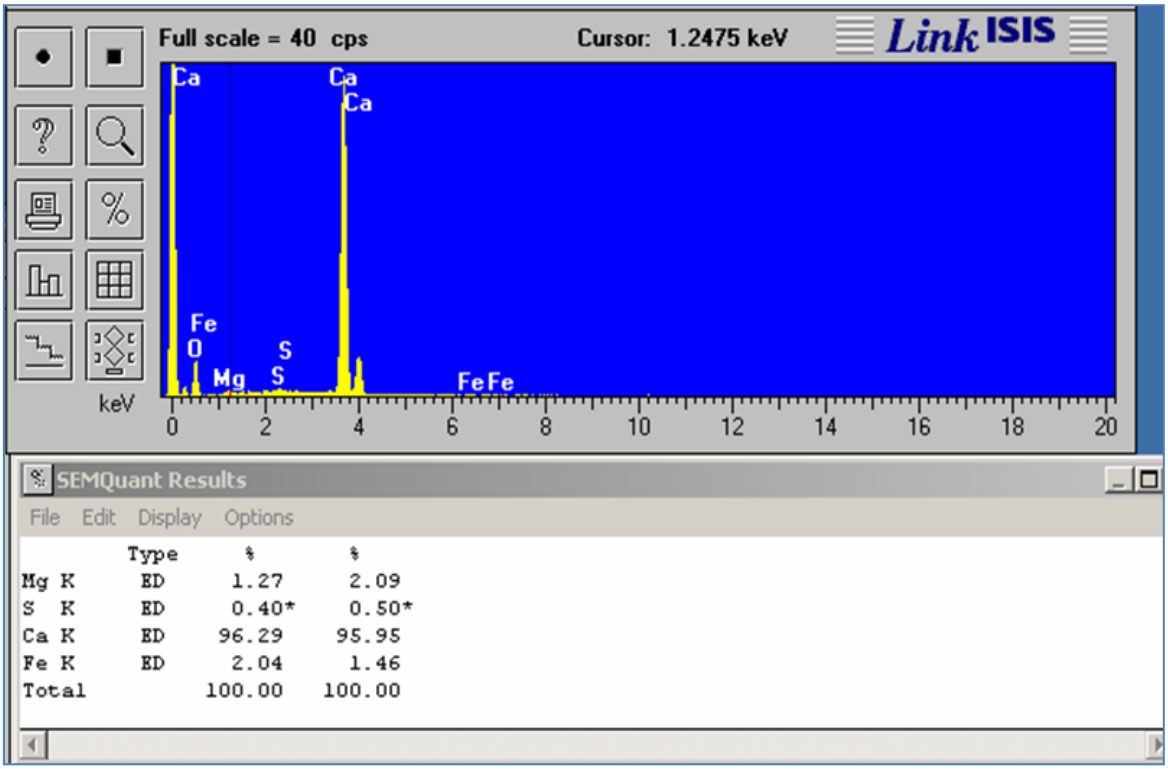

Figure 3-6: EDS spectrum of elements detected in sample of the scale content

3.1.3 Full-scale simulation

In order to understand the results in a large-scale production scheme, the MD facility is assumed to be connected to the district heating network, where the heating is supplied by the district heating supply line, and the cooling is provided by the district heating return line. The thermal energy consumption is thus calculated based on the difference between the supplied heat and the heat added to the sink. Figure 3-7 illustrates a simplified scheme of the layout.

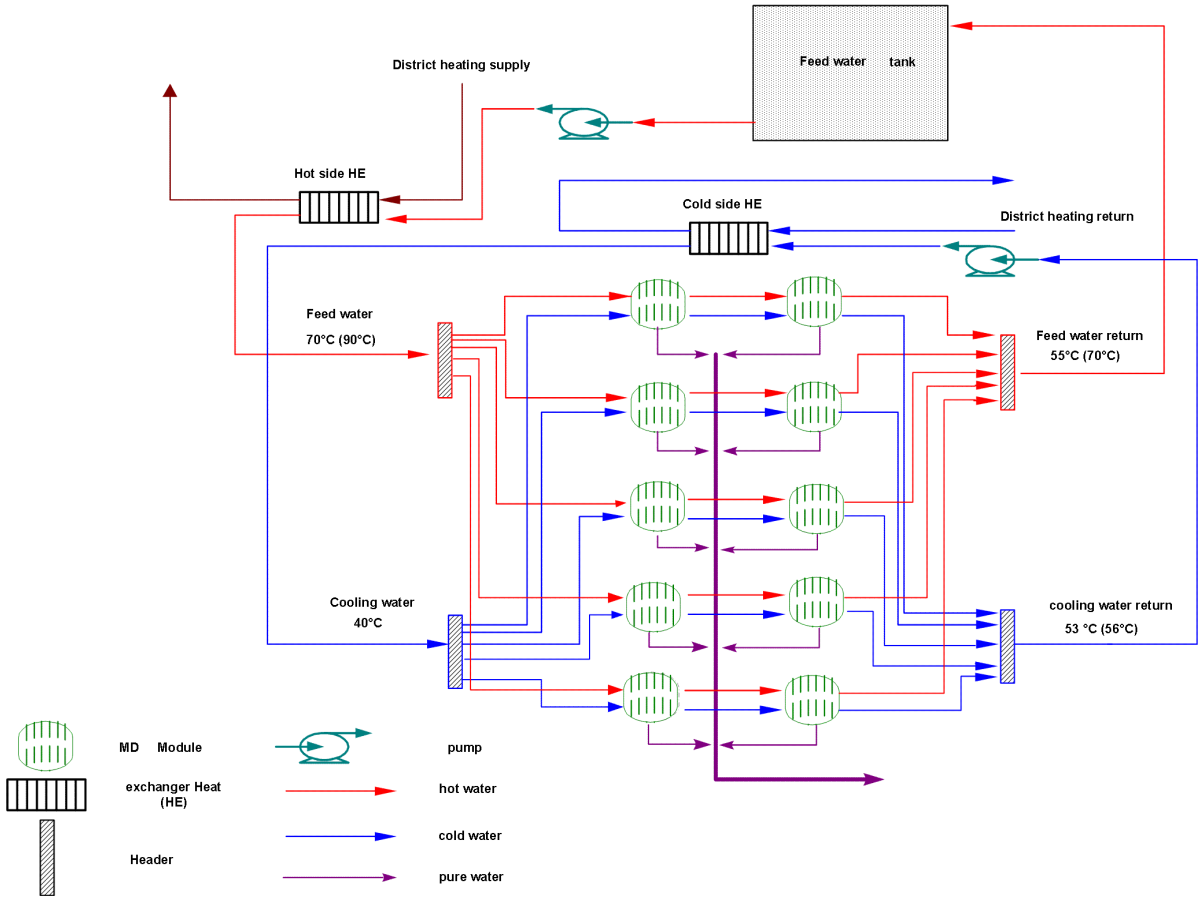

Figure 3-7: Simulation layout

The feed water temperature (assumed to be supplied by district heating supply) was chosen to be either 70 or 90 ºC based on different possible district heating operation conditions in different cogeneration plants. The district heating return line temperature is assumed to be 40 ºC. The assumed flow rate is chosen to be 1200 l/h per cascade, and the targeted production rate is 10 m^3/h. Numerical model describing AGMD developed by Jönsson et al [1985], was modified based on the experimental results (including previous ones) to include the effect of thermal boundary layer effect and heat losses to the environment. Aspen Utilities® was employed as the simulation software tool, and the other major assumptions are included in the prestudy done by Liu and Martin [2005].

Table 3-4 presents the simulation results for hot side feed temperatures of 70 and 90 ºC.

Table 3-4: Simulation results

Parameter	Case I	Case II
Cascade flow rate (l/h)	1200	1200
MD hot side temperature (°C)	70	90
MD cold side temperature (°C)	40	40
Pure water output (m^3/h)	10	10
Specific thermal energy consumption (kWh_t/m^3)	5,5	12,1
Specific electricity consumption (kWh_e/m^3)	1,3-1,5	0,6-0,7
Membrane area (m^2)	2392	1141

It is clear that the best results in terms of efficient membrane use are obtained with higher feed water temperatures. Reducing the area of the membrane and subsequent number of modules used is crucial since they comprise the most expensive part of the investment (around 40% of the total cost of the MD facility [Liu and Martin; 2005]). This is also true for the operational cost, since less MD modules means less maintenance cost. As shown in comparing Case I and II in table above, the thermal energy consumption is almost doubled if the operation temperature is raised from 70 to 90 ºC, while the specific electrical consumption is halved. The reason for this increase in the specific thermal energy consumption is due to the higher energy carried by the production flow rate and the relatively high level of heat lost to the environment (Heat loses by the module was included in the calculation as a varying percentage).

To compare these figure with other technologies adopted in flue gas condensate treatment, a rough estimate of 1,5 kWh/ m^3 for electrical energy consumption can be considered in a Reverse Osmosis (RO) system [Liu and Martin; 2005]. Based on the literature survey conducted during this particular study, there is no record of using similar thermal treatment process such as MED or MSF in this subject area, to compare results with. The cost of water for the system studied in Case II was calculated with a margin of safety/error (associated with lack established industrial scale experience) is 14-20 SEK/m^3 [Kullab and Martin, 2007].

3.1.4 Concluding remarks

The performance of MD concerning production rate is highly dependent on the feed stock temperature, flow rate and temperature difference across the membrane. The performance of the MD modules was stable for approximately 370 hours of continuous operation. However, after thirteen days of continuous operation, the first permeate flow rate deterioration was encountered. The reason for this was attributed to scale formation on the membrane cassettes feed inlets, flow distributors inside each cassette and the membranes upper half. Such scale caused a total or partial clogging for these channels/distributors/membrane pores, reducing the feed flow and hence the permeate flow rate. It must be mentioned that the MD modules were previously subjected to several discrete test periods which must be added to the operation

time. The main problem encountered during the long-time test was scaling due to the high content of hardness in the feedstock (Ca and Mg). This problem can only be overcome with some kind of pre-treatment. The most common way to deal with hardness is by using acid water softeners. Moreover, the mechanism of scale formation was also affected by the hydrodynamic conditions inside the module.

Though the permeate flow rate was affected by scaling problems, the permeate quality was stable over time and did not deteriorate. For municipal water feedwater (467 μS/cm) the product water conductivity was 1-3 μS/cm as measured on-site and lay below the detection levels in the sample analyzed at external laboratory. Important parameters like silica and sodium levels met the requirements for make-up water in boilers when running with municipal feed water. However, when running with the flue gas condensate feedstock, high conductivity level was recorded in the product water due to the presence of ammonia and alkalinity (measured as HCO_3). Also, some ions like Na^+ and Cl^- were present in the product water at relatively high levels. There is no specific known reason for that taking in consideration that the purification is evaporative process. However, since treating flue gas condensate took place after the scale formation, it is possible that such scale caused partial damage for the membrane's hydrophobic character. The performance of the MD unit concerning removal of heavy metals is encouraging.

Full-scale simulations were performed, based on the experimental results assuming that a 10 m^3/hr production capacity MD facility is connected to the district heating network. Specific thermal energy consumption ranged from 5 to 12 kWh/m^3, while specific electricity consumption ranged from 0,6 to 1,5 kWh/m^3 for two different scenarios.

3.2 Membrane Distillation: Experimental and Simulation of and Air Gap Membrane Distillation System for Solar Driven Desalination System (Appended Paper II)

The work included in this section, was carried out within EU MEDESOL project, which started in 2006, with aim of developing an environmentally friendly, cost-effective, low maintenance and easy to handle desalination technology driven by thermal solar energy. Within the project scope, and regarding MD modules part of the project, several experimental campaigns were carried out with different configurations (single module, two and three modules connected in series), and different operation modes (directly connected to solar field, temperature step-wise operation and combined operation mode). The experimental results from direct connection to the solar field were reported by the project partners [Guillén-Burrieza et al; 2011]. In the following sections, only step-wise operation on one module is covered. The aim was to establish an operation data base to be employed in a system simulation to design and evaluate a three-step MD desalination system.

3.2.1 Experimental work

3.2.1.1 Test facility and plan

The test facility was located in Plataforma Solar de Almería (PSA), Spain, and consisted of two independent hydraulic loops connected through a heat exchanger. The solar loop supplied the thermal energy and operated with RO treated tap water. The desalination loop operated with artificial seawater (NaCl) solution of varying concentration. The desalination loop consisted of two independent 2 m^3 fiber glass reinforced polypropylene tanks used as hot and cold water reservoirs. Feed solution was heated up passing through the heat exchanger and pumped into the MD unit/units where the desalination process took place. **Details of experimental set up can be found in Appended Paper II.**

Experiments were carried out during a two-week period. The main experimental work aim was to evaluate the MD performance with saline water of 35 g/l NaCl (similar to normal sea water salinity level. The salinity level was kept stable during these experiments by adding fresh water to the feed tank proportionate to the distillate production. Feed temperatures were kept stable during measurements ranging from 50 to 85 °C at three cooling temperature levels; 30, 40 and 50 °C. Feed flow rates for feed and cooling loops were kept stable at 20 l/min (the nominal flow rate) and each measurement was repeated three times to ensure the reliability. Several comparison measurements were taken at 45 and 60 g/l of salinity to establish a production versus salinity relations.

The membranes used were subjected to partial permanent damage after a previous long term experiments resulted from crystallization and dilution (during long shutdown periods and restart operation [Guillén-Burrieza et al, 2011] The conductivity of the distillate was ranging from 1 to 10 mS/cm depending on the distillate flow rate (the higher distillate, the lower conductivity) and feed concentrations. However, since the membrane leakage pattern was stable, it was possible to carry the experiment and correct the distillate flow rates.

3.2.1.2 Test results and discussion

Figure 3-8 shows the distillate flow rate at varying feed temperatures at different cooling inlet temperature. Feed and cooling flow rates were kept constant at 20 l/min and salinity was 35 g/l. The distillate flow rate for 1 g/l salinity is shown as well for comparison.

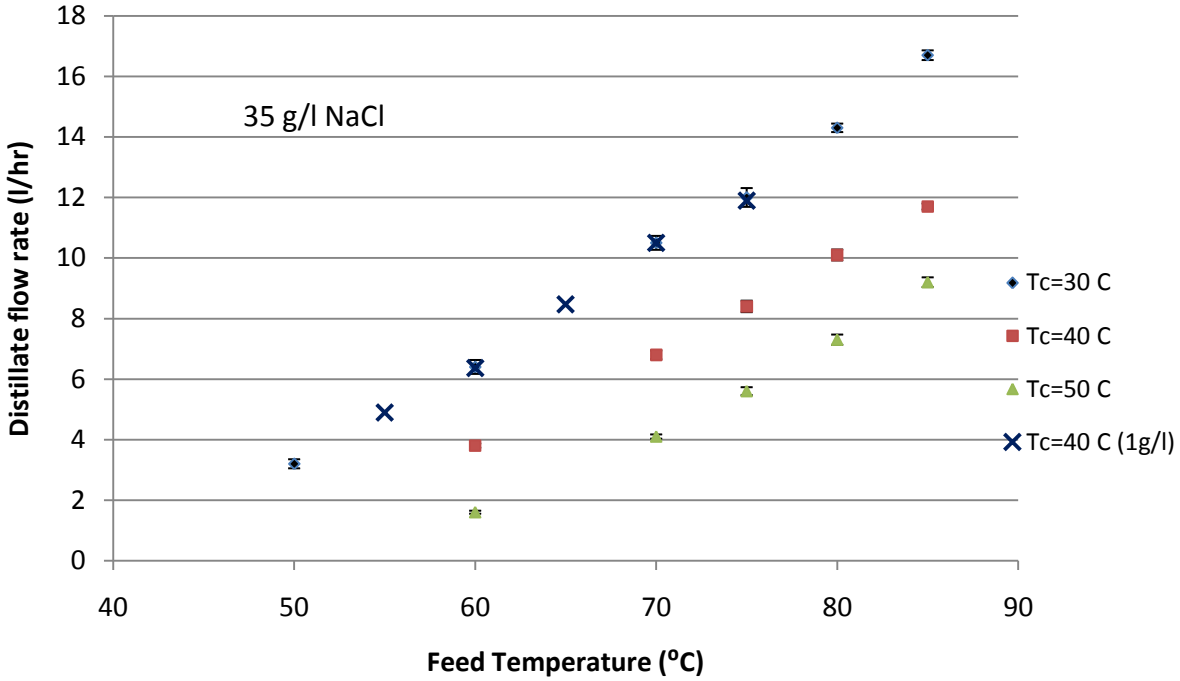

Figure 3-8: Experimental results for varying feed temperature at three different cooling inlet temperature (feed flow rate= 20 l/min; salinity 35 g/l and 1 g/l)

The results generally show a linear increase of distillate output as the feed temperature increases. As the theoretical curves should follow an exponential pattern, the linearity of the three plots highlights the effect of concentration boundary layer and thermal boundary layer in reducing the actual temperature at the membrane surface. Comparing the black plot with both red and green, indicate that the relative effect of concentration boundary layer increases and causing a lower slope of the plots. Such effect is demonstrated more clearly when the distillate output for 1 g/l solution at cooling inlet of 40 °C is added. Comparing the two plots of cooling inlet temperatures of 40 ^{0} C for 1 g/l and 35 g/l salinity, confirms the previous conclusion of salinity effect on the plot trend. Generally, the increase in salinity from close to fresh water up to close to sea water salinity level resulted in decrease in distillate output flow rate of 30-40 %.

Such level of distillate output reduction is generally higher than what was reported in previous literature [Alkalibi and Lior, 2004; Banat and Simandl, 1990; Schofield et al, 1990]. The difference is partially related to the difference in flow conditions (linear velocity) between the reported literature and this test. For example, Schofield et al [1990] reported a decrease of 10 % when the feed concentration was increased from pure water to sea water salinity feed. However, in their experiment, the flow regime was turbulent and linear velocity was 0,9 m/s; almost nine times higher than the one used in the test.

To assess the effect of salinity on distillate production, Figure 3-9 shows the distillate flow rate at 35 g/l, 45 g/l and 60 g/l salinity levels.

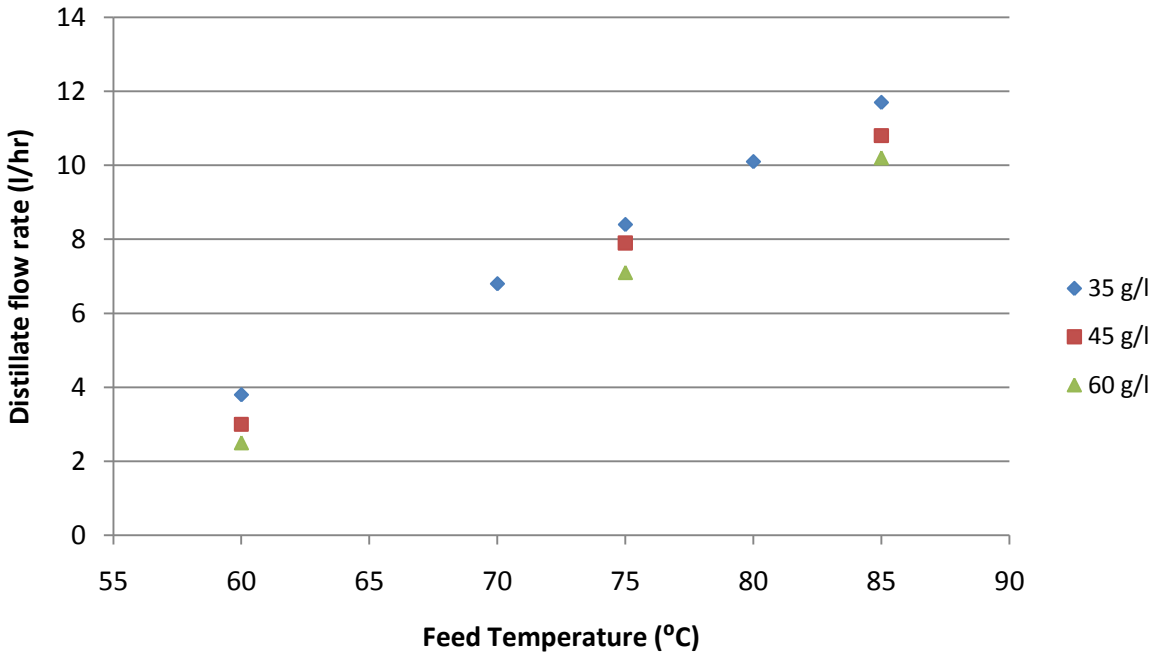

Figure 3-9: Experimental results for varying feed concentration (feed flow rate= 20 l/min; cooling temperature =40 ° C)

Results showed the previous figure confirms the previous finding of the poor hydrodynamic conditions in the feed channel. The reduction in distillate flow rate is relatively significant as the salinity increases. An increase of 30 % of salinity would generally result in a decrease of 10 to 20 % in distillate output.

To assess the thermal efficiency, performance ratio (PR) is a general parameter used to evaluate the thermal performance of thermal desalination processes. The PR indicates the amount of distillate (in kg) produced per each 2326 kJ of thermal energy supplied to the process to evaporate 1 kg of water at atmospheric pressure. As the MD module used for this experimentation was not designed to recover heat, PR values greater than one could not be expected. Figure 3-10 shows the development of PR in relation to the inlet temperature difference ($\Delta T=T_h-T_c$) for different feed inlet temperatures.

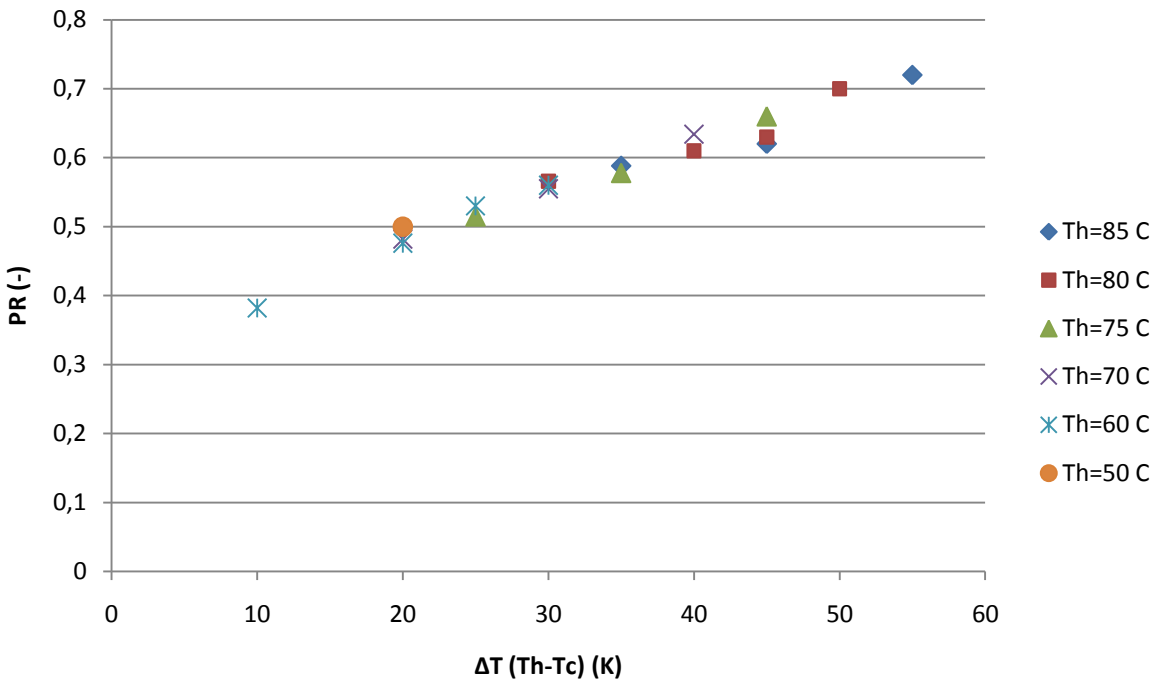

Figure 3-10: PR as a function of temperature difference at different feed temperatures (° C); (feed flowrate= 1200 l/hr & salinity 35 g/l)

Results confirm a linear increase of PR as the temperature difference increases. However, they show that PRs are slightly less for the same temperature difference as the feed temperature increases. This can be explained by the fact that as the feed temperature increases, the heat losses to the surrounding increases which reduces the energy efficiency of the module.

3.2.2 Experimental-based simulation of three-step MD system

Based on experimental results, computer simulations of a three step MD system were performed to evaluating two options to arrange the three single MD units; in a series mode in one layout, and rearranging the modules in the second one in order to recover part of the heat supplied to the system. Figure 3-11 and Figure 3-12 show the two simulation layouts. The simulations represent only the MD part and do not represent and actual system design that includes the solar field or thermal storage. Feed inlet temperatures varies from 85 °C to 70 °C at 5 °C steps, while cooling inlet temperature varies from 20 °C to 50 °C at 5 °C steps. Feed and cooling flow rates were kept constant at 1200 l/hr and feed salinity in the range 35 to 40 g/l.

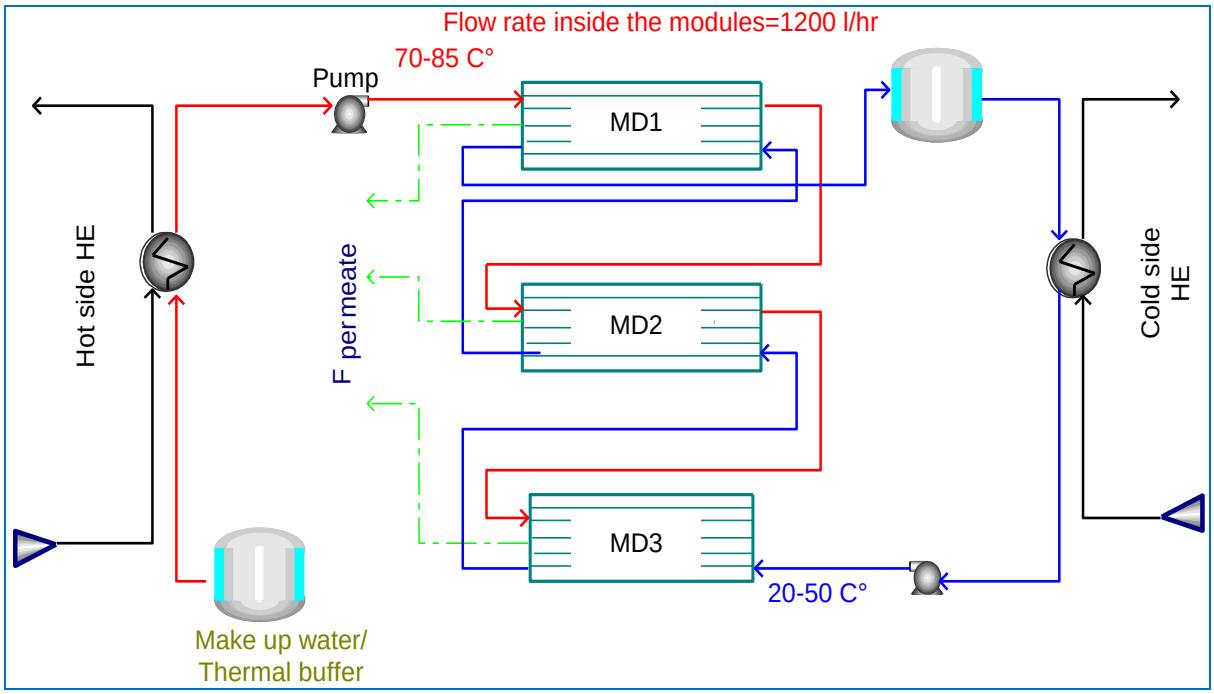

Figure 3-11: Simulation layout I

Layout I comprise of three MD modules connected in series where with feed and cooling circuits are in counter current flow mode. Layout II has the same number of MD units connected in series with the cooling outlet of MD1 is used as a feed inlet for MD3.

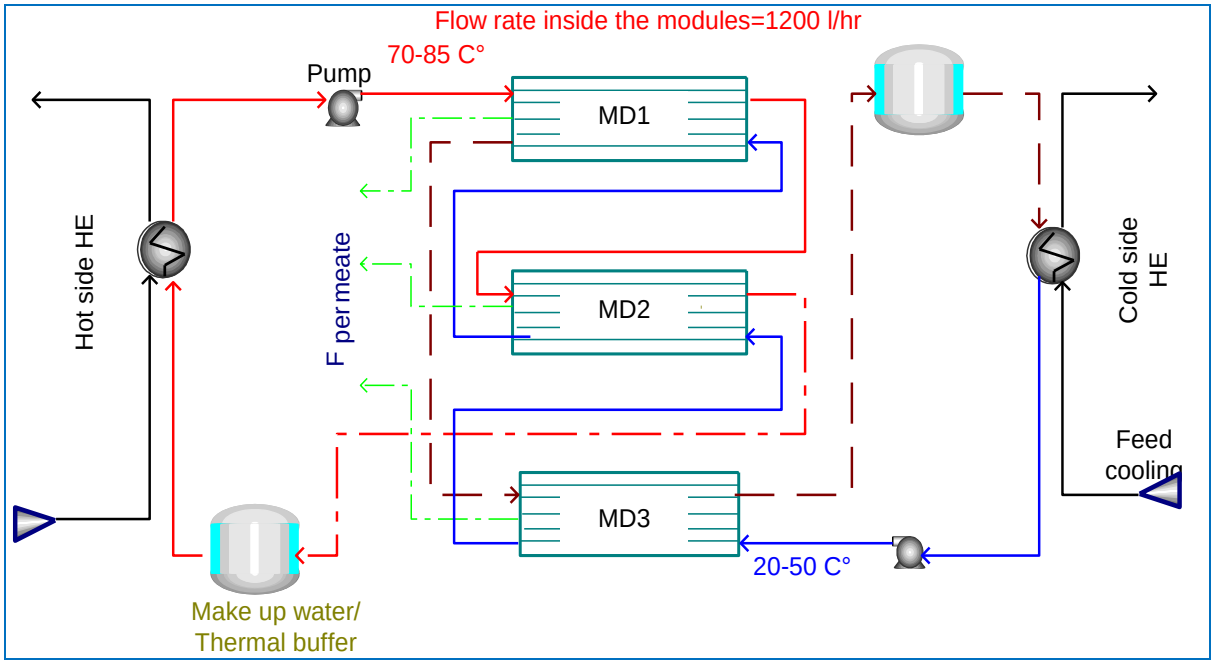

Figure 3-12: Simulation layout II

The results of the simulations are summarized in the following two figures, which show the total production and PR, respectively, for the two layouts (I & II), at different feed and cooling inlet temperatures.

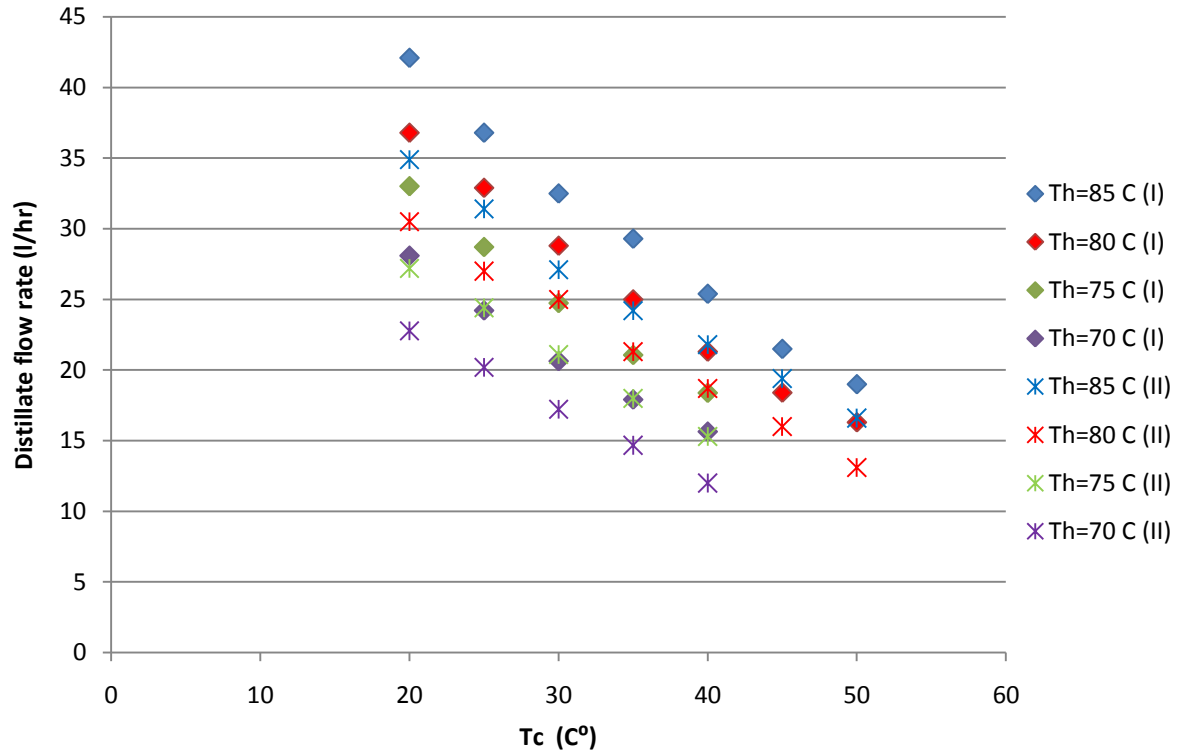

Figure 3-13: Total water production (for three MD modules) for the two layouts (I & II) at different feed inlet temperature Th (°C) Vs cooling water inlet temperature Tc (°C)

Figure 3-13 shows that the total water production (three MD modules with total of 8,4 m^2 membrane area) for layout I is higher by 10 to 20 % due to higher temperature difference available mainly in MD3.

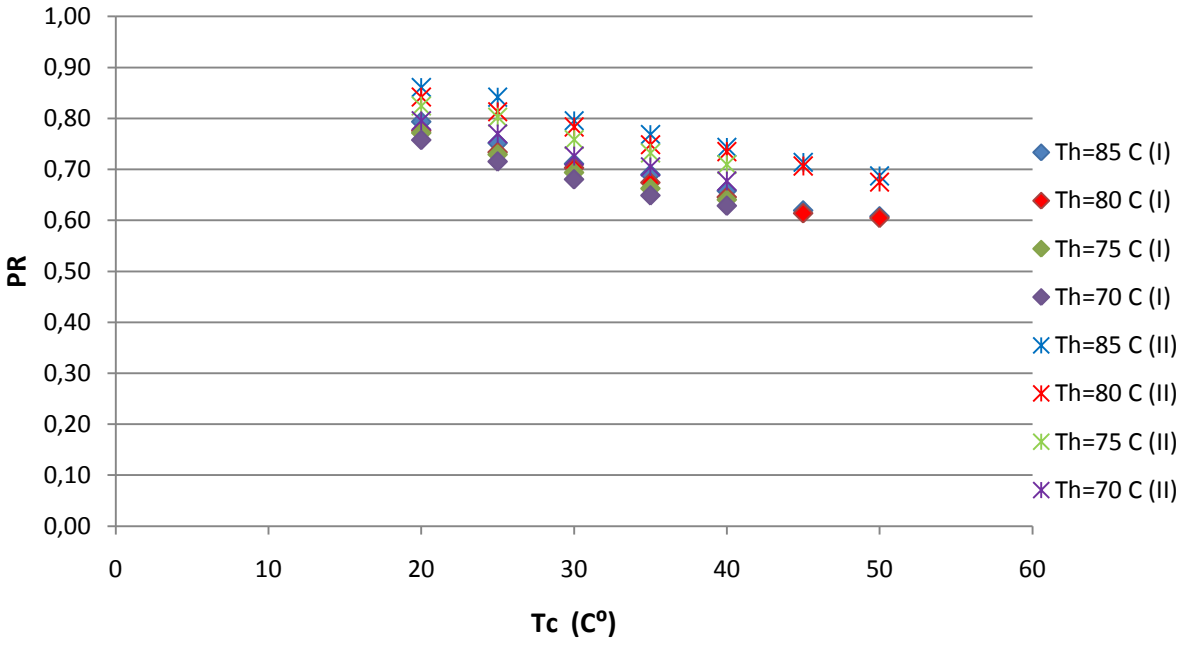

Figure 3-14: PR as a function of cooling water inlet temperature for different feed water inlet temperatures for the two layouts (I & II)

Figure 3-14 shows the PR for the three-Module-unit for both layouts. Layout II has a slightly higher PR compared to Layout I due the fact that part of the recovered heat in the cooling circuit was used as heat supply in one of the modules. However, the penalty was lower production as shown in Figure 3-13. The heat demand (from the solar field) in the layout II is lower by 20 % roughly, which make it a favorable option in such case of heat supplied by solar field. Specific thermal energy consumption for Layout I and II, were calculated as 950 kWh_t/m^3 and 850 kWh_t/m^3.

3.2.3 Concluding remarks

Experiments were carried out during a two-week period. The main experimental work aim was to evaluate the MD performance with saline water of 35 g/l NaCl (similar to normal sea water salinity level). The salinity level was kept stable during these experiments by adding fresh water to the feed tank proportionate to the distillate production. The distillate production was 30-40% less in the case of using 35 g/l salinity compared with 1g/l. Further decrease of 10-20% was noted when the salinity was increased by 30%. Experimental-based simulations of a three step MD system of two arrangement layout were employed to assess the system heat demand. Specific thermal energy consumption was calculated as 950 kWh/m^3 for the layout without heat recovery, and 850 kWh/m^3 for the layout with one stage heat recovery.

It can be concluded, in light of the specific thermal energy consumption, that any solar driven membrane distillation system based on the current technology, must be integrated with other process in order to make use of the recovered heat in the cooling water.

4 CFD ANALYSIS OF AGMD UNIT (Paper III)

In order to improve the understanding of the internal flow conditions within the MD module, as a first step in finding new areas for improvement. This part of the work is intended to be a preliminary step; CFD analysis was used as a tool to analyze the flow conditions in both hot feed channel and cooling channels. The first section cover the analyses of flow conditions under varying spacer geometries in order to understand their effects on velocity boundary conditions, flow distribution, pressure drop and wall (membrane) sheer stress. The second section covers the flow distribution in the existing cooling channel in order to analyze the flow conditions and effect of its structure on the boundary conditions.

4.1 Spacer obstructed flow channel

As the MD is a heat driven process, several methods have been used to enhance heat transfer coefficient and reduces temperature polarization coefficient. Spacers introduced in the flow channel have several roles: keeping the two membrane sheets (constituting the flow channel) apart, achieve better mixing in the direction of the flow and across the flow channel thickness (reduction of the velocity boundary layer and thermal boundary layer). On the other hand, they impose an additional pressure drop across the flow channel. While this task main focus was on selecting the most appropriate spacer for the modified MD design, it was extended in scope to generalize the understanding of flow in spacer-obstructed flow channels.

Computational fluid dynamics (CFD) has been used recently as a method to investigate the effect of spacer on trans-membrane flux in Reverse Osmosis (RO) and Ultrafiltration (UF) processes [Fimbres-Weihs and Wiley, 2007; Li et al, 2005; Koutsou et al, 2009; Shakaib et al, 2007; 2009]. The uses of spacers in these processes have slightly different purposes. Most importantly, they form the flow channel by their thickness, as they separate adjacent membrane sheets, in addition to promoting flow disturbance, enhance mass transport and mitigate fouling and concentration polarization phenomena [Koutsou et al., 2007]. Cipollina et al [2009] presented a thermo-fluid analysis in spiral wound MD module channel. A spacer with longitudinal filament (direction of the flow) and transverse filament was used; evaporation was modeled indirectly by imposing a value for the heat flux.

In case of plate and frame flat sheet MD modules, spacers are not needed to separate the membrane sheets and form the flow channel, though they are still needed as a physical separator to prevent membrane physical contact (for membrane integrity reasons), in addition to their hydrodynamic and thermal role. The relative spacer to channel thickness will be one of the areas covered in this study using CFD as a tool to analyze the hydrodynamic conditions (in particular, flow distribution, pressure drop and wall/membrane sheer stress) in spacer obstructed flow channel. The physical means by which a spacer that is thinner than the flow channel is kept in a vertical position in the middle of the flow channel will not be discussed in this study (one way is to attach the spacer element to the frame forming the flow channel). Void ratio and flow of attack angle are two geometrical aspects of spacer that will be covered as well.

4.1.1 Modeling and boundary conditions

Three dimensional geometries representing different spacer-obstructed channels were created and simulated. Although the heat transfer is the driving force for MD process, it is not the comparison criteria in such a study. Since the mass loss per channel pass is typically two orders of magnitude lower than the channel-averaged mass flow, the mass transfer across the membrane boundary is neglected.

The model used for the simulation was steady, laminar and three-dimensional flow with the governing equations of continuity and momentum for steady incompressible fluid:

$$\frac{\partial u}{\partial x}+\frac{\partial v}{\partial y}+\frac{\partial w}{\partial z}=0$$
$$u\frac{\partial u}{\partial x}+v\frac{\partial u}{\partial y}+w\frac{\partial u}{\partial z}=-\frac{1}{\rho}\frac{\partial p}{\partial x}+\nu\nabla^2 u$$
$$u\frac{\partial v}{\partial x}+v\frac{\partial v}{\partial y}+w\frac{\partial v}{\partial z}=-\frac{1}{\rho}\frac{\partial p}{\partial y}+\nu\nabla^2 v$$
$$u\frac{\partial w}{\partial x}+v\frac{\partial w}{\partial y}+w\frac{\partial w}{\partial z}=-\frac{1}{\rho}\frac{\partial p}{\partial z}+\nu\nabla^2 w$$

where ∇ is the laplacian operator; ν is kinematic viscosity; ρ is density. Velocity magnitude was normalized according to the following relation:

$$V^*=\frac{V}{V_{inlet}}$$

The analyzed cases represent specific spacer geometry types; flow of attack angle θ, spacer to channel thickness ratio and void ratio , which is volume of opening compared to total volume of the spacer cell containing the opening and solid part, based on the following relation:

$$Void\ Ratio=\frac{V_{tot}-V_{sp}}{V_{tot}}$$

where V_{sp} is the volume of the solid part of the spacer cell. Figure 4-1 shows a schematic of the spacer geometry parameters.

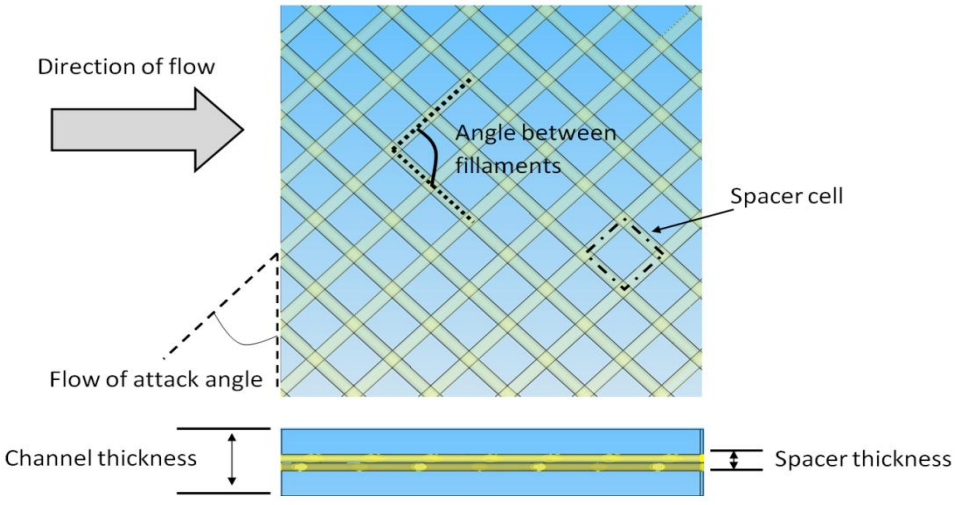

Figure 4-1: Schematic presentation of parameters used to define spacer

Table 4-1 summarizes the geometrical details of these cases/spacers. All spacers are round-filament non-woven types with identical diameters of the two filaments constituting the spacer.

Table 4-1: Simulation cases

Case	Flow of attack angle θ (angle between filaments α)	Spacer to channel thickness ratio %	Void ratio %
1	37 (105)	23	80
2	52 (75)	23	80
3	45 (90)	23	80
4	45 (90)	46	80
5	45 (90)	69	80
6	45 (90)	100	79
7	45 (90)	46	61
8	45 (90)	46	69
9	45 (90)	46	85
10	45 (90)	46	89

All the cases were simulated using CD-Adapco® CCM+ software package. The domain size was chosen large enough to alleviate the entrance region effect. Domain mesh size ranged from 900,000 to 1,500,000 polyhedral finite volume cells depending on the domain size. Mesh was refined and structured close to the membrane surface, and unstructurally refined in the vicinity of the spacer solid and opening parts. When the global mesh number was increased by 10% and near membrane domain mesh by 40%, the difference in results was less than 2%. Figure 4-2 shows an example of meshed domain for case 3.

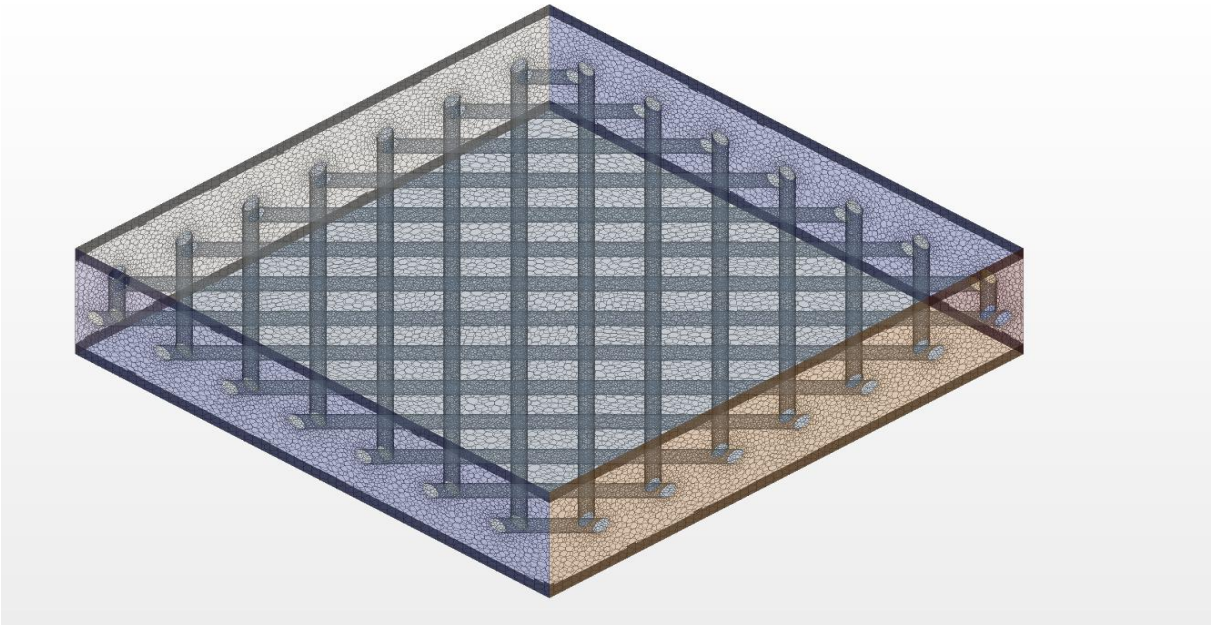

Figure 4-2: Overview mesh domain

Convergence criterion for residual of error was set to a minimum of 1×10^{-3} for continuity and the three velocity components. The stability was of the solution was judged by at least 1000 iterations.

Water with constant density was assumed as a fluid. Inlet boundary was chosen as inlet mass flow condition to represent a free stream velocity of 0,011 m/s in all cases, and outlet boundary condition was chosen as pressure (atmospheric). Membrane boundary was chosen to be non-slip condition.

4.1.2 Results and Discussion

4.1.2.1 Flow of attack angle

Figure 4-3 shows an overview of the normalized velocity fields and particle streamlines for cases 1 to 3 (θ=37, 52 and 45°) including three cross sections: one in the direction of flow over the crossing of the spacer filaments (E), one in the direction of flow avoiding the crossing (F), and one perpendicular to the direction of flow (I). Note that the three black lines represent three area of interest to examine the velocity profile development close to the membrane area; A is the center of the cell, B is point above the filament intersection and C is the point above the filament. This illustration will follow in all cases.

The spacer filaments forced the flow towards the membrane surface as expected with higher velocity values over the spacer filaments. It can be noted that the velocity in the center of the channel is very low and comes close to zero in the vicinity of the spacer filaments. In the newly formed two flow channels, the average velocity magnitude is roughly 60-70 % more than the original inlet velocity. In cases 1 and 3, the velocity in the newly formed channels are slightly higher than in case 2, mainly over the crossing of the spacer which that due to the higher resistance of flow caused by the decrease of flow angle. The higher flow of attack angle in case 2 makes the filaments become closer to the direction of flow, which in turn, ease the flow resistance.

The streamline has uniform resolution 5×30 (horizontal × vertical). The particles' streamlines show a clear trend of the flow being forced with the horizontal direction of the filaments. However, such trend is less significant close to the membrane surface due to the low spacer to channel thickness (in these particular cases).

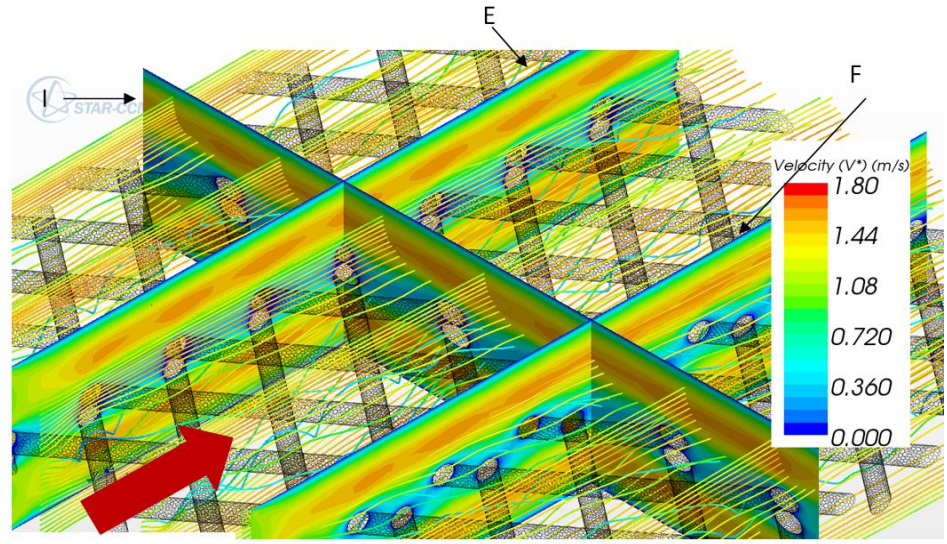

Case 1 (θ=37)

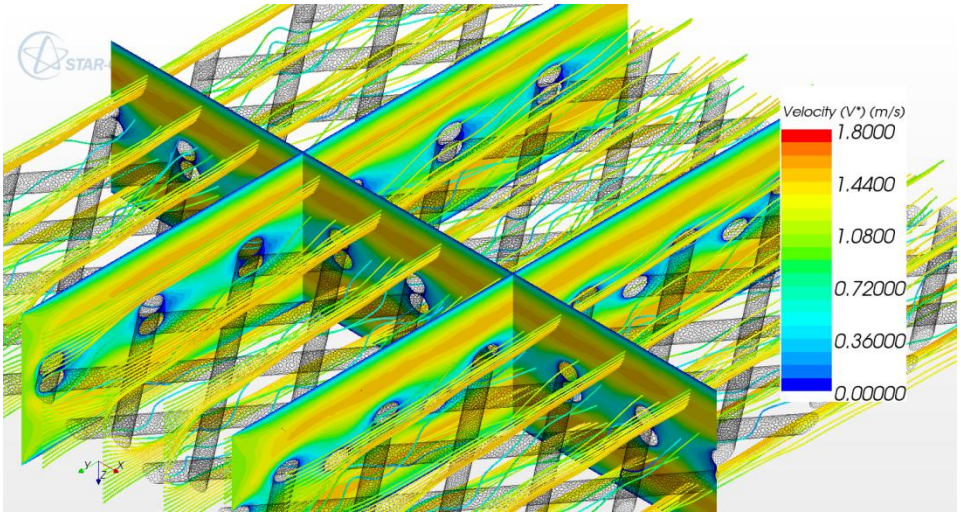

Case 2 (θ=52)

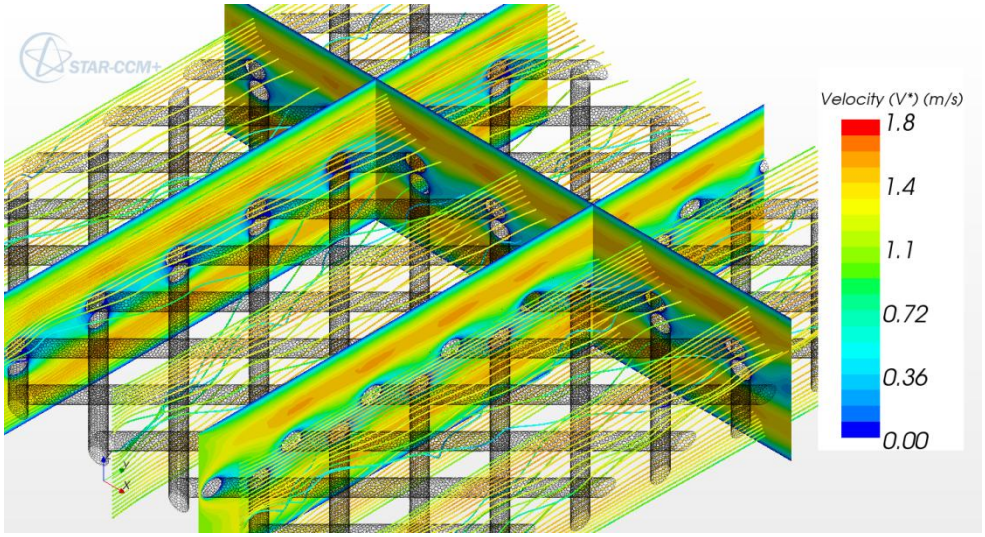

Case 3 (θ=45)

Figure 4-3: Overview of velocity fields and stream lines (cases 1-3)

Figure 4-4 shows the velocity profiles from the membrane surface to the center of the channel, for the two longitudinal cross sections (E and F); for the three cases over their entire length. Generally, there is no significant difference in the velocity profile slope and magnitude between the two sections of each case due to the fact that the spacer to channel thickness ratio is low, which causes the flow to split into two flow channels. As can be seen from the general shape, that there is no significant mixing of the flow in the vertical direction (channel thickness), which is one of the motives to use spacer in flow channel. However, such effect shouldn't cause an instantaneous judgment of the efficiency of a specific spacer since the assessment depends on the other factors mentioned previously. Moreover, the flow mixing that is desired in other membrane separation (RO, UF), is mainly intended for disturbing the concentration boundary layer which is crucial these applications; but less significant in MD. Note that there few horizontally scattered points represent the velocity values at and close to the inlet boundary.

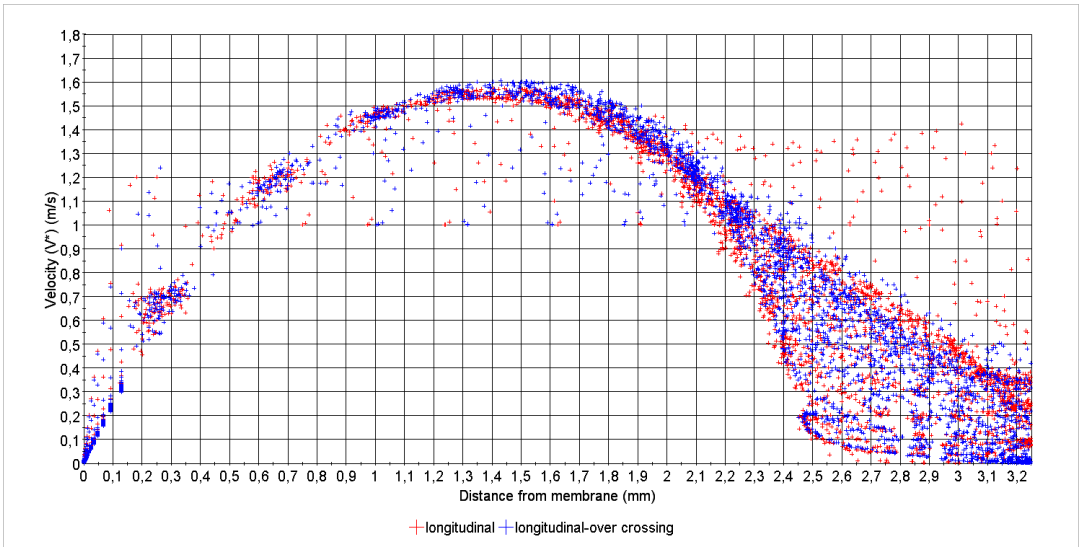

Case 1

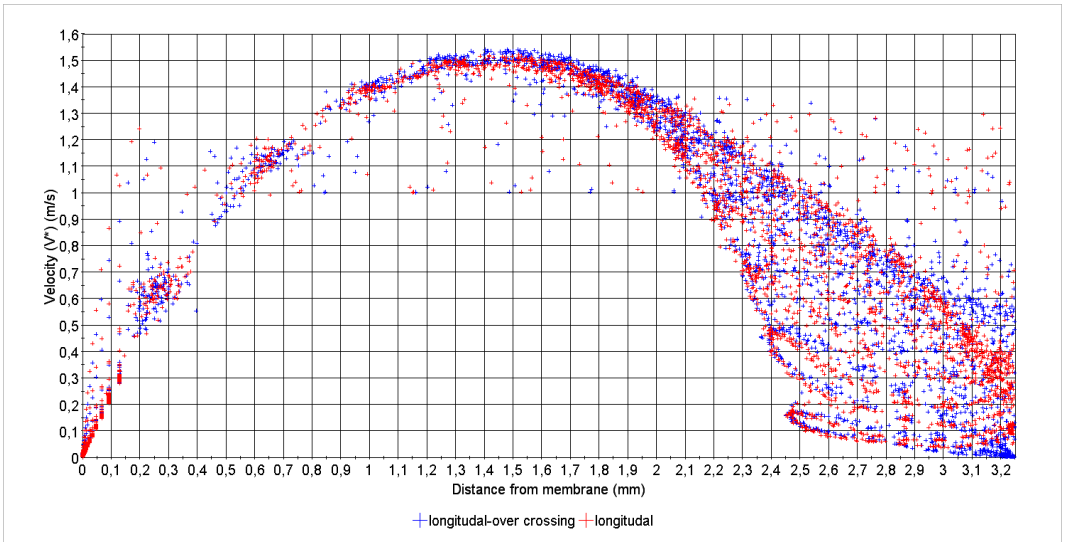

Case 2

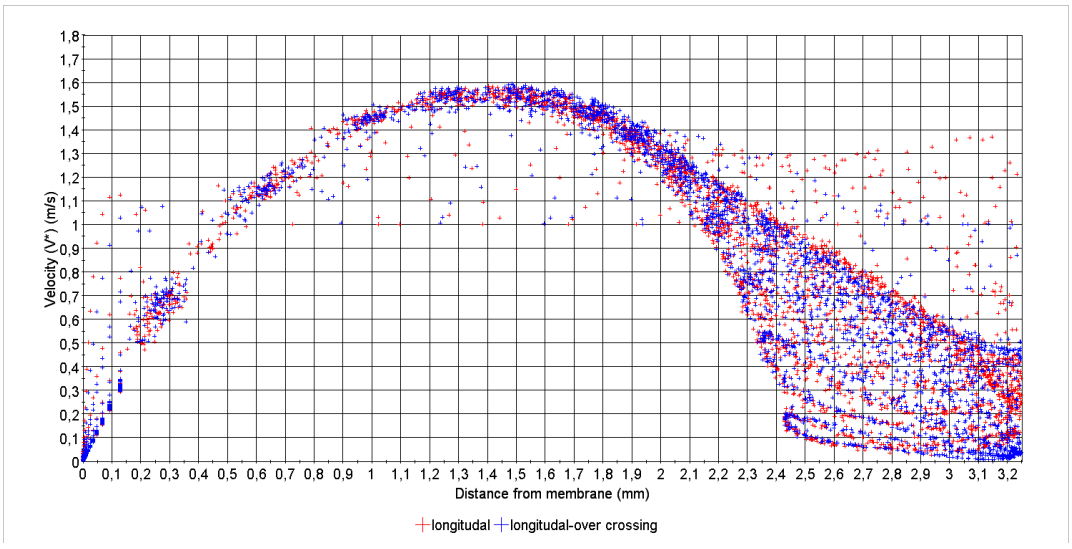

Case 3

Figure 4-4: Velocity profiles for the two longitudinal cross sections over their entire length; distance from membrane surface to channel center (cases 1-3)

Table 4-2 lists the average sheer stress and pressure drop for the three cases. To quantitatively assess the spacers, the ratio of average sheer stress to pressure drop is used.

Table 4-2: Average sheer stress and pressure drop (cases 1-3)

Cases	Average sheer stress (Pa)	Pressure drop per m length (Pa)	Sheer stress/pressure drop ($\times 10^3$)
1 (θ=37°)	2,77E-02	21,45	1,29
2 (θ=52°)	2,61E-02	19,2	1,36
3 (θ=45°)	2,76E-02	21,11	1,31

As a general conclusion, and within the range of angle used, the flow of attack angle has a very minimum effect of the hydrodynamic conditions. This finding somewhat differ from results reported in literature. Phattaranawik et al [2003] reported relatively large difference in mass flux (7-14 %) achieved experimentally for a similar range of angles (note: the hydrodynamic angle considered was the one between the spacer filaments; i.e, α in this paper) in DCMD. However, since the results reported in their work were for mass flux and a fully spacer filled channel; the numerical discrepancies cannot be assessed. The significant difference is that the spacer which achieved the highest flux was the one with flow of attack angle of 45° (90° in their annotation). A similar finding was reported by Chernyshov et al [2003] for experimental work done on DCMD configuration and Da Costa et al [1994]. However, Shakaib et al [2007] found that the average shear stress increase with decrease of flow attack angle in their CFD analysis of spacer-filled feed channels (RO and UF systems). A possible explanation for the cases related to optimum spacer having a 45° in MD is related to the fact that, in case of spacer-filled channels (which is not the case covered in this paper), having smaller angles, means more number of filaments per membrane surface area. This means that a larger area of membrane is in contact with spacer body and hence less area available for evaporation. While such suggestion means that the spacer with larger angle should achieve higher fluxes, the lower flow disturbance caused by such spacer means lower shear stress and hence higher thermal boundary layer, i.e, lower heat transfer; which in turn suggest that the trade off is for spacers of moderate angle, the ones with 45°.

4.1.2.2 Spacer to channel thickness ratio

Spacers 3 to 6 were chosen to represent the spacer to channel thickness ratio (23, 46, 69 and 100 %). Flow of attack angle and void ratio were kept constant (case 6 has a slightly less void ratio). Figure 4-5 shows the normalized velocity contours and stream lines, with more visual details of the cross sections (case 3 was presented in the previous section).

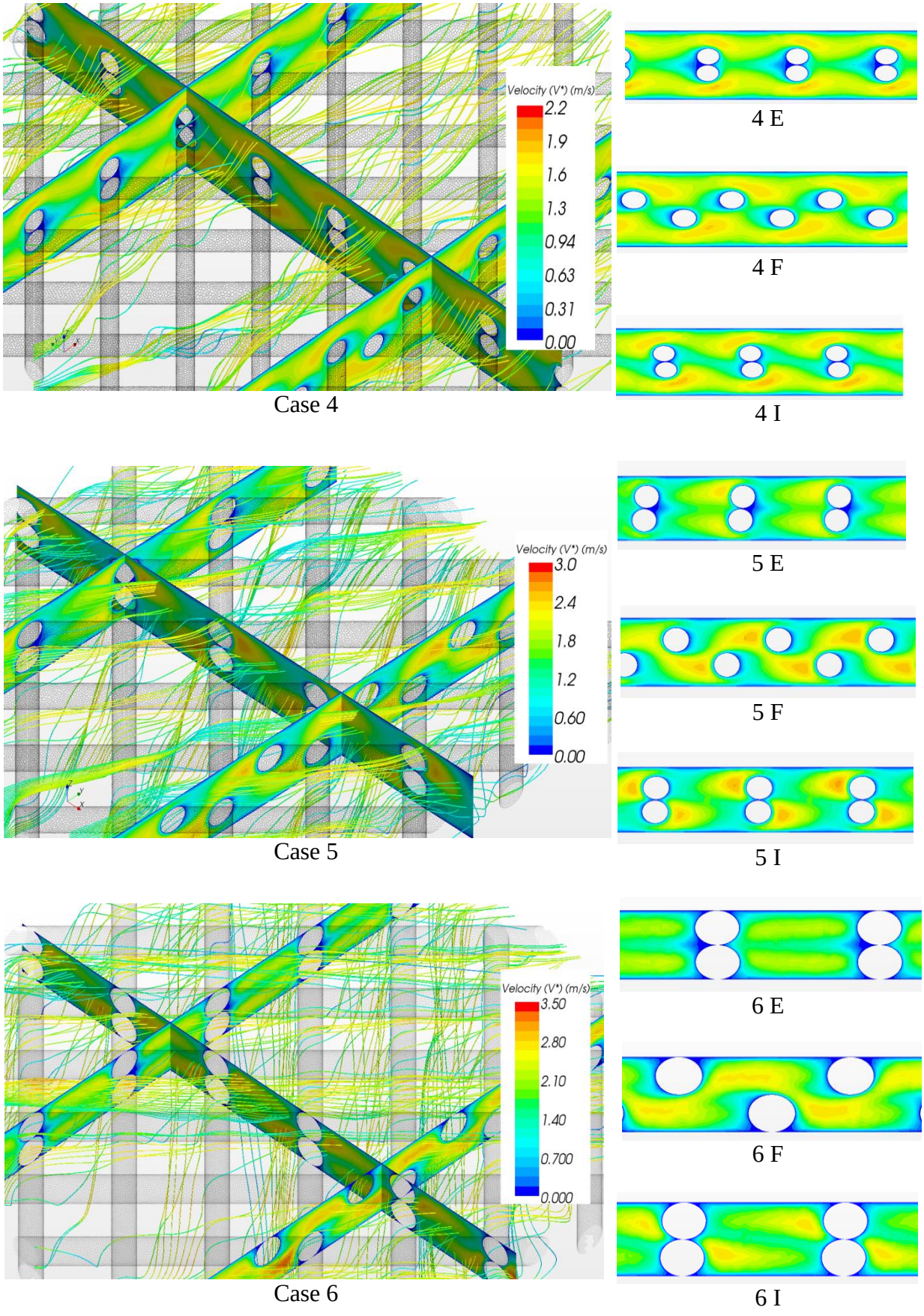

Figure 4-5: Overview of velocity contours and streamlines (cases 4-6)

The velocity increase as the volume of the obstacle increase; however, the main concern here to study is how the flow distribution and velocity profiles develop. When thickness ratio increased to 46 % (case 4), a noticeable horizontal and vertical change of flow direction can be seen mainly close to the center of the spacer cell, due to resistance that the upper or lower filament poses. The transversal cross section (view 4 I) in this case, shows higher velocities in the areas close to the spacer filament; to the left of the upper filament, which direct the flow to the left; and to the right of the lower filament which direct the flow to the right. Although the normalized velocity fields and streamlines indicate a noticeable vertical mixing of the flow, still the thickness ratio is not sufficient to cause a general flow block, and the flow is still divided into two flow channels. When the thickness ratio is increased to 69% (case 5), a clear flow blockage can be seen over the spacer crossing (view 5 E), and a zig zag flow pattern on the middle of the cell (view 5 F). The transversal cross section shows large differences in velocity contours across the flow channel width with half of the area has an average of double the inlet velocity and the other with value of 1. When the thickness ratio is increased to 100%, a complete mixing of the flow happens because of the flow blocking by the two non-woven filament sets. Velocity fields in views 6 E, 6 F and 6 I indicate a close to even distribution of the flow in void area of the cell. While such even distribution and mixing might seem favorable, it must be noted that area covered by such case is relative to the spacer surface area and void ratio, i.e, in such case around 15% of the membrane.

Figure 4-6 shows the velocity profiles for the two longitudinal cross sections over their entire length for the three cases (case 3 was presented previously). It can be seen clearly that as the thickness ratio increases, the flow distribution increases as mentioned in the previous paragraph. Moreover, the differences between the velocities close to the membrane surface along the two sections becomes clear; as the thickness ratio increases, the velocities over the void area of the cell increases in comparison to the area over the filament area and the velocity profile development becomes higher.

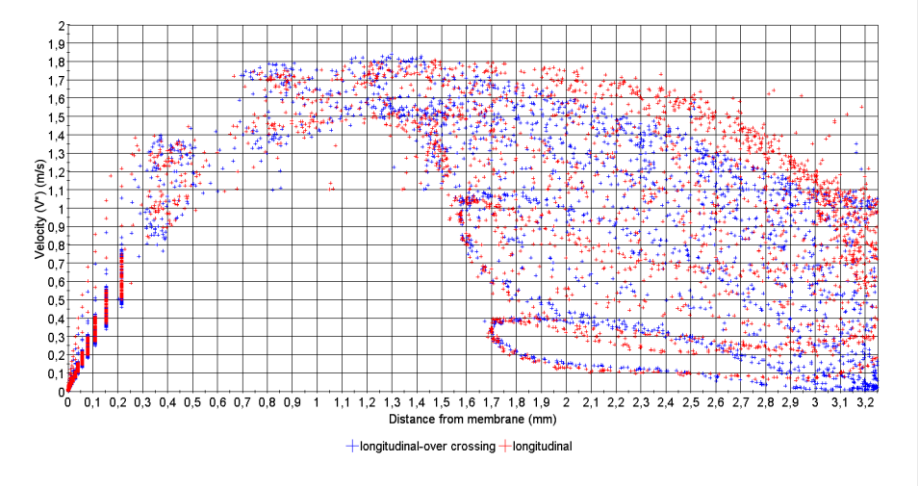

Case 4

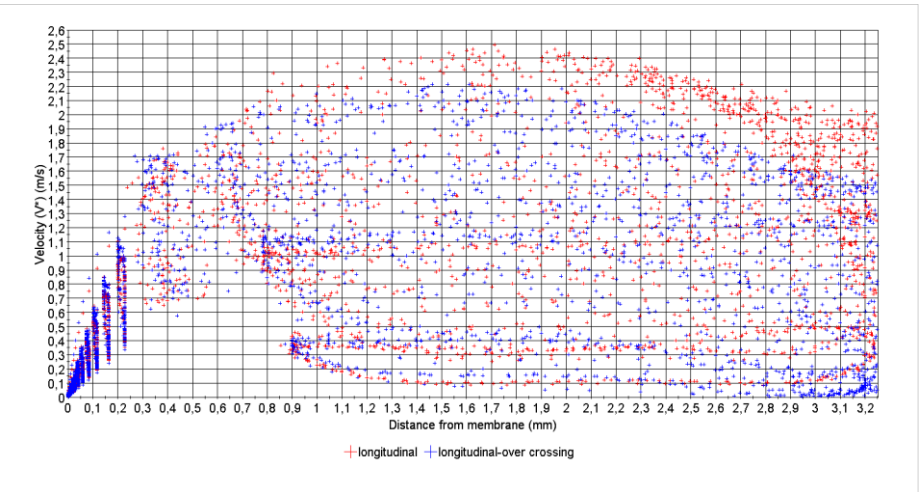

Case 5

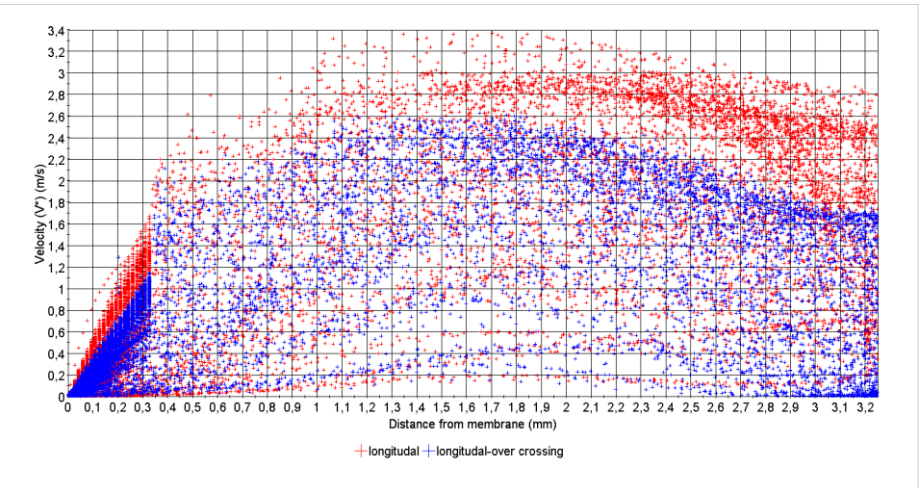

Case 6

Figure 4-6: Velocity profiles for the two longitudinal cross sections over their entire length; distance from membrane surface to channel center (cases 4-6)

Figure 4-7 shows the shear stress contours plotted on the same scale, and shear stress distribution as a function of percentage of the membrane for the cases 3 to 6. As the thickness ratio increases, the sheer stress distribution becomes less uniform. As the shear stress is directly related to velocity profiles, the values of the membrane areas over the spacer filament are higher than the empty part of the cell. The fully spacer-filled channel (case 6) has the highest sheer stress concentrated in the center of the cell. The histogram of the spacer filled channel shows that large percentage of membrane area has zero or almost zero values.

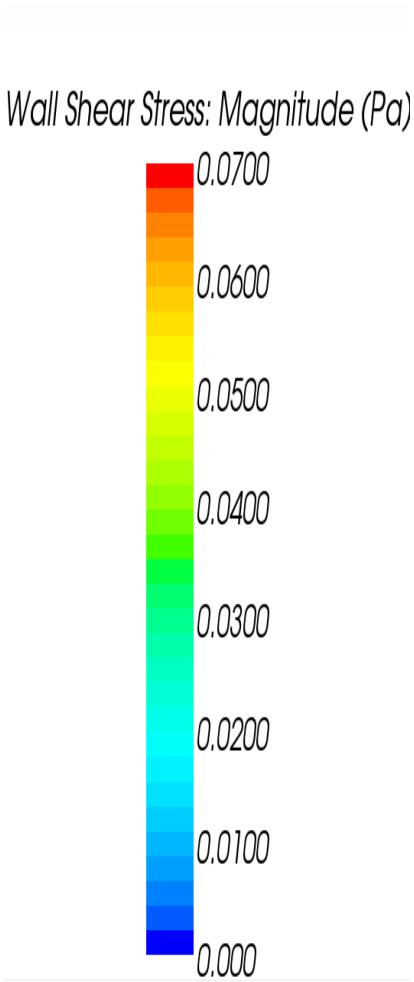

Case 3: thickness ratio 23%

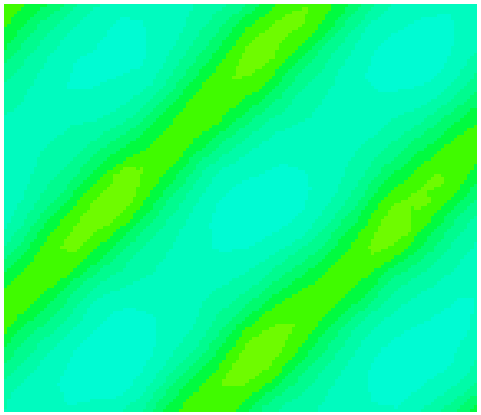

Case 4: thickness ratio 46%

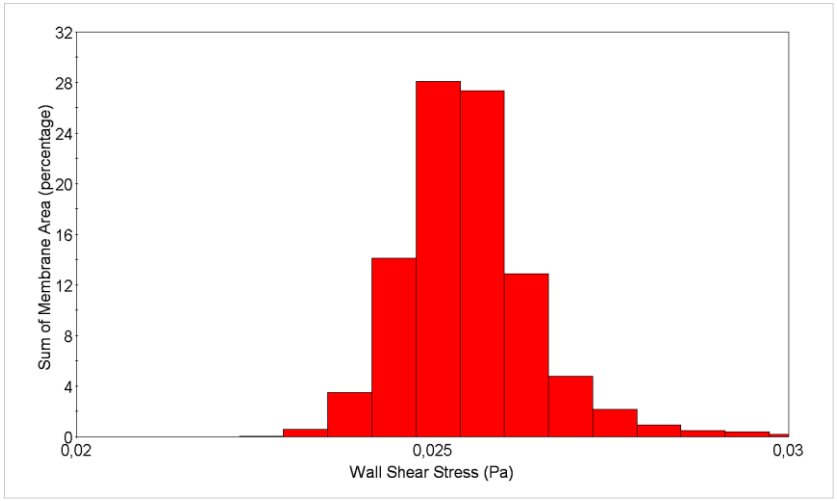

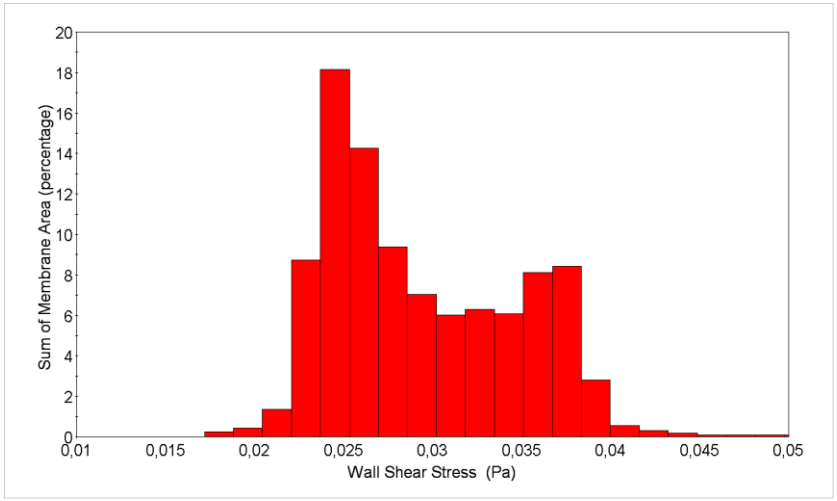

Figure 4-7: shear stress on membrane surface (case 3-6)-continued in the following page

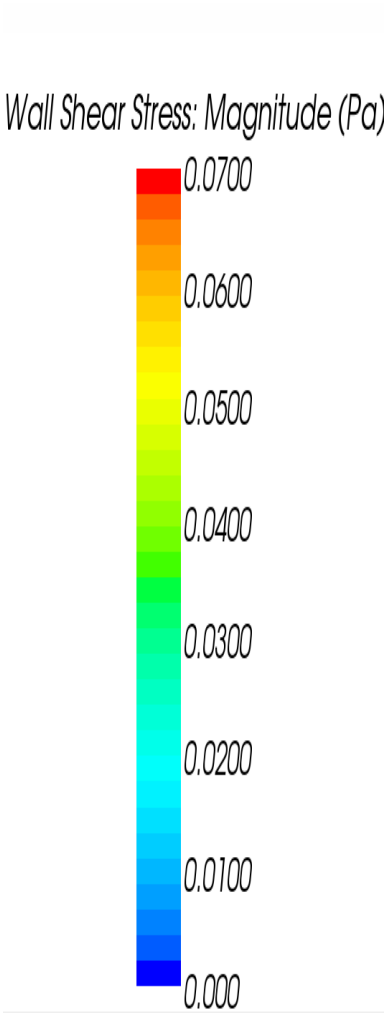

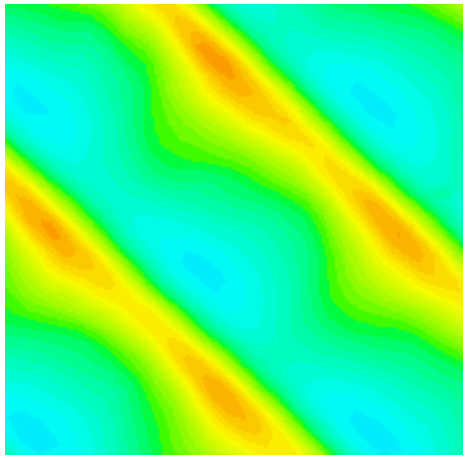

Case 5: thickness ratio 69%

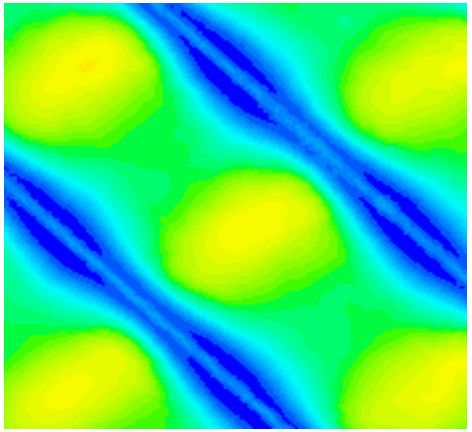

Case 6: thickness ratio 100%

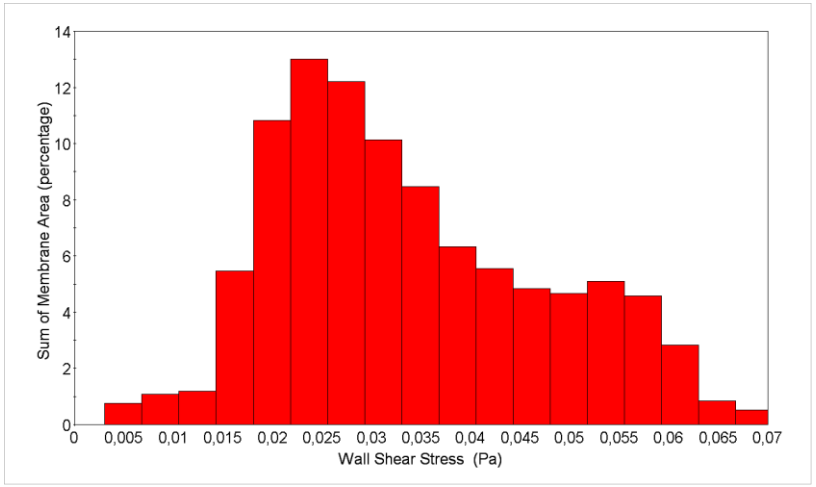

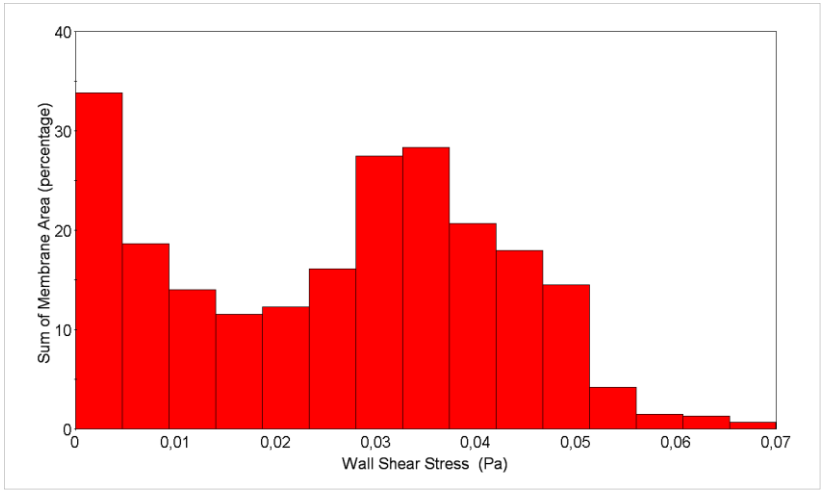

Figure 4-7: shear stress on membrane surface (case 3-6)-continued

The following table gives a clear numerical indication of performance. Numerically, case 6 is the least efficient; it has the lowest average sheer stress and highest pressure drop. Another disadvantage that a spacer-filled channel (similar to case 6) has is the possible thermo-physical interaction between the membrane material and spacer material, which might damage the membrane surface. In experiments on spacer filled channel performed at the EGI-KTH lab, a rapid deterioration of flux/permeate quality was observed. The inspection on the membrane revealed a physical damage to the membrane surface along all the filaments length causing loss of hydrophobicity.

Table 4-3: Average sheer stress and pressure drop (cases 3-6)

Cases	Average sheer stress (Pa)	Pressure drop per m length (Pa)	Sheer stress/pressure drop ($\times 10^3$)
3	2,76E-02	21,11	1,31
4	3,02E-02	26,0	1,16
5	3,48E-02	35,79	0,97
6	2,73E-02	38,49	0,71

4.1.2.3 Void ratio

Spacers 7, 8, 4, 9 and 10 were chosen to represent the spacer void ratio (VR= 61, 69, 80, 85 and 89 %). Flow of attack angle (45°) and spacer to channel thickness ratio (46%) are kept constant. Figure 4-8 shows the normalized velocity contours and streamlines for 7, 8 9 and 10 cases (case 4 was shown in Figure 4-5).

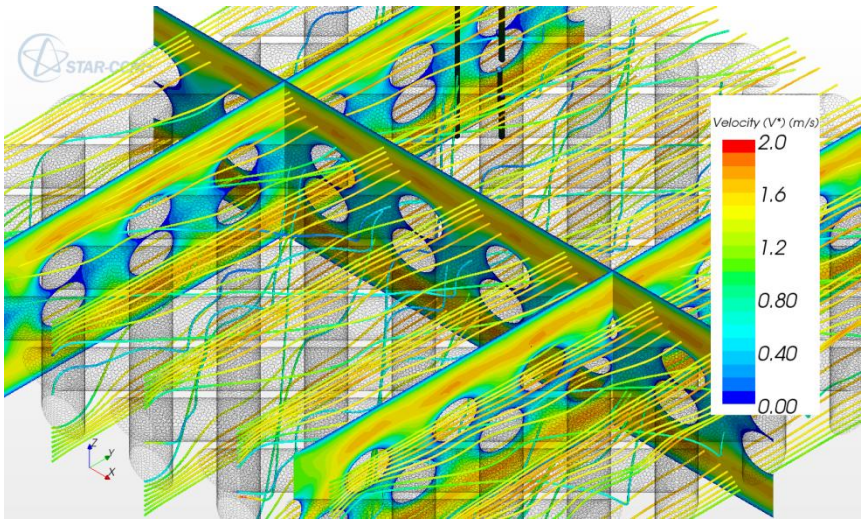

Case 7: Void ratio 61%

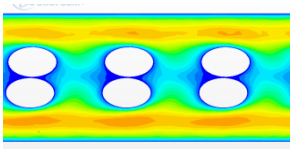

7 E

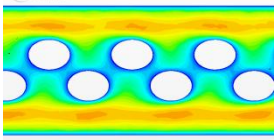

7 F

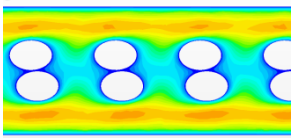

7 I

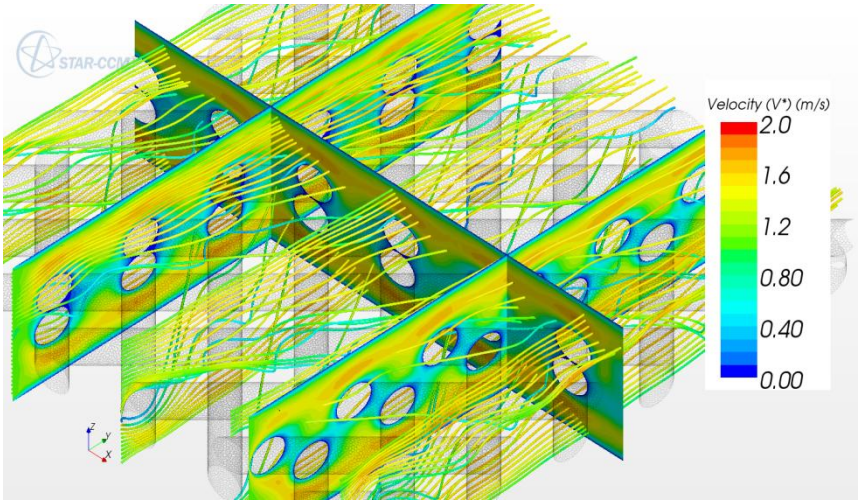

Case 8: Void ratio 69%

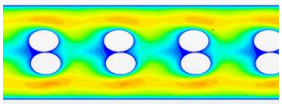

8 E

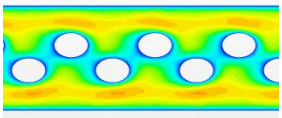

8 F

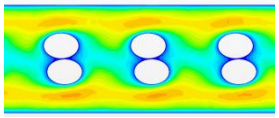

8 I

Figure 4-8: Overview of velocity contours and streamlines (cases 7,8, 9 and 10)-continued in the following page

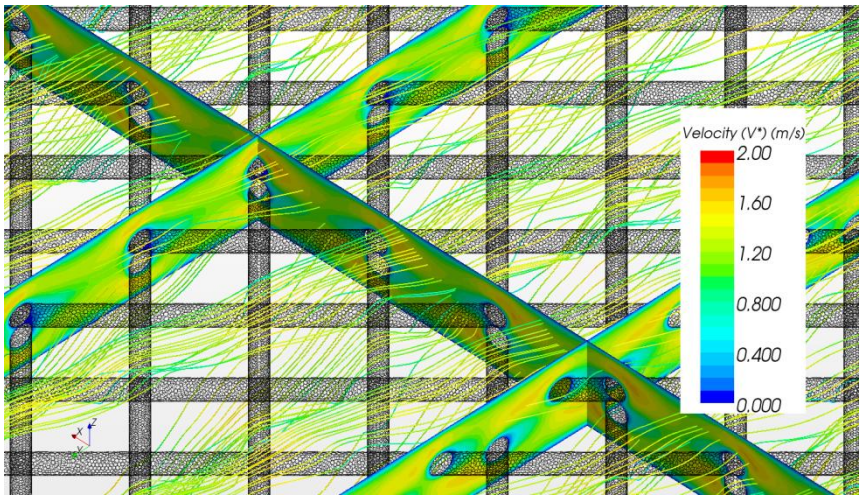

Case 9: Void ratio 85%

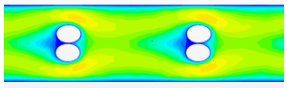

9 E

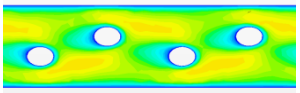

9 F

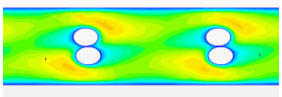

9 I

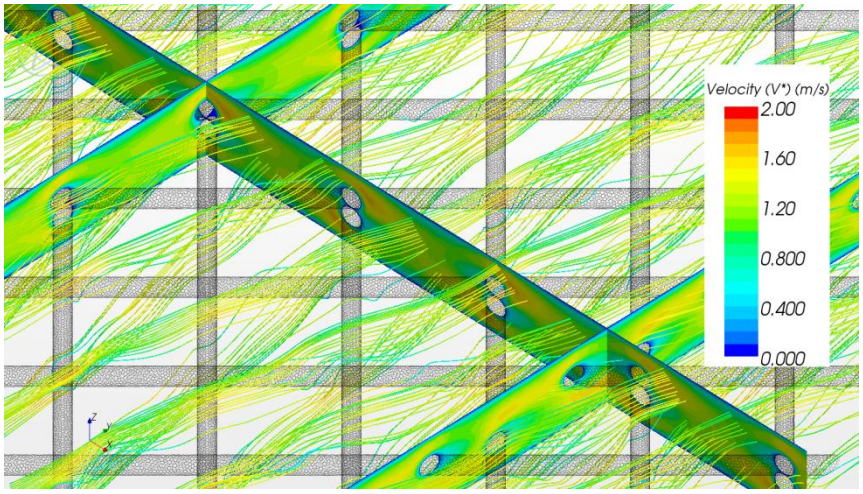

Case 10: Void ratio 89%

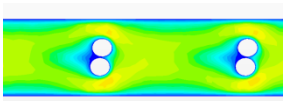

10 E

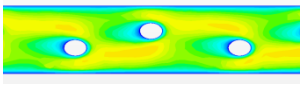

10 F

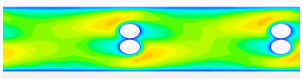

10 I

Figure 4-8: Overview of velocity contours and streamlines (cases 7,8, 9 and 10)-continued

Recalling the previous analyses of case 4 as a starting point, the thickness ratio allows some small degree of flow mixing in the vertical direction, though it was not enough and the flow still distributed into a newly formed two channels. Reducing the void ratio to 61% minimizes the vertical flow direction, yielding a two flow channel regime similar to the cases 1 to 3, with a relatively more increase in the velocity over the spacer filaments. The clear pattern of velocity "stress and relax" regions in these two formed flow channel, compared to 1-3 cases, is due to the higher thickness ratio and lower void ratio which is small enough to hinder the flow vertical mixing. Case 8 (void ratio 69%) clearly validate such condition; the similar velocity "stress and relax" regions, with lower values; and yet, the void ratio is not enough to promote vertical mixing. It should be kept in mind that the relatively less flow resistance in the region above and under the spacer compared with spacer region, at this specific spacer to channel thickness. It could be assumed, even at this early stage of analysis, that these two cases will have the lower efficiency in all aspects.

As the void ratio increases, the two flow channel regime diminishes and a larger vertical mixing increases. However, the larger void ratio, the smoother the zigzag flow path becomes. The flow takes a close to the center of the channel path rather than close to the membrane. Figure 4-9 visualize the previously described flow distribution for the four new cases.

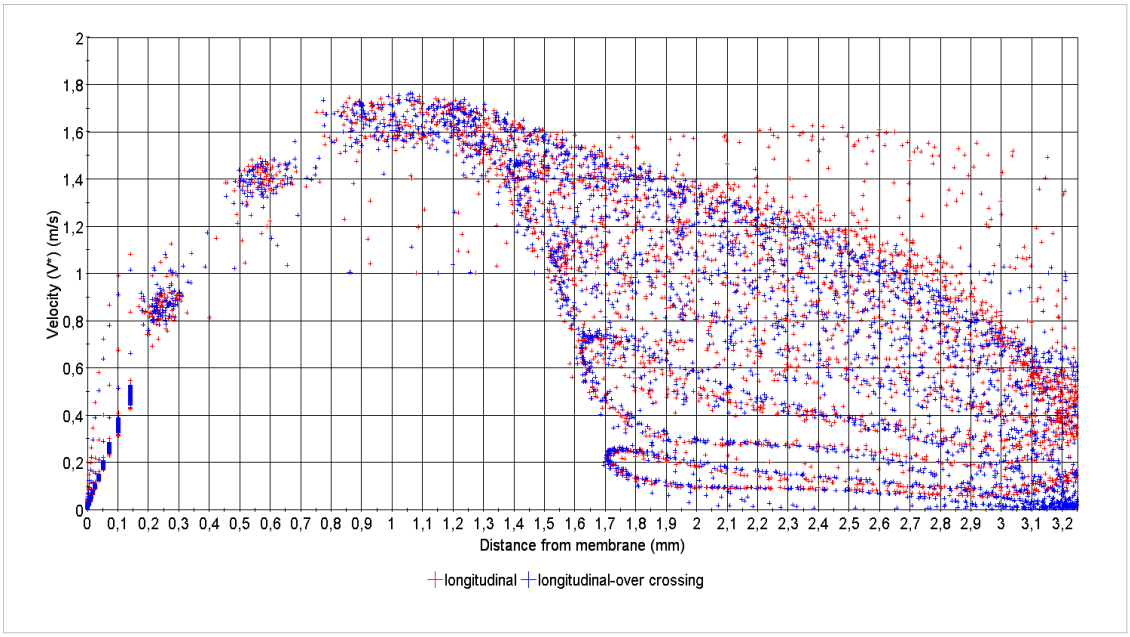

Case 7

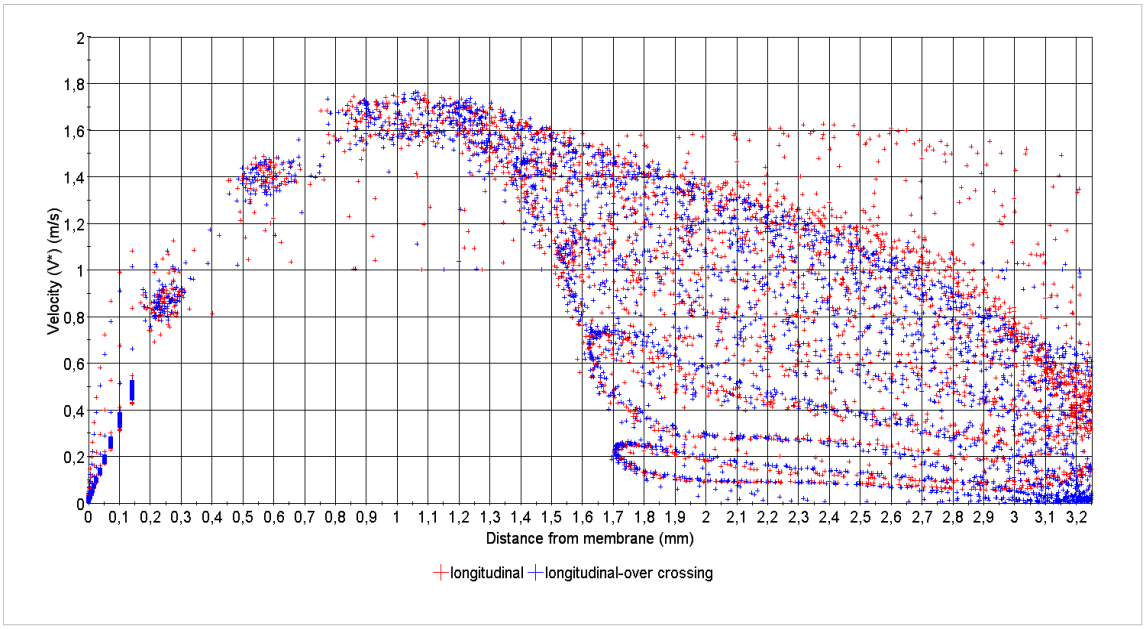

Case 8

Figure 4-9: Velocity profiles for the two longitudinal cross sections over their entire length; distance from membrane surface to channel center (cases 7, 8, 9 and 10)- continued in the following page

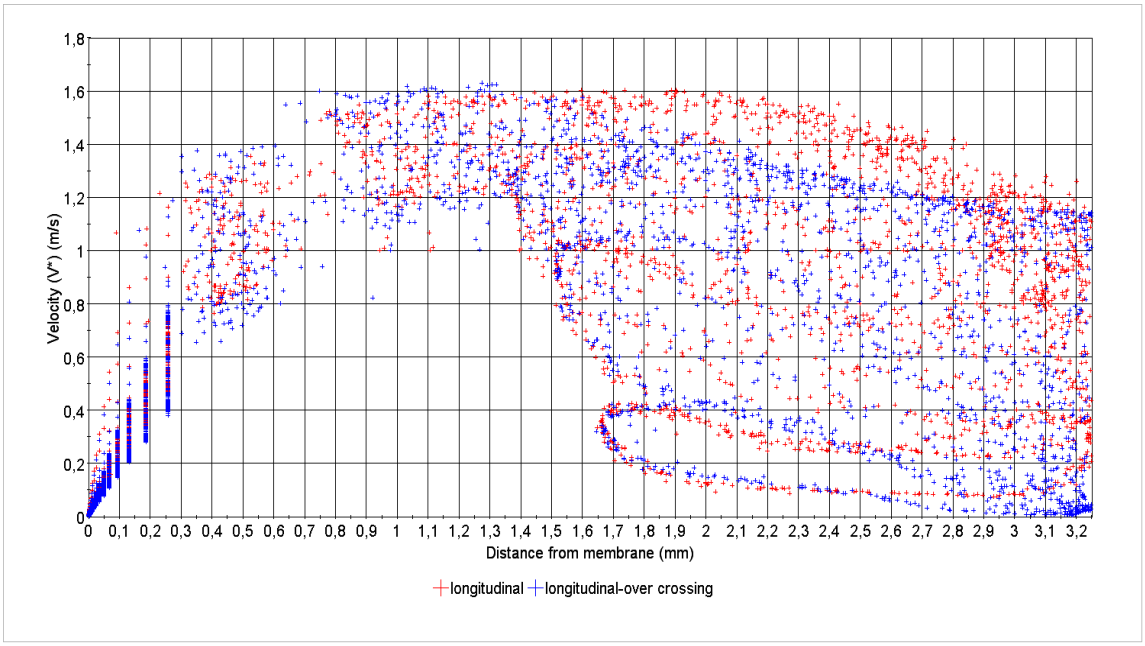

Case 9

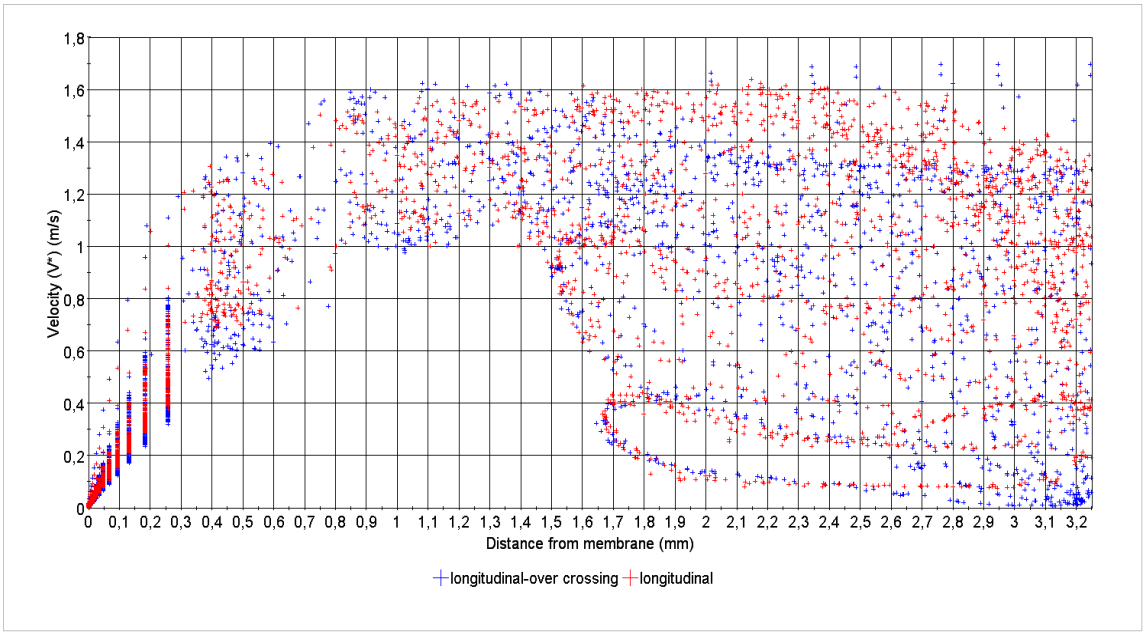

Case: 10

Figure 4-9: Velocity profiles for the two longitudinal cross sections over their entire length; distance from membrane surface to channel center (cases 7, 8, 9 and 10)-continued

Examining the velocity profiles close to the membrane surface, it can be seen that when the void ratio is low, the highest value and uniformity of velocity is achieved. Such uniformity starts to decrease by the increase of void ratio; and split once the void ratio is exceeds 80 %. In case 9 and 10, the difference between the profile developments close to the membrane becomes clearer. From this figure; less void ratio is favorable from a uniformity of velocity gradient point of view; nevertheless, the other factor, mainly pressure drop should be taken in consideration.

Figure 4-10 shows the wall sheer stress and distribution for the 7, 8, 9 and 10 cases (all are in the same scale). Clearly the more uniformity and hence membrane usage is higher in lower void ratio.

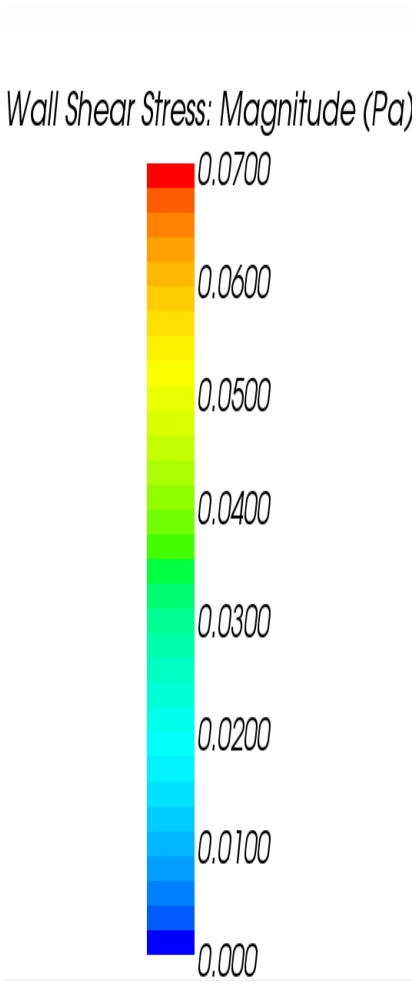

Case 7: void ratio 61%

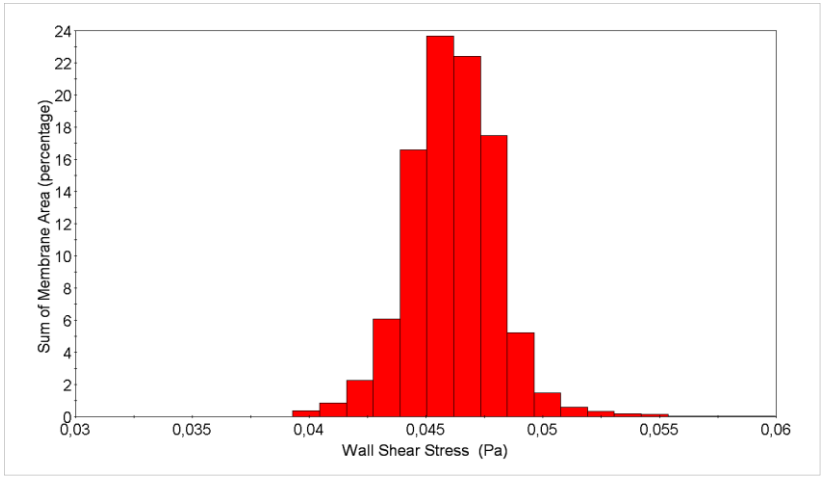

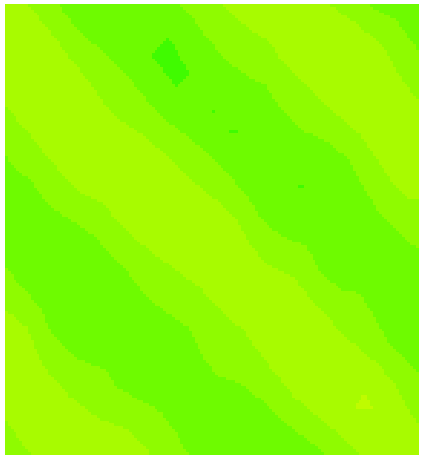

Case 8: void ratio 69%

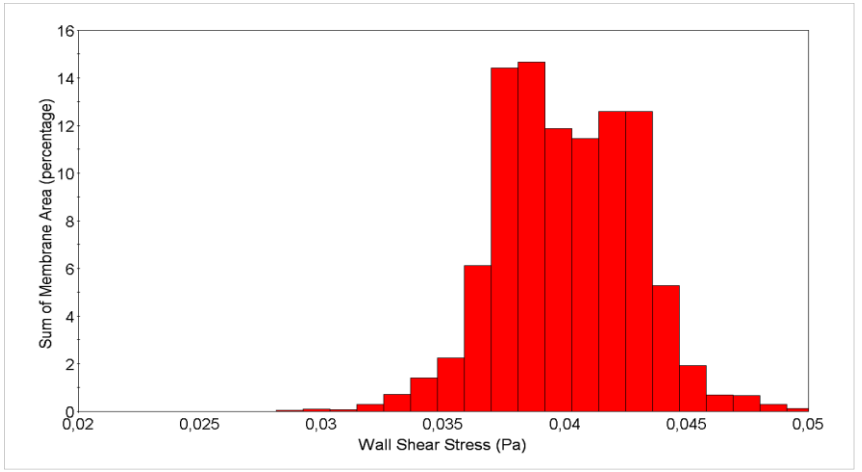

Figure 4-10: shear stress on membrane surface (cases 7,8,9 and 10)-continued in the following page

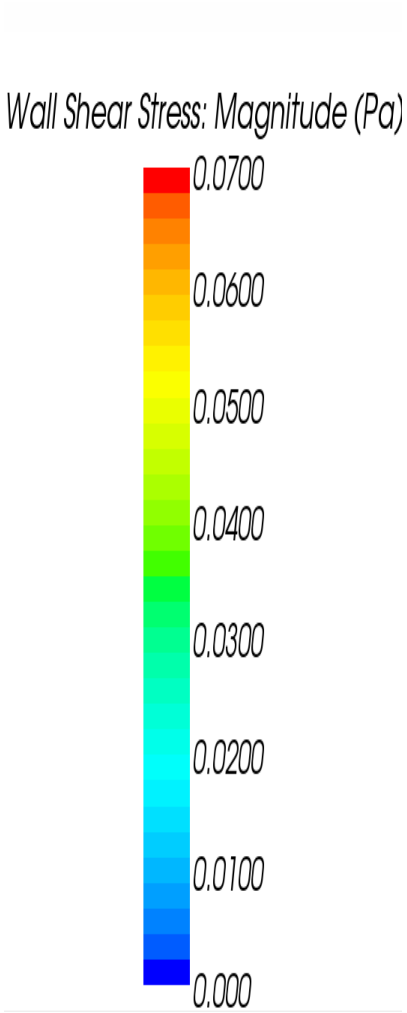

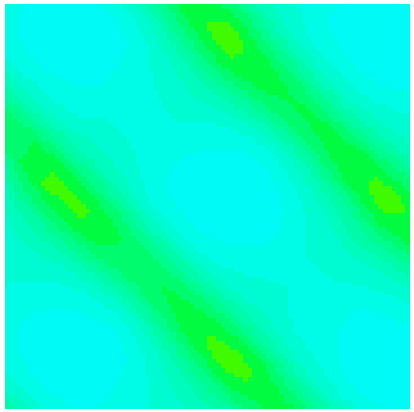

Case 9: void ratio 85%

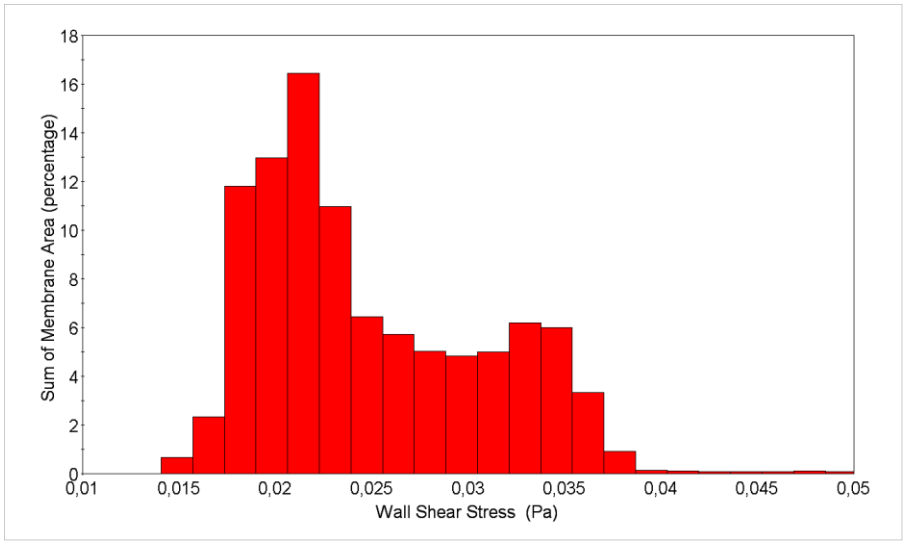

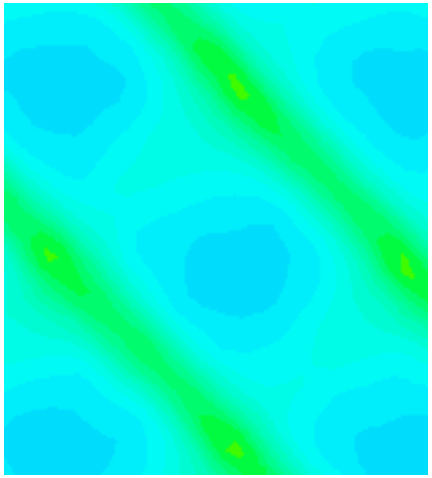

Case 10: void ratio 89%

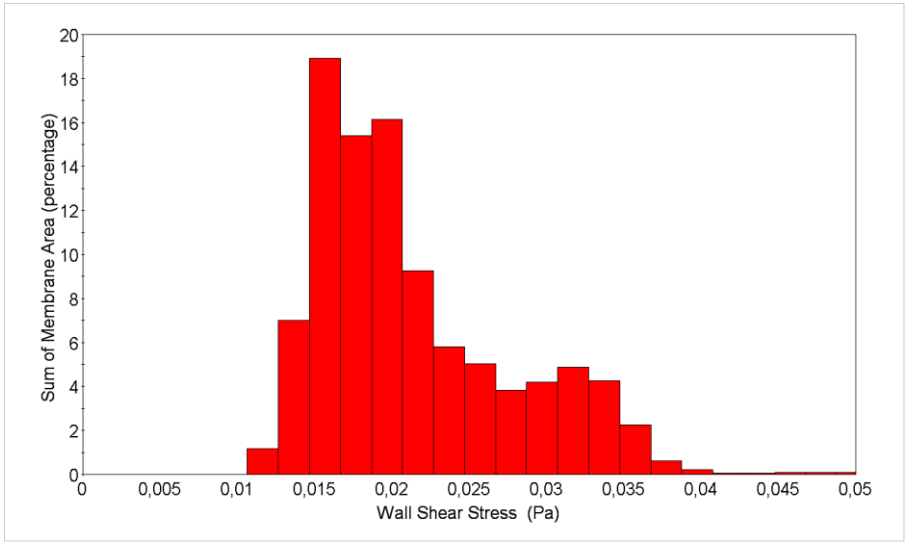

Figure 4-10: shear stress on membrane surface (cases 7,8,9 and 10)-continued

Cases 9 and 10 have a very low shear stress in the membrane area corresponding to center of spacer cell. The following table indicates the overall assessment factors. Numerically case 10 would be the favorable spacer. However, such result should be weighed against the membrane cost as the average shear stress, and hence, the heat transfer and specific mass flux would be low.

Table 4-4: Average sheer stress and pressure drop (cases 7,8,4,9 and 10)

Cases	Average sheer stress (Pa)	Pressure drop per m length (Pa)	Sheer stress/pressure drop ($\times 10^3$)
7 (VR=61)	4,820E-02	53,9	0,89
8 (VR=69)	4,209E-02	43,5	0,97
4 (VR=80)	3,023E-02	26,0	1,16
9 (VR=85)	2,524E-02	19,76	1,28
10 (VR=89)	2,176E-02	15,3	1,42

To compare these results with the ones reported by Pattaranawik et al.[2003] work on several spacers with different void ratio; they found that the mass flux in DCMD increased moderately by increasing the void ratio from 35 % until it reaches a maximum value at approximately 60%. Increasing the void ratio further more resulted in a rapid decline in mass flux. Though the average shear stress in the table above suggest a similar trend, increasing the void ratio from 61 to 69%, resulted in a moderate decrease, while the rapid decline starts at void ratio of 70%, but slows again. Da Costa et al. [1991] reported different results with experimental work on different spacers used in UF; increasing the void ratio from 46% to 80% resulted in a minor drop in mass transfer (2-10%), and concluded that void ratio has a negligible effect. However, in later work, Da Costa et al. [1994] produced correlations for spacers performance estimation based on their geometrical characteristics and calculated that the maximum mass transfer coefficients would be achieved at void ratio around 40%. They also showed that the mass transfer coefficient dropped significantly when the ratio increased over 50%.

4.1.2.4 Special cases

Some special cases were simulated for different reasons. Case 11 represent two spacers similar to case 3 inserted in the flow channel, in which both can be compared to case 4; i.e, similar spacer to channel thickness ratio and void ratio. This case was simulated because it represents the actual case of MD current design spacer. The other two cases, 12 and 13, have similar characteristic geometries (angle of attack: 45°, spacer to channel thickness ratio: 52% and void ratio: 87%). The difference is that case 13 has a varying filament diameter with center value of half the value at the crossing node.

Figure 4-11 shows the velocity contours, stream lines and velocity profiles for the longitudinal cross sections for the three cases. In case 11 (which should be compared with case 4), the flow is divided into two flow channel as the cases 1-3. Unlike case 4, the two spacer constituted a two-level blockage in front of the flow which eliminated the effect of increase spacer to channel thickness in case 4; the vertical mixing. The results were higher shear stress for case 11 compared with case 4 by 50 % and higher pressure drop by 100%. Having two-level obstruction in front of the flow cause part of the flow in the center to take a vertical zigzag path, this resulted in such higher pressure drop. The numerical spacer efficiency of such case (Table 4-5) is lower than case 4.

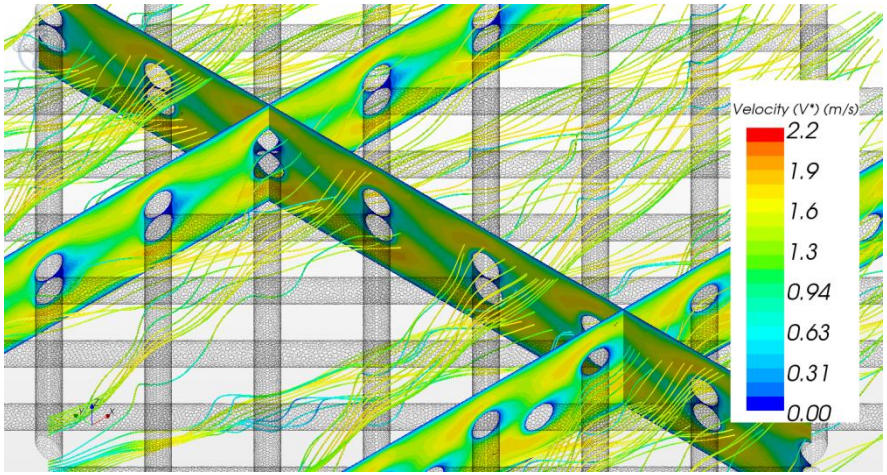

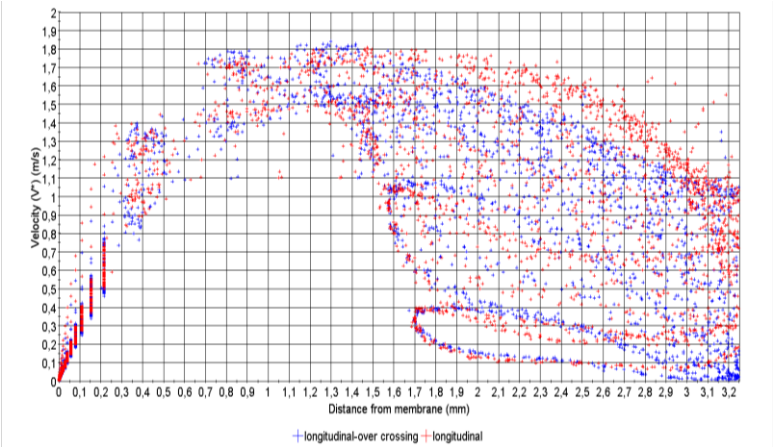

Case 4

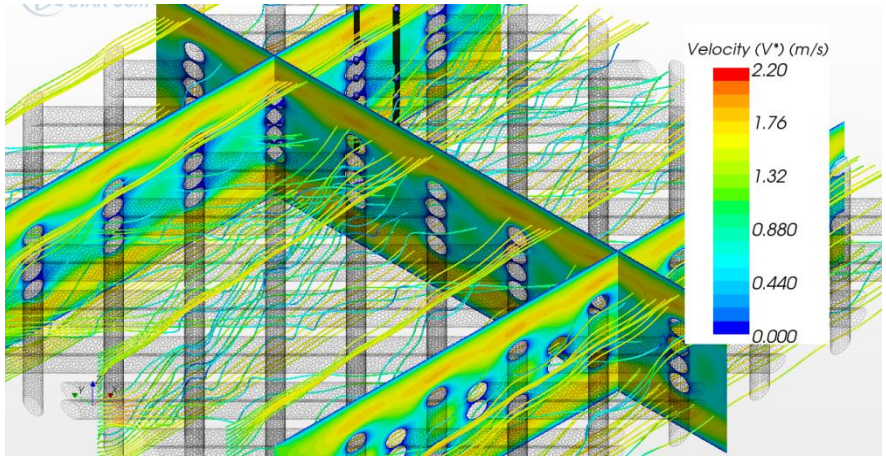

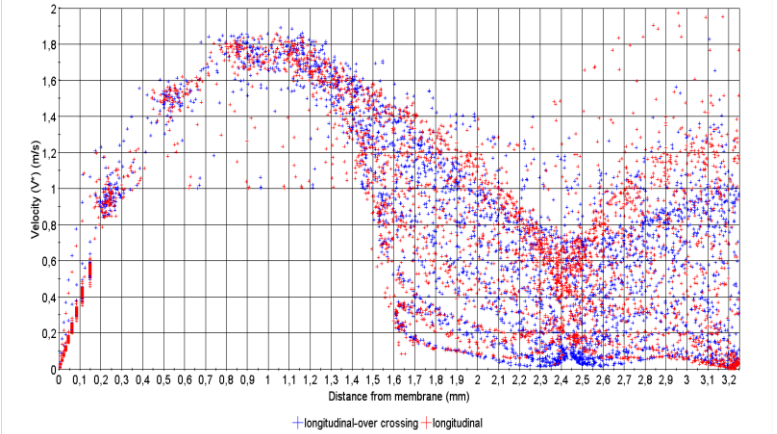

Case 11

Figure 4-11: Velocity contours, streamlines and velocity profiles for the two longitudinal cross sections (cases 4 ,11,12,13)-continued in the following page

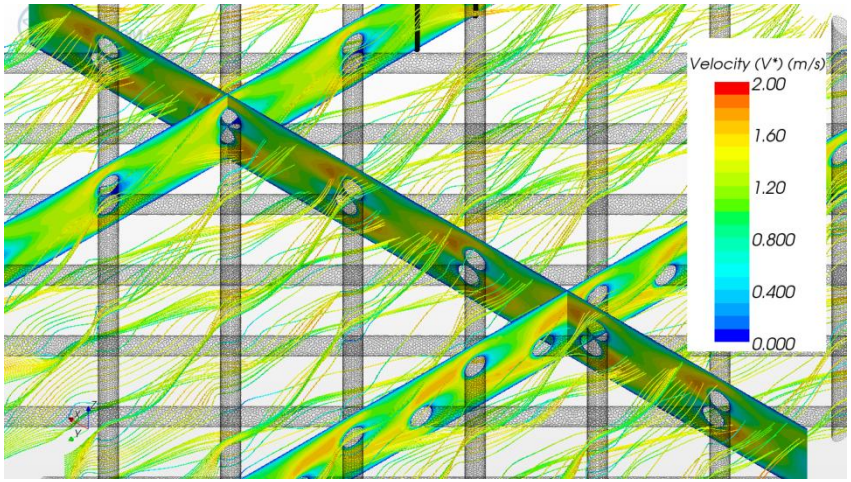

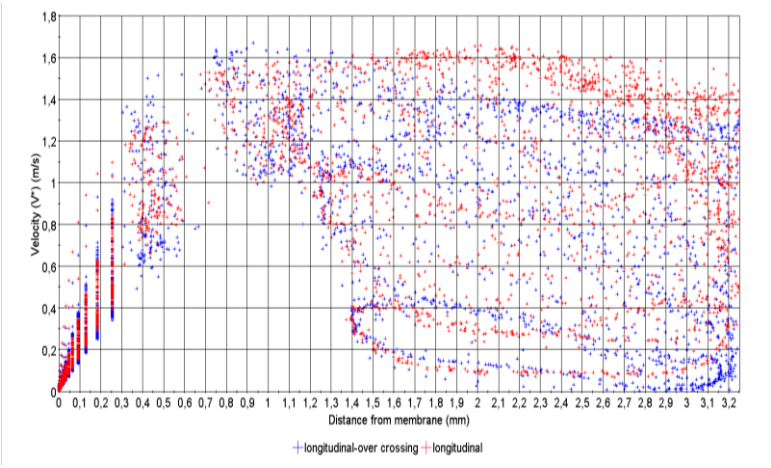

Case 12

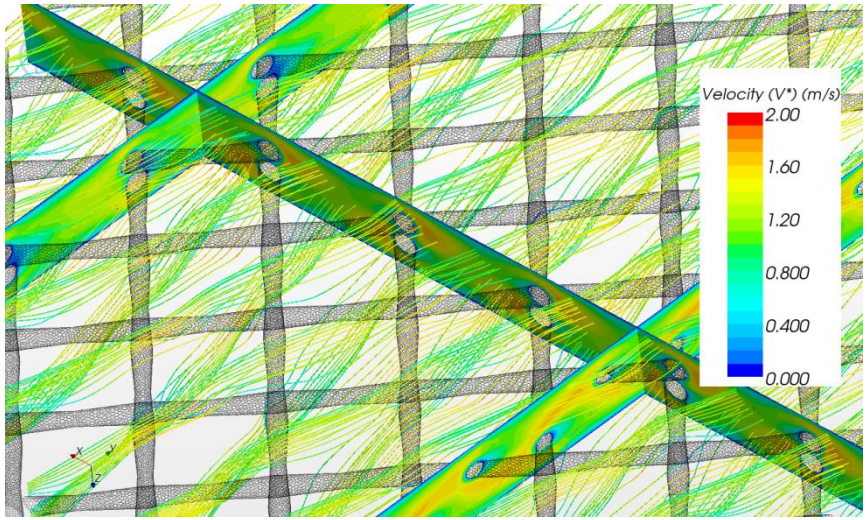

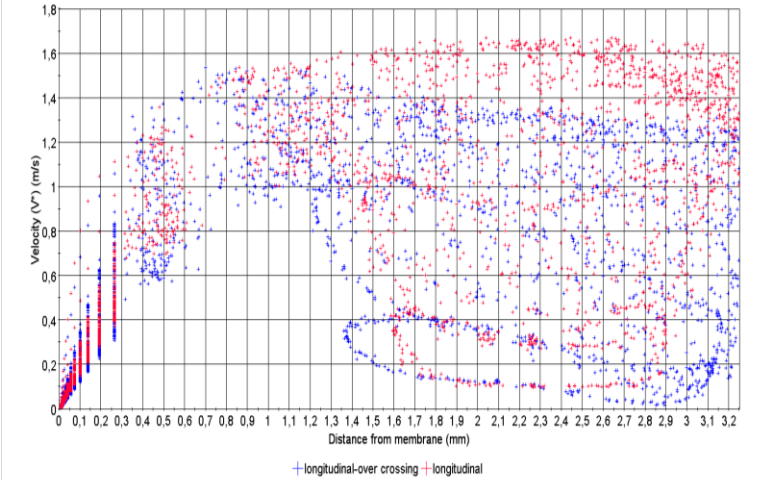

Case 13

Figure 4-11: Velocity contours, streamlines and velocity profiles for the two longitudinal cross sections (cases 4 ,11,12,13)-continued

Results from cases 12 and 13 are almost similar with flow in the later one having a smoother flow in the vertical and horizontal directions. The numerical efficiency indicator suggests that case 13 is more efficient.

Table 4-5: Average sheer stress and pressure drop (cases 11-13)

Cases	Average sheer stress (Pa)	Pressure drop per m length (Pa)	Sheer stress/pressure drop ($\times 10^3$)
4	3,02E-02	26,0	1,16
11	4,45E-02	49,6	0,9
12	2,49E-02	19,6	1,27
13	2,27E-02	17	1,33

4.1.2.5 Concluding remarks and future work

From previous results of cases 1 to 10, the flow of attack angle has a very minimum effect on the performance of spacers. All results of wall shear stress and pressure drop were very close to each other. When it comes to the spacer to channel thickness ratio, the numerical assessment criteria results suggest the lower ratio is the better; however, one should think that such numerical comparison is very qualitative. In practice, the selection of best case would include a trade-off between the cost of membranes needed to produce the required production and cost of electrical energy needed. Not only, the cost of membranes; with that comes number of MD modules, piping, fittings, etc. In all cases, the full channel spacer seems to be the least favorable, due to reduction in membrane area and higher pressure drop. In addition, the pressure in such case on specific location of the membrane will increase the high risk of membrane wetting. When it comes to the void ratio, the higher void ratio, the better the spacer is. Again, this based on the rough numerical indicator. A similar trade off is needed to make required selection.

Generally, the choice of higher spacer to channel thickness ratio should be accompanied with higher void ratio. Such combination would enhance the vertical and horizontal mixing of the flow with a relatively lower pressure drop compared to lower void ratio.

However, since the MD is a heat driven process, the previous results is not conclusive; rather than it serves as starting point for advanced work. The obvious next step is to fully model the heat and mass transfer; in particular the relation between the choice of spacer type and the channel length; in other words what type spacer would achieve the optimum ratio of evaporation to specific pumping power.

4.2 Cooling channel

The cooling channel in the existing MD module has another role beside the thermal one. It serves as a mechanical support for the MD cassettes. For that, the design is mainly depending on small rectangular channels, separated by ridges. The flow in each of these channels is separated from another, and each one has an inlet receiving the flow from the cassette upstream header and collected in the downstream header. The channel thickness to width ratio is 1. Figure 4-12 shows a schematic view of the cooling channel cassette (the specific details of the channel are not shown due to intellectual property rights).

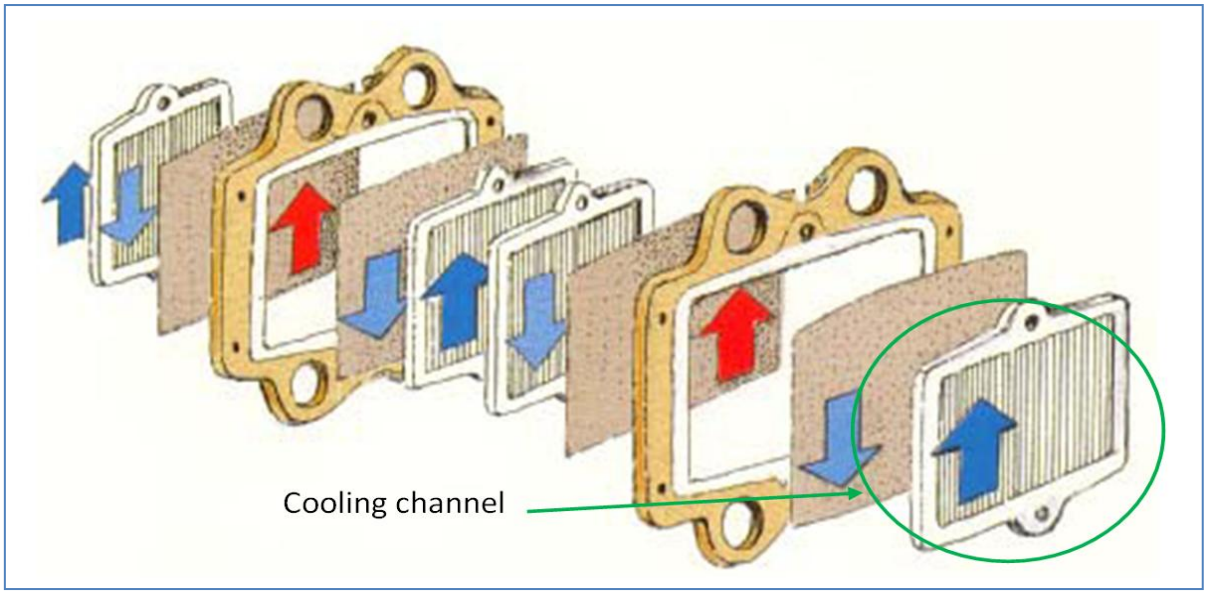

Figure 4-12: Schematic view of the cooling channel [courtesy of SCARAB Development AB]

The objective of this analysis is to examine the horizontal distribution in these channels and to assess the velocity boundary layer gradient. The number of mesh cells was 3,000,000 polyhedral with structured refinement close to the heat exchanging walls Inlet boundary layer was set to velocity boundary layer of average value in the four header inlets 0,611 m/s; and outlet boundary layer is set to atmospheric pressure.

Figure 4-13 shows the over view of the normalized velocity contours (normalized by the average inlet velocity of all the channels) along the flow channel. As it could be seen, the horizontal distribution is not uniform among the flow channels. Roughly, they are divided into three regions with different velocities (denoted by red circles).

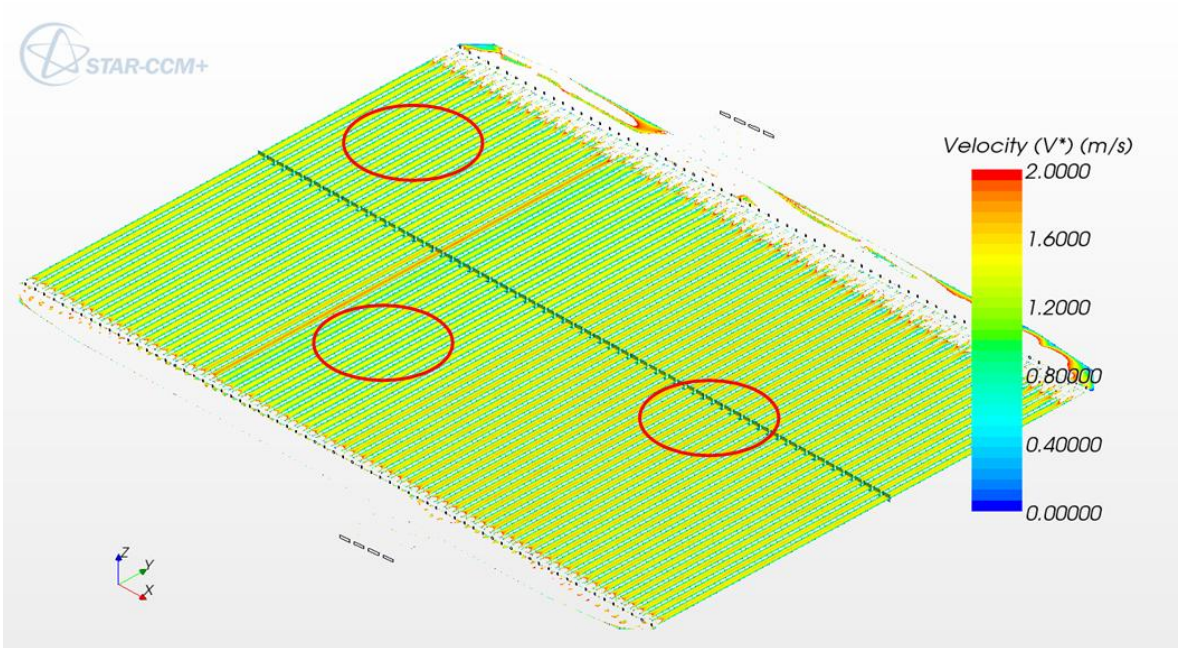

Figure 4-13: Normalized velocity contours along the flow channels cross section (general view)

Data extracted from several probe lines in these three regions for the normalized velocity along the channels' thickness (distance between the cooling plates) are plotted in Figure 4-14

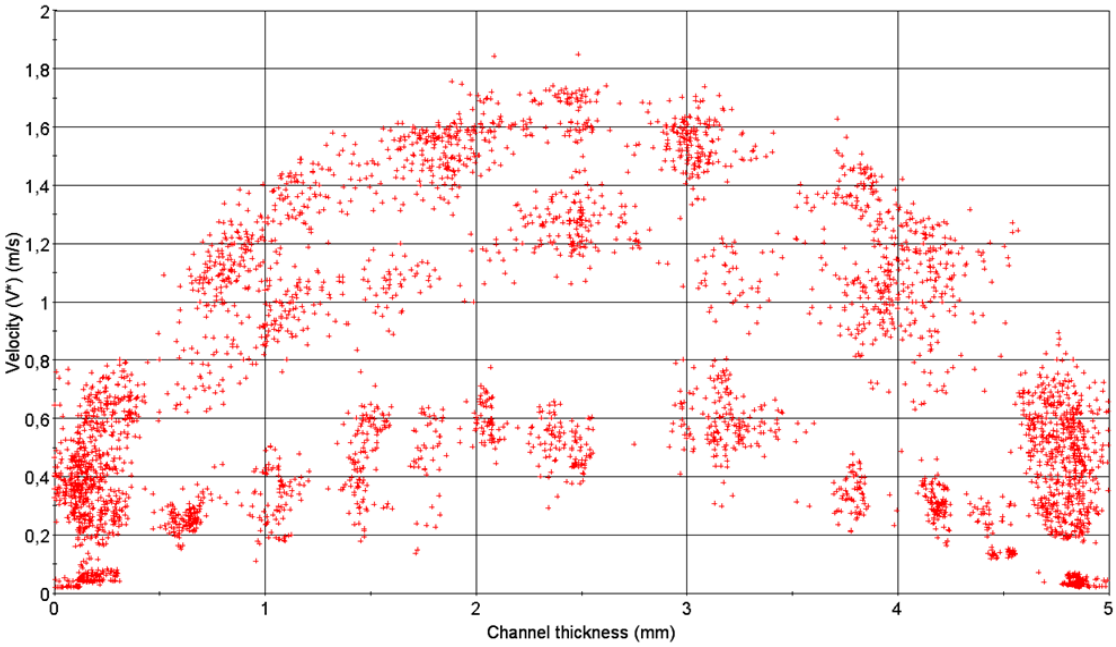

Figure 4-14: Normalized velocity profiles for probe lines representing the three different flow condition regions (data from the center of the flow channels)

The figure shows clearly the differences in the velocity profiles between these three regions, which indicate some degree of flow maldistribution. It must be noted that these velocity profiles corresponds to the center of the small flow channels which have the highest velocity gradient development. At the corners of the flow channels, the velocity profile development is significantly lower.

5 AGMD MODIFIED DESIGN (Appended paper IV)

As the MD is a heat driven process, several methods has been used to enhance heat transfer coefficient and reduces temperature polarization coefficient. To analyze the heat transfer mechanism, a cross section of AGMD cassette (Figure 2-2) is considered. Heat transfer from feed channel to cooling channel is carried out in four steps: (1) heat flux from the feed solution to the liquid-vapor interface across the thermally boundary layer in the feed channel (2) heat flux by conduction and latent heat of vaporization across the membrane; (3) heat transfer from the permeate side of the membrane to the condensation surface on condensation plate; (4) heat transfer from the condensation surface to the cooling liquid across the condensation plate and thermal boundary layer in the cooling channel.

The air-gap domain in AGMD configuration has the role of reducing the conductive heat losses through the membrane surface. Heat transferred from the air gap side of the membrane (*mp*) to the condensation interface is dependent upon the sensible heat flux (Q_S) and heat associated with mass transfer (Q_L) according to the following equation:

$$Q_T = (\frac{k_g}{b} + n_w C_g)(T_{mp} - T_{cf}) + n_w \lambda$$

where C_g is the specific heat at constant pressure in the gas phase of the water, n_w is the mass flux, λ is the latent heat of evaporation, k_g is the gas phase thermal conductivity and b is the air-gap width.

The first term of sensible heat comprises the conduction hear transfer and the second one is the sensible heat transferred by diffusing vapor. The later is relatively much smaller than the first. In the air gap, the vapor flow is affected by the natural convection and the relative importance of natural convection depends on Rayleigh number (Ra) [2005]. Alkalibi and Lior [2005] estimated that the natural convection is negligible in all typical AGMD configurations Ra is far below the critical value of 1000; and hence the heat transfer is mainly by conduction.

In all the theoretical models in AGMD, the assumption is made that the air gap domain is filled only air/vapor. However, in practice, the membrane must be supported or separated from the condensation surface by physical means. In trying to avoid the use of support in the lab test, small scale membrane areas have been considered [Khayet and Matsuura, 2011]. One way to support the membrane in plate-and-frame AGMD modules, small ridges or spacer could be used. These ridges can be built-in features of the condensation surface and hence made from the same material. These ridges/support, and despite their negative effect as they reduce the area of membrane and/or condensation surface; they act as a short cut or thermal bridge for thermal conduction. To illustrate this, Figure 5-1 shows a schematic presentation of such physical support in the air gap domain.

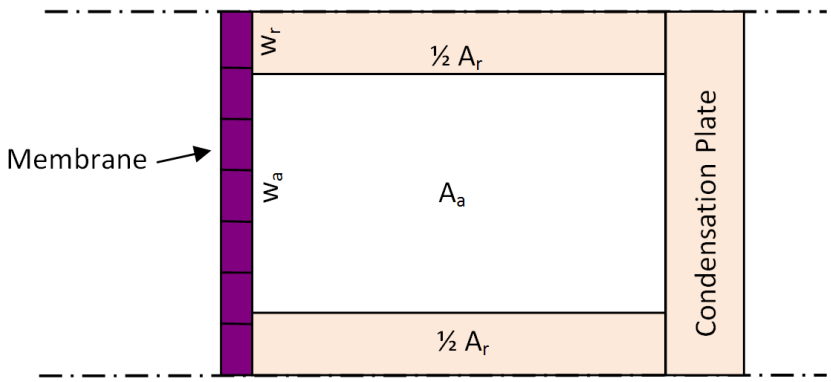

Figure 5-1: Schematic representation of air gap domain

Areas A_r and A_a represent the cross sections of the ridge and air-gap respectively, which are in contact with membrane with width w × ℓ (the length of the flow channel, i.e, the direction perpendicular to sketch). The relative relation of conduction heat transfer of air to the support ridges is defined by the following:

$$\frac{Q_a}{Q_r} = \frac{k_a}{k_r}\frac{A_a}{A_r}$$

where k_a and k_r are the thermal conductivities of the air/vapor and ridges respectively. The thermal conductivity of the air/vapor is more than one order of magnitude lower than the thermal conductivity of the ridge (in the case of ridge/condensation made of polypropylene (PP), covered in this study), which would require the cross sectional area of the air-gap to be 10 times more for the case of equal conduction shares. Such a case is practically impossible to deploy if the membrane deflection inside the air-gap should be minimized to maintain the designed air-gap thickness.

Figure 5-2 gives an indication of the percentage of heat conduction compared to total heat transferred, in the current module design. These figures are calculated from experimental results with saline feed of 35 g/l (MEDESOL project experimental work). The values range from 45 to 25 % roughly, which are quite high. It must be noted that these calculation is based on measurements in outdoor environment, where heat losses to the surroundings is varying depends on the ambient temperature and wind speed.

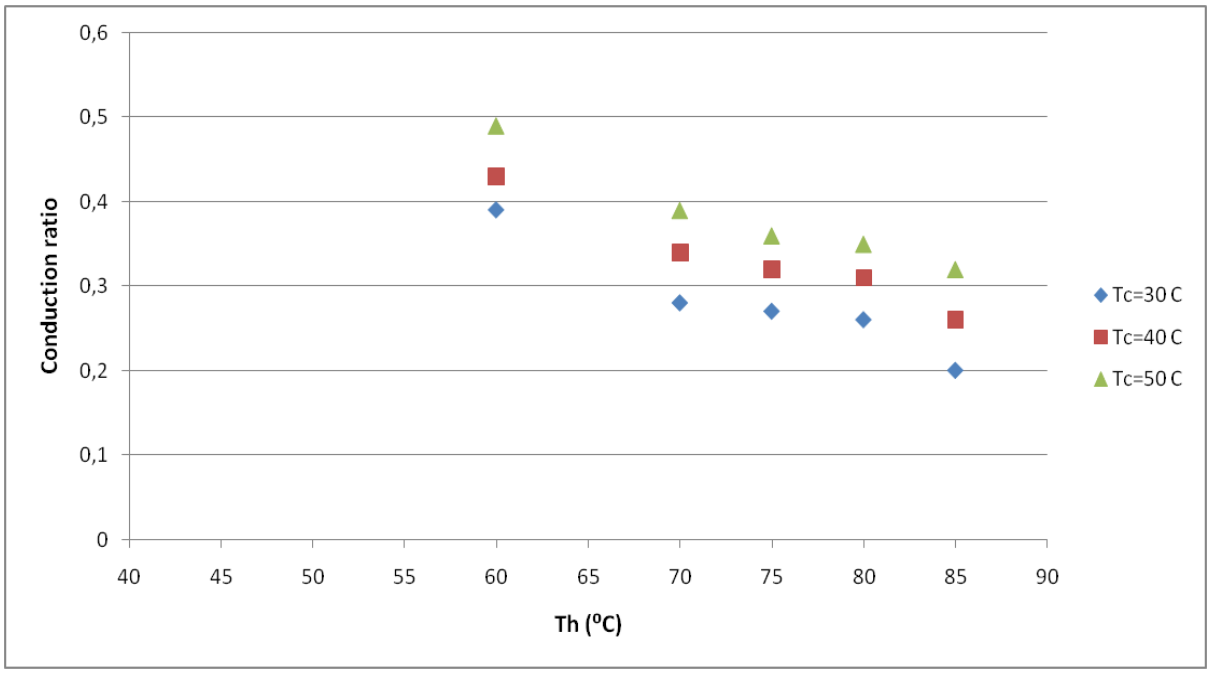

Figure 5-2: Conduction heat transfer ratio compared to total heat transfer (feed flow rate 20 l/min and salinity of 35 g/l)

The objective of the experimental work covered in this chapter, is to apply simple modifications on AGMD module in order to improve its performance. These modifications are bounded by the current module design limitations, which include the MD module global dimensions, feed and cooling flow channel thickness and condensation surface material. The main modifications were in the air-gap domain in order to lower the conduction heat transfer transported by the physical support (ridges). Moreover, several spacers that are used to promote flow mixing in the feed channel are tested.

5.1 Design consideration

5.1.1 Feed channel

As stated previously, the hydrodynamic conditions significantly affect the heat and mass transfer across the membrane. Spacers are used to affect the hydrodynamic conditions in flow channel in MD (as well as other desalination technologies like RO and UF) in terms of reducing the thermal and concentration boundary layers as well as enhancing the flow distribution perpendicular to direction of the flow, in addition to the basic task of separating the two membrane sheets forming the flow channel. The need for choosing optimized spacer is very crucial and depends on two main factors; maximum achievable mass transfer (i,e, lower thermal and concentration boundary layers and enhanced mixing) and lower induced pressure drop. The latter factor is crucial in maintaining the advantage of lower pumping power and hence minimizing electrical energy consumption. Two main types of spacers were used; small cell spacer (two spacers) and large cell spacer (*Table 5-1*).

5.1.2 Cooling channel

The cooling channel consists of 68 small square flow channels formed by molded PP ridges. These solid ridges reduce the area available for heat transfer by 10 %. Moreover, they contribute significantly to higher pressure drop, compared to flow channel with equivalent cross sectional area) due to high wetted perimeter. While these ridges are important to maintain a structural stability for the stacked cassettes, removing these ridges and replacing them with appropriate net type spacer could be a solution to address the hydrodynamic and thermal considerations and in the same time, provide the structural stability.

5.1.3 Distillate/air gap channel

The distillate/air gap channel consists of small channels form by several built in ridges (as described in the CFD part). These ridges serve as a support that separate the membrane surface from the condensation surface and thus form the air gap. In working conditions, the membrane sheet is pressed over the ridges and distillate channels are formed. The built-in ridges constitute a thermal short circuit for undesirable conductive heat transfer between the membrane and the condensation surface, with approximate area of 25 % of the membrane surface. However, only half of these ridges actually serve as conduction medium to the cooling channel, as the other half is connected to the ridges constituting the cooling flow channel/channels (see next section). These ridges were removed and replaced with a non woven net-type spacer with aim to reduce the area of the conductive medium by 75 %.While area of the membrane in contact with spacer (covered by the horizontal filaments) is reduced by 50%, the membrane effective area is still the same as the vertical filaments are in contact with condensing surface. Figure 5-3 shows a scheme of the employed spacer. The calculated conductive heat reduction is 30% of original.

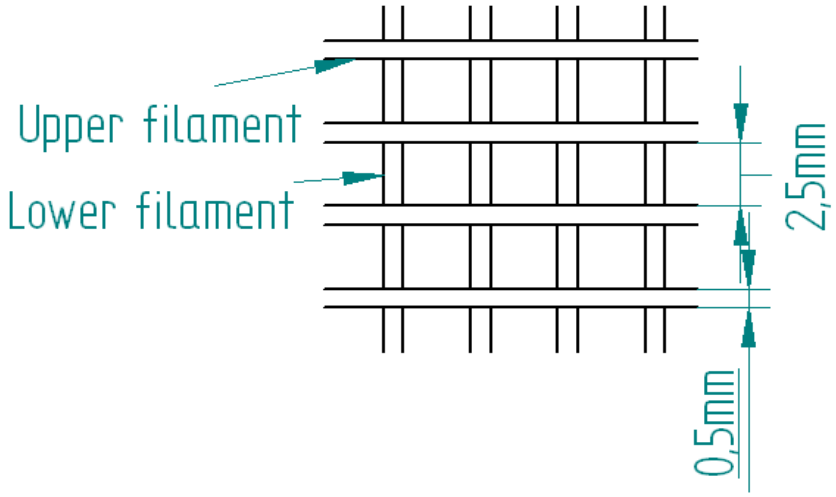

Figure 5-3: Schematic illustration of the net type spacer employed as membrane support in the condensation channel

5.2 Experimental work

5.2.1 Experimental set up

The test facility (Figure 5-4) comprises six-cassette AGMD module with total membrane area of 1,7 m^2. The cassette consists of injection molded plastic frames containing two parallel membranes, feed and exit channels for the warm water, and two condensing walls. Two sets of condensation/cooling channels plates were used; the original one for establishing a baseline for comparison and the modified one for testing the modified design. The membrane material is PTFE with a porosity of 80%, thickness of 0,2 mm, and average pore size of 0,2 micrometer. The width of air gap of AGMD is 1 mm. The size of module is 63 cm wide and 73 cm high. System control and primary data acquisition were handled via PLC connections to Citect Runtime software installed on a standard PC. Flow rates were measured by visual flow meters (accuracy ± 5%), temperatures were measured by Pt 100s (accuracy 0,2%) and differential pressure with differential pressure transmitters (accuracy 2,5 %). On site conductivity measurements were also introduced to check the instant bulk quality of the product water. Product water flow rate was determined manually. Feed and cooling flow rates were identical for both sides in all sets of experiments. Tap water of 300-400 µS/cm of conductivity was maintained in the experiments; distillate conductivity was 1-3 µS/cm.

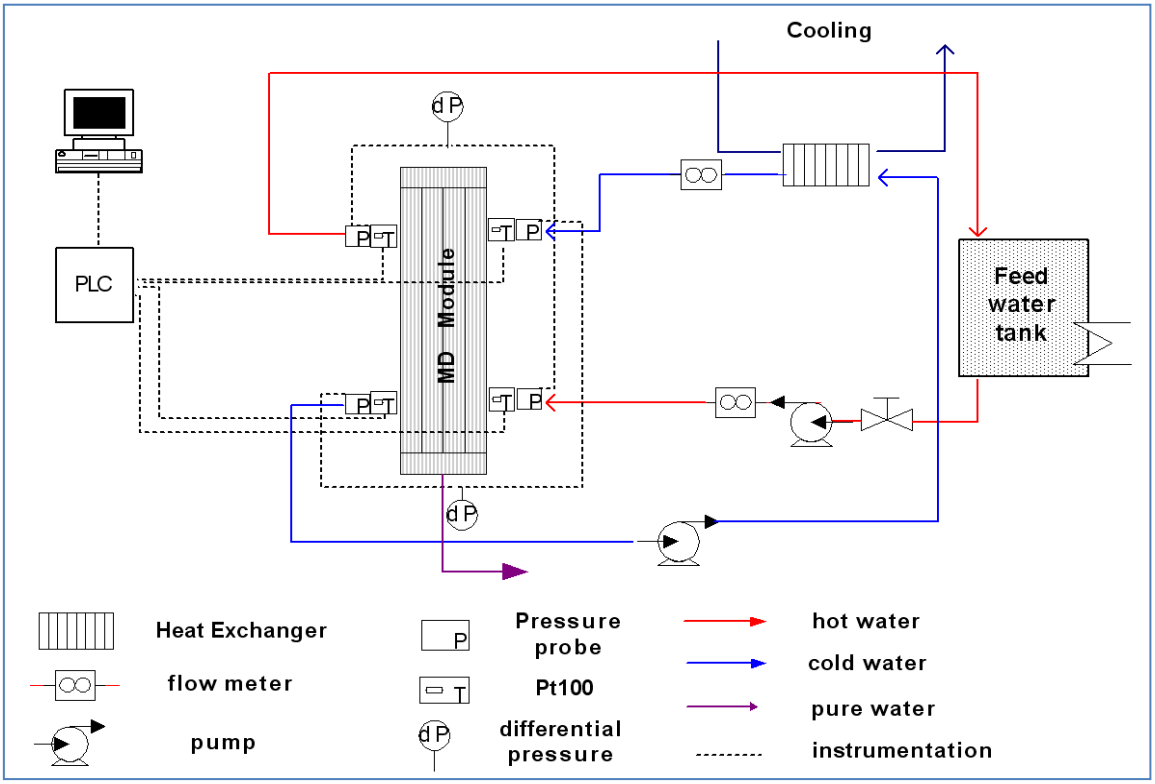

Figure 5-4: Schematic illustration of the test rig

Experimental work on several configurations was divided into three main stages:

- Experiment to evaluate the effect of replacing the solid ridges with spacers in the condensation/air gap and cooling channel.
- Spacers' experiments: aims at choosing the optimum spacer in terms of maximum mass transfer and lower pressure drop (among available spacers).
- Based on results obtained from the above stages, a combined experiment was performed on the favorable configuration.

5.2.2 Experimental results

In all experiments, results were scaled up for standard MD unit of 10 cassettes.

5.2.2.1 Original versus modified condensation/air gap experiment

Experiments were conducted for both case at the same operation condition, feed and cooling flow rates, temperature and similar type of spacers in the feed/hot channel (spacer 2 in *Table 5-1*). Figure 5-5 shows the results.

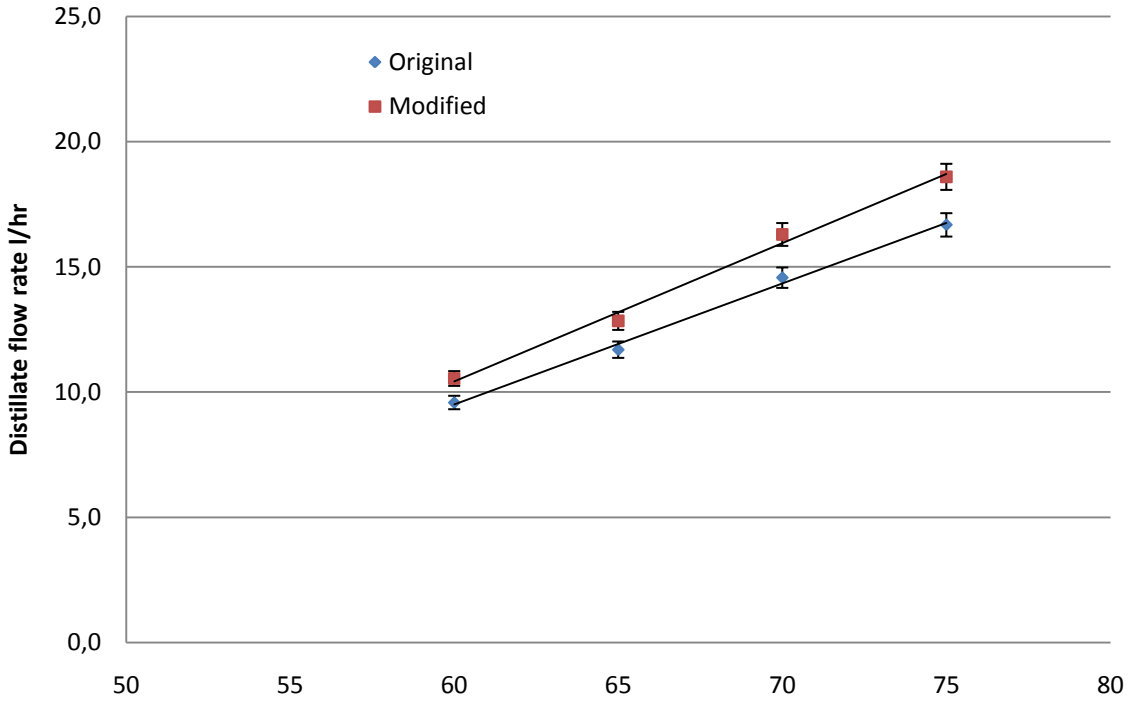

Figure 5-5: Experimental results for original Vs modified designs (flow rate of 20 l/min (1200 l/hr), cooling water inlet at 25 ⁰C); error bars depict combined uncertainty

As shown in the figure, the modified configuration is 9 to 11 % higher in distillate flow rate compared with original. These results indicate the effects of reducing the temperature loss along the feed/hot channel caused by conductive heat transfer; hence, increased vaporization caused by partial pressure difference.

Figure 5-6 shows the thermal efficiency for both original and modified design at varying feed temperatures. The thermal efficiency is defined as:

$$\eta = \frac{Q_L}{Q_T}$$

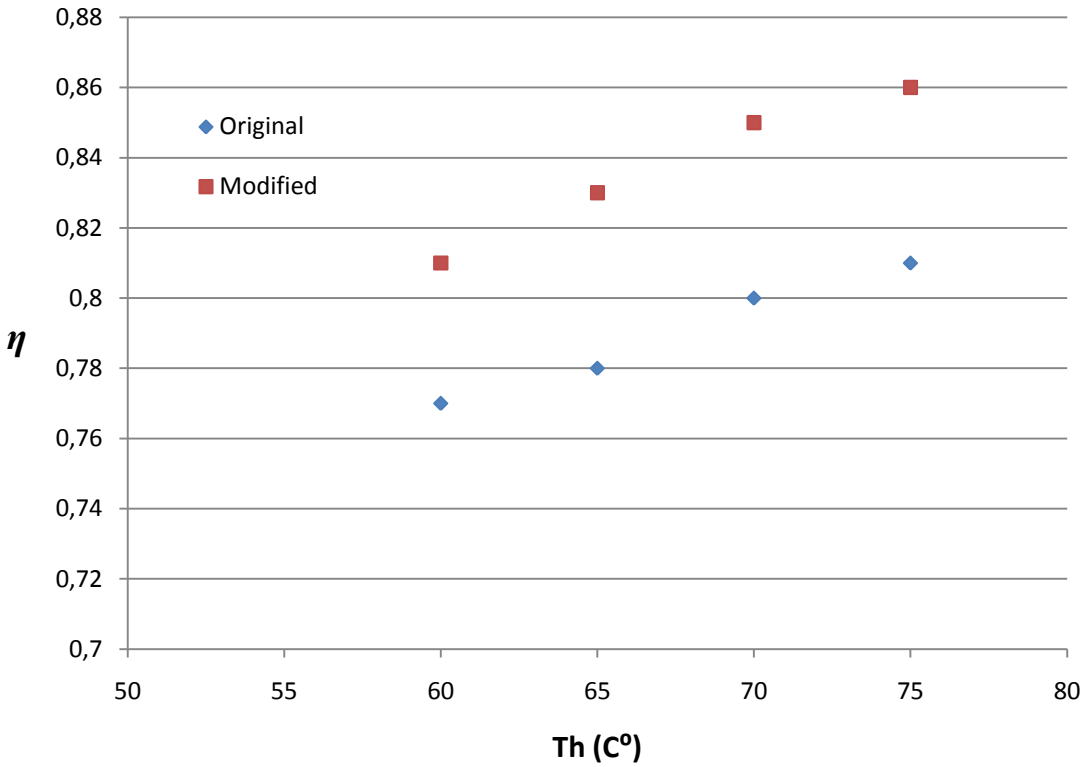

Figure 5-6: Thermal efficiency for original Vs modified designs (flow rate of 20 l/min (1200 l/hr), cooling water inlet at 25 °C)

The thermal efficiency increases (i.e, conductive heat transfer ratio decreases) with the increase in feed inlet temperature in both cases as known, due to the fact that the rate of increase of latent heat of evaporation is higher, compared to heat transferred by conduction. The thermal efficiency increased by 6 % approximately, corresponding to 20-24 % conductive heat transfer reduction compared to the original design.

5.2.2.2 Spacers experiment (in hot channel)

Table 5-1 presents the geometrical details of three different spacers. Spacer 2 represents the original spacer adopted by the manufacturer of the current module. In addition, in one case, the membrane sheet was switched so the backing side (PP backing material) was on the flow channel side. This case was tested mainly to check the performance if applied. The backing side is physically and thermally less affected by the friction caused by the spacer body, which might damage the membranes. However, such surface is less smooth than the typical side, which may increase the risk of fouling.

Table 5-1: Geometrical characteristics of the spacer used in experiments

Spacer	Filament diameter (mm)	cell size (mm)	Flow of attack angle (°)	Void ratio
1	1,2-2 (varying)	11×11	45	≈86
2	0,75	3×3	≈37	80
3	1	3,5×3,5	≈35	78

To use approximately similar spacer to flow channel thickness ratio, one element of spacer 1 was used, three of spacer 2 and 2 of spacer 3. Figure 5-7 illustrates the scaled experimental results in terms of distillate flow rate at different feed temperatures.

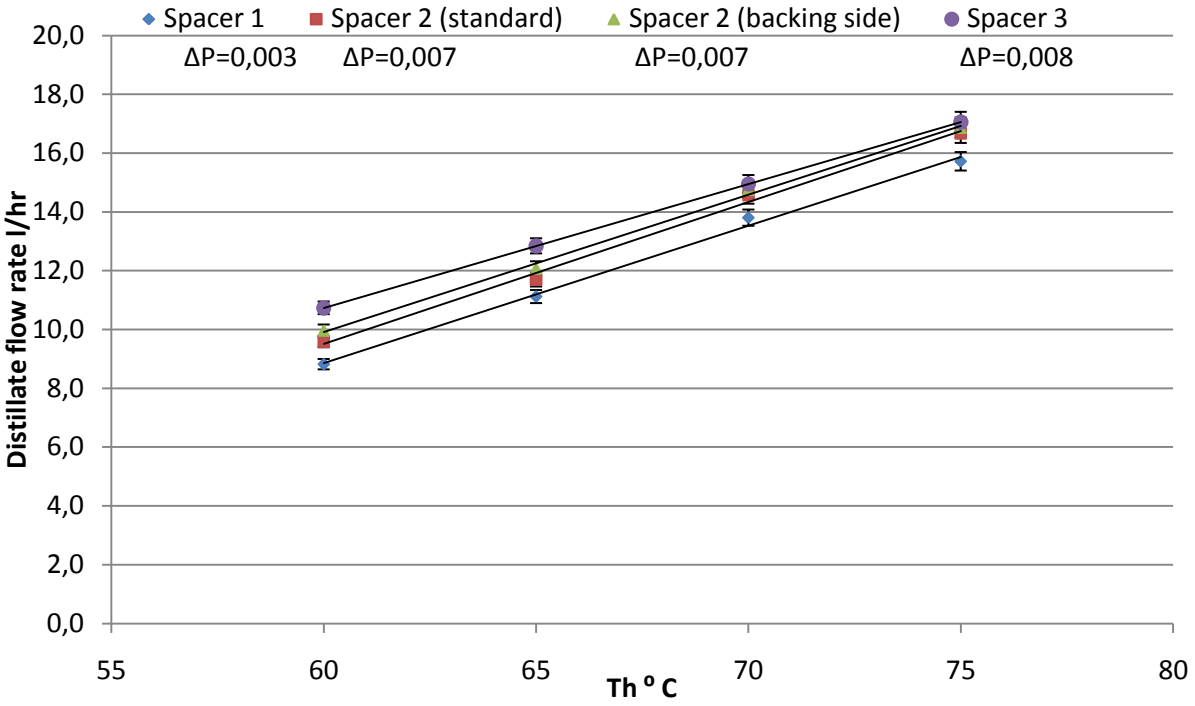

Figure 5-7: Experimental results for different spacers (flow rate of 20 l/min (1200 l/hr), cooling water inlet at 25 ° C); error bars depict combined uncertainty

As shown, spacer 1 and 2 (spacer 2 with backing side of the membrane) have almost the same linear slope while spacer 3 has lower one. Spacer 3 achieved the best result in term of distillate flow rate especially at low feed temperature. However, the pressure drop is significantly higher compared to spacer 1. Spacer 2 with backing side has achieved slightly better performance compared with the original case. While spacer 1 has a lower performance in terms of distillate flow rate, it has the significantly better performance in term of pressure drop. Spacer 1 has 8 to 18 % lower distillate production, but has a significantly reduced pressure drop. It should be noted that these pressure drops include the pressure drop from the module header and the cassette flow distribution header.

5.2.2.3 Combined experiments

The previous results indicate that the effect of reducing the pressure drop (and hence electrical consumption) is much larger than increasing the distillate flow rate, and hence has more

weight in choosing the desired configuration. The favorable choice would be using spacer number 1 (in both hot and cooling channels) with the modified condensation/cooling channel design in combined experiment configuration. The set of experiments were performed with varying feed/hot channel and cooling temperatures; and varying feed and cooling temperature (while maintain similar flow rates on both sides in each case). Figure 5-8 summarizes the performance of the configuration at varying flow rates. It must be noted that the flow rates appear in the figure below are for the whole module which have 10 feed flow channels which means that the feed flow rates must be divided by 10 to obtain the flow rate in each feed channel.

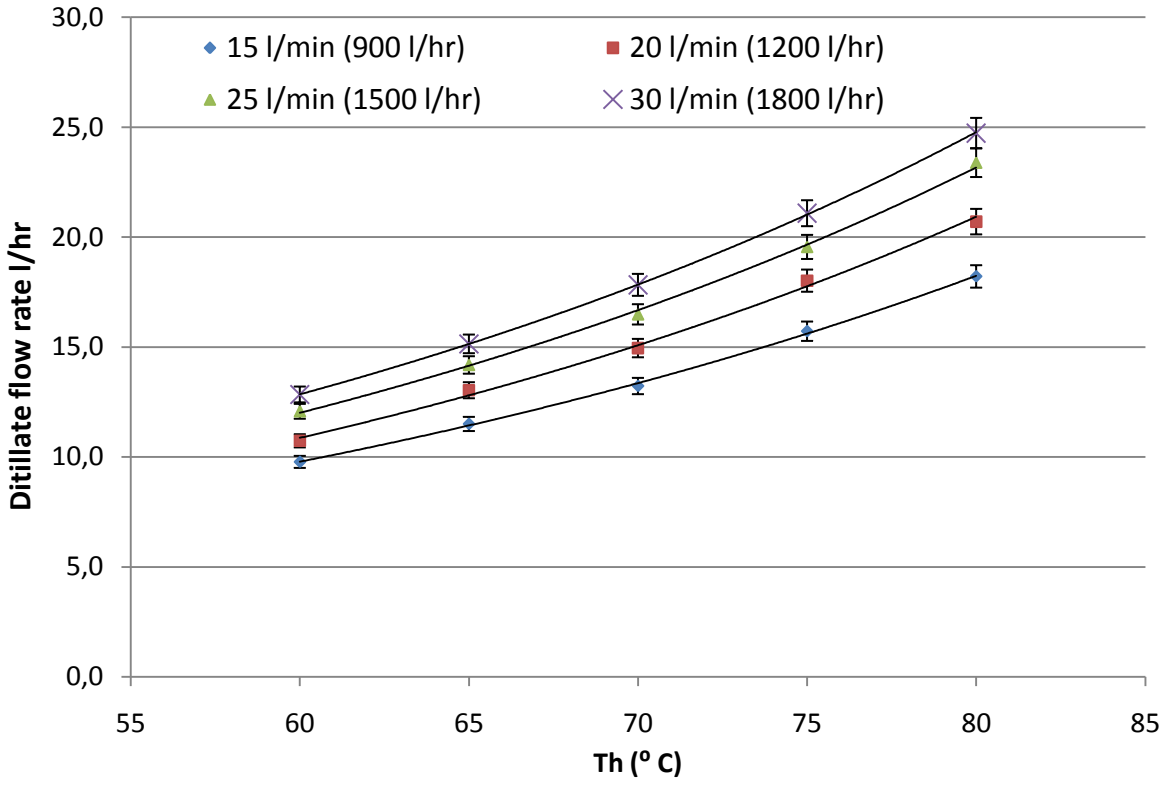

Figure 5-8: Experimental results for the modified configuration at varying feed flow rates and temperature (cooling water inlet at 25 °C); error bars depict combined uncertainty

The results indicate a slightly-curved increasing trend for 25 l/min and 30 l/min feed flow rates as the inlet temperature increases, while almost linear for lower flow rates. Such results confirm with the expected trend since the vapor pressure increases exponentially with temperature. However, the curvature is significantly lower than the theoretical one which indicates the high effect of thermal boundary layer (the average linear velocity is one order of magnitude compared with the ones used in most theoretical models). At low feed temperatures, the differences in distillate production are almost constant, and increase as the feed inlet temperature increases. However, the rate of increase for such differences decreases between each successive flow rates. As expected, such increase in flow rate would reach a maximum until the effect diminishes. Understanding these results and with comparison with pressure drop is crucial in adopting the optimized flow rate at certain temperatures available in real applications. Figure 5-9 shows the corresponding thermal efficiency for the varying feed flow rates.

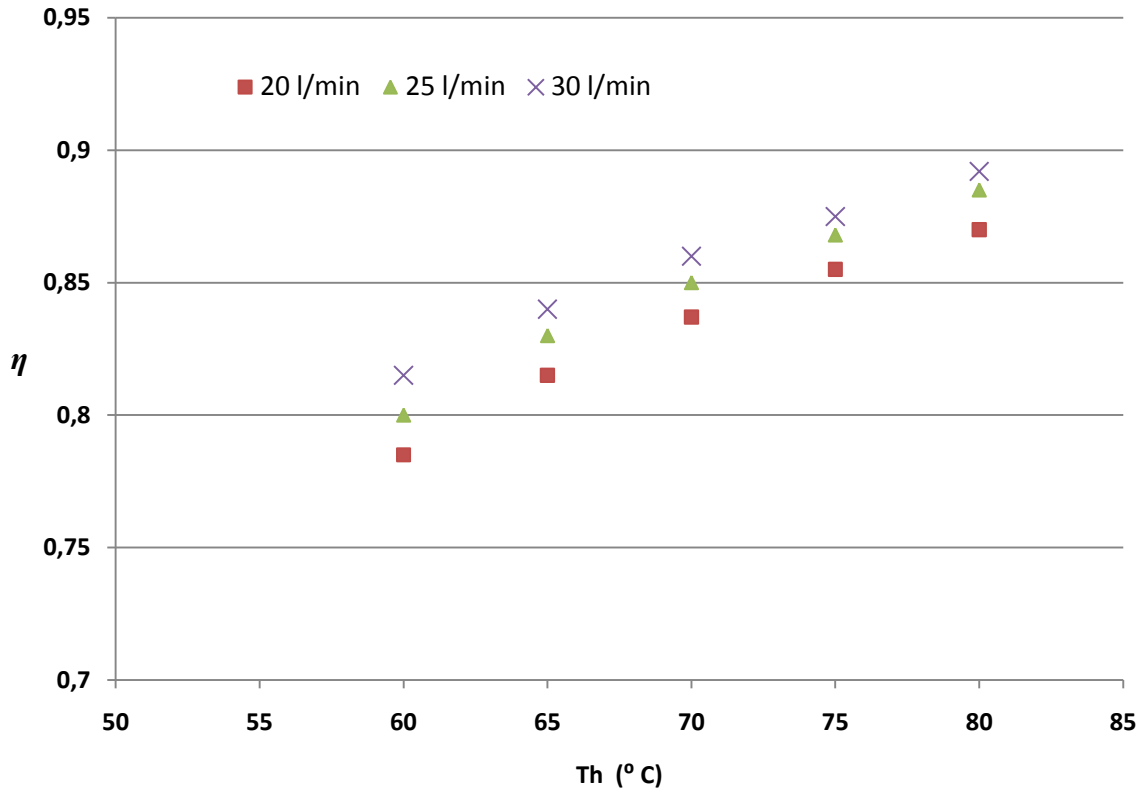

Figure 5-9: Thermal efficiency for modified design at varying feed flow rates and temperature (cooling water inlet at 25 °C)

The efficiency increases with increasing flow rates as the thermal boundary layer in the feed and cooling channel (mainly the feed) decreases, meaning higher actual temperature (lower temperature difference across the membrane. The difference in efficiencies at low feed temperature is slightly higher indicating the relative effect of increasing the flow rate (linear velocity) at lower feed temperatures, on thermal efficiency. It must be noted that calculating the thermal efficiency at feed flow rate of 15 l/min was not possible as the outlet temperatures were unstable. The reason for that is related to the fluctuating partial flow in the pipes hosting the temperature sensor.

Figure 5-10 shows the distillate production as a function of temperature difference between feed/hot and cooling inlets, at different feed temperatures.

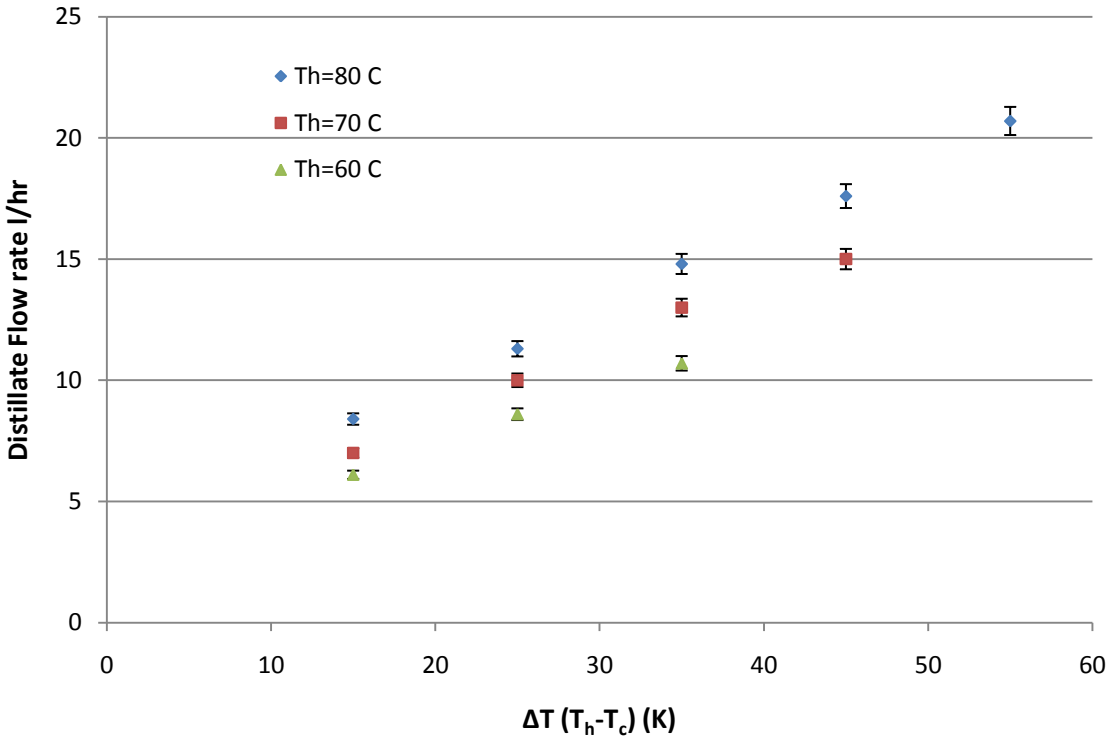

Figure 5-10: Experimental results for distillate production in relation to temperature difference at different feed inlet temperatures (feed and cooling flow rates of 20 l/min); error bars depict combined uncertainty

The results show the higher distillate production at higher feed inlet temperatures for the same temperature difference. A moderate increase in such difference of distillate production is maintained as the ΔT increases, which lay in the expected theoretical pattern. Such result shows a less effect of the thermal boundary layer compared to the original design.

5.3 Concluding remarks

The previous experiments show a possibility of a slight improvement in thermal energy efficiency with small modifications within the boundaries of geometry and material. Such improvement came as a result of reducing the conductive heat losses, and increasing the area available for heat transfer in general. Since the module was not originally designed with internal heat recovery, a further increase of energy efficiency would be limited.

In this specific case of module design (no internal heat recovery), the effect of spacer geometrical characteristics on the thermal performance is very minor regardless the variation. However, the corresponding pressure drop is significantly large. To put these results in perspective, the modified design was employed in assessment of energy consumption of the thermal cogeneration application (section 3-1). Table 5-2 summarizes the results for case II in Table 3-4, compared with the new calculation made based on the modified design for the same case.

Table 5-2: Comparison of main assessment parameter for application in cogeneration (original vs modified design)

Parameter	Case II	Case II(modified)
Pure water output (m^3/h)	10	10
Specific thermal energy consumption (kWh_t/m^3)	12,1	11,5
Specific electricity consumption (kWh_e/m^3)	0,6-0,7	0,2-0,3
Membrane area (m^2)	1141	1045

The reduction in thermal energy consumption is insignificant, particularly in such specific application where heat is recovered back into the cogeneration plant; the specific thermal energy consumption is low anyway. The main significant reduction is the electrical energy consumption needed for the pumping which is reduced to one third of the original figure. Such reduction, would allow utilizing a higher feed flow that significantly reduce the membrane area (and hence number of modules) with maintaining the original specific power consumption, which is also low in the original case.

6 CONCLUSION AND FUTURE WORK

6.1 Conclusions

The performance of MD in industrial scale application varies depending on the application. Full-scale experimental simulations for a 10 m^3/hr water treatment capacity system in a thermal cogeneration plants, were performed. Specific thermal energy consumption ranged from 5 to 12 kWh/m^3; specific electricity consumption ranged from 0,6 to 1,5 kWh/m^3 for two different scenarios. When MD is utilized in cogeneration or industrial facilities, the possibility of integrating the technology with available heat sources and sinks would support the positive assessment of the technology from energetic point of view. The economy part in the assessment hinders the possibility of employing it on large scale. The cost of water for the system studied was calculated to be 14-20 SEK/m^3 (2-2,8 \$/m^3). However, as such economy is strongly related with the high capital cost associated with current phase of MD module production and high costs of membrane; the possibility of significant cost reduction relies on mass production of modules and availability of suitable membranes at low cost.

When the technology is employed in a solar system, the picture is significantly different. Experimental-based simulations of a three step MD system of two layouts were employed to assess the heat demand. Specific thermal energy consumption was 950 kWh_t/m^3 for the layout without heat recovery, and 850 kWh_t/m^3 for the layout with partial heat recovery. The lack of internal heat recovery in the current MD module means that most of the heat supplied to MD system is not recovered and hence, the thermal energy consumption is high. This would mean that a large solar field is needed.

CFD analysis was used as a tool to analyze the flow conditions in both hot feed channel (spacer analysis) and cooling channels. The analyzed cases for the feed channel represent specific spacer geometry types; flow of attack angle, spacer to channel thickness ratio and void ratio. Results showed that the flow of attack angle has little or no dependency on this parameter. When it comes to the spacer to channel thickness ratio, the selection of best case would include a trade-off between achieving high wall sheer stress and pressure drop. In all cases, the full channel spacer seems to be the least favorable, at least in case of flat plate MD configurations. When it comes to the void ratio, similar trade off is needed to make required selection. As the void ratio increases, the vertical mixing increases. Generally, the choice of higher spacer to channel thickness ratio should be accompanied with higher void ratio. Such combination would enhance the vertical and horizontal mixing of the flow with a relatively lower pressure drop compared to lower void ratio.

Modifications aiming to improve the flow conditions in the hot and cold channels and to reduce the conductive heat losses were tested. The experimental results show a slight improvement in thermal energy efficiency (6 %) as a result of reducing the conductive heat losses. In addition, an average of 10 % increase in the module production flow rate was achieved at the same operation conditions. In this specific case of module design (no internal heat recovery), the effect of spacer geometrical characteristics on the thermal performance is very minor regardless the variation; hence, the choice should be for the spacer that impose the lower pressure drop.

6.2 Concluding remarks and future work

Possible implementation of MD technology in the near term would first require the resolution of a few issues. The permeate flux is relatively low comparing with the recirculation rate, which has a negative impact on the electricity consumption. To be able to overcome this problem, appropriate redesign of the module that takes in account enhancing the mass transfer and increasing the membrane area per module volume (compactness) is needed. With current performance, MD utilization would only be feasible in small scale application, where it could be thermally integrated with other process, or in application for treatment of special feed stock (such as landfill leachate) and where other treatment process has a limited capacity in terms of treated water quality.

Utilizing CFD in designing AGMD module dimensions and their interactions with operation conditions would be an area that can move the technology forward, in terms of module design. Fully modeling the heat and mass transfer; in particular the relation between the choice of spacer type and the channel length; in other word what type spacer would achieve the optimum ratio evaporation to specific pressure drop.

A further fundamental study of the module design will eventually have a significant effect on flux enhancement and potentially, increase the technology efficiency. Though it was not part of the experimental nor CFD work included in this thesis, a main area which the author believe would significantly improve the technology in general is in the membrane design. As most of the membrane used for MD are originally made for a different type of water treatment (UF), developing new membranes specifically for MD which take in consideration the need for low surface energy, low tortuosity and higher chemical and mechanical stability, would boost the industrial realization of the technology.

REFERENCES

Alklaibi, A; Lior, N; 2004
"Membrane-distillation desalination: status and potential"
Desalination 171 (2004) 111-131.

Alklaibi, A; Lior, N; 2006
"Heat and mass transfer resistance analysis of membrane distillation"
Journal of Membrane Science 282 (2006) 362–369.

Al-Obaidani, S; Curcio, E; Macedoniob, F; Di Profiob, G; Al.Hinaid, H; Drioli, E; 2008
"Potential of membrane distillation in seawater desalination: Thermal efficiency, sensitivity study and cost estimation"
Journal of Membrane Science 323 (2008) 85–98

Al-Shammiri, M.; Safar, M; 1999
"Multi-effect distillation plants: state of the art"
Desalination 126 (1999) 45-59

Axby, F.; 1998
"Avsaltning av varmt rökgaskondensat med Membranteknik"
VÄRMEFORSK Service AB, (1998) Stockholm.

Axby, F; Ekengren. O, Bjurhem, J-E; 2004
" Avancerad rening av rökgaskondensat"
VÄRMEFORSK Service AB, (2004) Stockholm.

Banat, F; Simandl, J; 1994
"Theoretical and experimental study in membrane distillation"
Desalination Vol. 95 (1994) pp. 39–52.

Chernyshov, M.N; De-Haan, A.B; Meindersma, G.W; 2003
"Modelling temperature and salt concentration distribution in membrane distillation feed channel"
Desalination 157 (2003) 315–324.

Cipollina, A; Di Miceli, A; Koschikowski, J; Micale, G; Rizzuti , L; 2009
"CFD simulation of a membrane distillation module channel"
Desalination and water treatment 6 (2009) 177-183

Criscuoli, A; Drioli E; 1999
"Energetic and energetic analysis of an integrated membrane desalination"
Desalination 124 (1999) 243–249.

Da Costa, A.R.; Fane, A.G.; Fell, C.J.D; Franken, A.C.M; 1991
"Optimal channel spacer channel spacer design for ultrafiltration"
Journal of Membrane Science 62 (1991) 275-291.

Da Costa, A.R.; Fane, A.G.; Wiley, D.E; 1994

"Spacer characterization and pressure drop modeling in spacer-filled channels for ultrafiltration"
Journal of Membrane Science 87 (1994) 79-98

Darwish, M.A.; Al-Najem, N.M; 2000
"Energy consumption by multi-stage flash and reverse osmosis desalters"
Applied Thermal Engineering 20 (2000) 399-416

Dhahbi, M; Bouguech, S; Chouik, R; 2002
"Numerical study of the coupled heat and mass transfer in membrane distillation"
Desalination 152 (2002) 245-252

Drioli, E; Wu, Y; 1985
"Membrane distillation: an experimental study"
Desalination 53 (1985) 339–346

Ding, Z; Liu, L; Liu, Z; Ma, R;
"Fouling resistance in concentrating TCM extract by direct contact membrane distillation"
Journal of Membrane Science 362 (2010) 317-325

El-Bourawi, M.S; Ding, Z; Ma, M; Khayet, M; 2006
"A framework for better understanding membrane distillation separation process"
Journal of Membrane Science 285 (2006) 4–29

El-Dessouky, Ettouney, H; Al-Fulaij, H.; Mandani, F.; 2000
"Multistage flash desalination combined with thermal vapor compression "
Chemical Engineering and Processing, 39 (2000) 343-356

Ettouney, H.; 2004
"Visual basic computer package for thermal and membrane desalination processes"
Desalination 165 (2004) 393-408

Fimbres-Weihs, G.A.; Wiley, E; 2007
"Numerical study of mass transfer in three-dimensional spacer-filled narrow channels with steady flow"
Journal of Membrane Science 306 (2007) 228-243

Goldschmidt, B; Ekdahl, E; Hellman, M; 2009
"Utvärdering av erfarenheter av membranteknik för rening av rökgaskondensat"
VÄRMEFORSK Service AB, (2009) Stockholm

Gray, S; Zhang, J; Dow, N; Duke, M; Ostarcevic, E; Li, J; 2010
"Identification of material and physical features of membrane distillation membranes for high performance desalination"
Journal of Membrane Science 349 (2010) 295–303

Gryta, M.; 2002
"The assessment of microorganism growth in the membrane distillation system"
Desalination 142 (2002) 79–88

Gryta, M.; 2005
"Long-term performance of membrane distillation process"
Journal of Membrane Science 265 (2005) 153–159.

Gryta, M; Barancewicz, M; 2010
"Influence of morphology of PVDF capillary membranes on the performance of direct contact membrane distillation"
Journal of Membrane Science 358 (2010) 158–167

Gryta, M; Karakulski, K; 1999
"The application of membrane distillation for the concentration of oil–water emulsions"
Desalination Vol 121 (1999) 23–29.

Gryta, M; Karakulski, K; 2005
"Water demineralisation by NF/MD integrated processes"
Desalination 177 (2005) 109-119

Gryta, M; Tomaszewska, M; Karakulski, K; 2006
" Wastewater treatment by membrane distillation"
Desalination 198 (2006) 67-73.

Guillén-Burrieza, E; Blanco, J; Zaragoza, G; D-C, P; M, W; 2011
"Experimental analysis of an air gap membrane distillation solar desalination pilot system"
Journal of Membrane Science 379 (2011) 386-396.

Hsu, S. T; Cheng, K. T; Chiou, J. S; 2002
"Seawater desalination by direct contact membrane distillation"
Desalination, 143 (2002) 279-287.

Izquierdo-Gil, M.A; Garcia-Payo, M.C; Fernandez-Pineda, C; 1999
"Air gap membrane distillation of sucrose aqueous solutions"
Journal of Membrane Science 155 (2) (1999) 291–307

Judd, S.; Jefferson, B.; 2003 Ed.
"Membranes for Industrial Wastewater Recovery and Re-use"
Elsevier Advanced Technology, The Boulevard, Langford Lane, Kidlington, Oxford OX5 lGB, UK (2003) ISBN 1-8561 7-389-5

Jönsson, A.S; Wimmerstedt, R; Harrysson, A.C; 1985
"Membrane distillation -- A theoretical study of vaporation through microporous membranes"
Desalination, 56 (1985) 237-249.

Karagiannis, Ioannis C.; Soldatos, Petros G.; 2008
"Water desalination cost literature: review and assessment"
Desalination 223 (2008) 448–456

Khayet, M.; J.I. Mengual; 2004
"Effect of salt concentration during the treatment of humic acid solutions by membrane distillation"
Desalination 168 (2004) 373–381

Khayet, M; Mengual, J; Matsuura, T; 2005
"Porous hydrophobic/hydrophilic composite membranes: application in desalination using direct contact membrane distillation"
Journal of Membrane Science 252 (2005) 101–113.

Khayet, M; Matsuura, T; 2011
"Membrane Distillation-Principles and application"
Elsevier B.V., Oxford, UK, 2011.

Kimura, S.; S.I. Nakao, S.I. Shimatani; 1987
"Transport phenomena in membrane distillation"
Journal of Membrane Science 33 (1987) 285–298.

Kubota, S; Ohta, K; Hayano, I; Hirai, M; Kikuchi, K; Murayama, Y; 1988
"Experiments on seawater desalination by membrane distillation"
Desalination 69 (1988) 19-26

Koutsou, C.P.; Yiantsios, S.G.; Karabelas, A.J; 2007
"Direct numerical simulation of flow in spacer-filled channels: Effect of spacer geometrical characteristics"
Journal of Membrane Science 291 (2007) 53–69

Koutsou, C.P.; Yiantsios, S.G.; Karabelas, A.J; 2009
"A numerical and experimental study of mass transfer in spacer-filled channels: Effects of spacer geometrical characteristics and Schmidt number"
Journal of Membrane Science 326 (2009) 234–251

Kullab, A.; Martin, A.; 2007
"Membrane Distillation and Applications for Water Purification in Thermal Cogeneration - Pilot Plant Trials"
VÄRMEFORSK Service AB, (2007) Stockholm.

Kullab, A.; Liu, C.; Martin, A; 2005
"Solar Desalination Using Membrane Distillation – Technical Evaluation Case Study"
International Solar Energy Society Conference, Orlando, FL, August 2005.

Lawson, K.W.; Lloyd, D.R; 1997
"Membrane distillation Review"
Journal of Membrane Science 124 (1997) 1–25

Li, F; Meindersma, W; de Haan, A.B.; Reith, T; 2005
"Novel spacers for mass transfer enhancement in membrane separations"
J. Membr. Sci. 253 (2005) 1–12

Li, J; Li, Y; Wai, N; Wong, F; Khaing, K; 2010
"Feasibility study on petrochemical wastewater treatment and reuse using a novel submerged membrane distillation bioreactor"
Separation and Purification Technology. 74 (2010). 138–143

Liu, C.; Martin, A.; 2005
"Membrane Distillation and Application for Water Purification in Thermal Cogeneration- A Pre-study"
VÄRMEFORSK Service AB, (2005) Stockholm.

Mandani, F; Ettouney, H; El-Dessouky, H; 2000
"LiBrî—¸H2O absorption heat pump for single-effect evaporation desalination process"
Desalination 128 (2000) 161-76

Martínez, L; Florido-Díaz, F.J; 2001
"Theoretical and experimental studies on desalination using membrane distillation"
Desalination 139 (2001) 373-379.

Meindersma, G.W; De-Haan, A.B; Guijt, C.M; 2006
Desalination and water recycling by air gap membrane distillation"
Desalination 187 (2006) 291-301.

Peng, P; Fane, A; Li, X; 2005
"Desalination by membrane distillation adopting a hydrophilic membrane"
Desalination 173 (2005) 45–54.

Phattaranawik, J; Jiraratananon , R; Fane, A.G., 2003
"Effects of net-type spacers on heat and mass transfer in direct contact membrane distillation and comparison with ultrafiltration studies"
Journal of Membrane Science 217 (2003) 193–206

Ribeiro, J.; 1996
"Desalination Technology: Survey and Prospect"
Institute for Prospective Technological Studies, European Commission Joint Research Center, EUR 16434 E.

Schneider, K.; W. Holz; R.Wollbeck; S. Ripperger; 1988
"Membranes and modules for transmembrane distillation"
Journal of Membrane Science 39 (1988) 25–42

Schofield, R; Fane, A; Fell, C; 1987
"Heat and mass transfer in membrane distillation"
Journal of Membrane Science 33 (1987) 299–313.

Shakaib, M; Hasani, S.M.F.; Mahmood, M; 2007
"Study on the effects of spacer geometry in membrane feed channels using three-dimensional computational flow modeling"
Journal of Membrane Science 297 (2007) 74–89.

Shakaib, M; Hasani, S.M.F.; Mahmood, M; 2009
"CFD modeling for flow and mass transfer in spacer-obstructed membrane feed channels"
Journal of Membrane Science 326 (2009) 270–284

Sharma, V.K; Fiorenza, G; Braccio, G; 2003

"Techno-economic evaluation of a solar powered water desalination plant"
Energy Conversion and Management 44 (2003) 2217–2240

Sirkar, K.K; Li, B; 2004
"Novel membrane and device for direct contact membrane distillation-based desalination process: Phase II"
Desalination and Water Purification Research and Development Program, Final Report No. 96, July 2004

Srisurichan, S; Fane, A.G; Jiraratananon, R; 2006
"Mass transfer mechanisms and transport resistances in direct contact membrane distillation process"
Journal of Membrane Science 277 (2006) 186-194.

Sudoh, M; Takuwa, K; Iizuka, H; Nagamatsuya, K; 1997
"Effects of thermal and concentration boundary layers on vapor permeation in membrane distillation of aqueous lithium bromide solution"
Journal of Membrane Science. 131 (1997) 1–7.

Tun, C.M; Fane, A.G; Matheickal, J.T; Sheikholeslami, R; 2005
"Membrane distillation crystallization of concentrated salts-flux and crystal formation"
Journal of Membrane Science. 257 (2005) 144–155

Van der Bruggen, B.; 2003
"Desalination by distillation and by reverse osmosis — trends towards the future"
Membrane Technology 2003, (2003) 6-9

Walton, J.; H. Lu; C. Tumer; S. Solis; H. Hein; 2004
"Solar and waste heat desalination by membrane distillation"
Desalination and Water Purification Research and Development Program Report No. 81, 2004.

Wang, Xiao-lin; Gong, Y.; Yu, Li-xin; 2004
"Process simulation of desalination by electrodialysis of an aqueous solution containing a neutral solute"
Desalination 172 (2005) 157-172

Wu, Y; Kong, Y; Lin, X; Liu, W; Xu, J; 1992
"Surface-modified hydrophilic membranes in membrane distillation"
Journal of Membrane Science 72 (1992) 189–196.